INVESTIGATION OF GEOMETRIC AND ELECTRONIC PROPERTIES OF CONDUCTING POLYMERS USING SEMIEMPIRICAL APPROACH

HAMSA SUBRAMANIAN

INVESTIGATION OF GEOMETRIC AND ELECTRONIC PROPERTIES OF CONDUCTING POLYMERS USING SEMIEMPIRICAL APPROACH

By

©Hamsa Subramanian

A THESIS SUBMITTED TO THE SCHOOL OF GRADUATE STUDIES IN PARTIAL FULFILLMENT OF THE REQUIREMENTS FOR THE DEGREE OF MASTER OF SCIENCE

DEPARTMENT OF PHYSICS & PHYSICAL OCEANOGRAPHY
MEMORIAL UNIVERSITY OF NEWFOUNDLAND

January, 1997

ST. JOHN'S NEWFOUNDLAND

Abstract

In this work, we present theoretical evidence illustrating that cyano derivatives of conducting polymers such as polythiophene, polycyclopentadiene and polyfulvene have smaller intrinsic band gaps than their parent polymers. The geometric and electronic properties of the parent and the derivative polymers are studied with the use of two methodologies: (1) the pseudo one-dimensional band structure calculations performed at the level of the semiempirical molecular orbital theory (Modified Neglect of Diatomic Overlap (MNDO) and Austin Model 1 (AM1)) and (2) oligomer calculations performed at the level of the *ab initio* molecular orbital theory. In particular, we have found that an organic polymer, poly-(dicyano-methylene-cyclopenta-difulvene) (PCNFv) has a comparable (possibly lower) band gap to the one observed in poly-(dicyano-methylene-cyclopenta-dithiophene) (PCNTH) (which has a band gap of 0.8 eV). The precursor of PCNFv is poly-(dicyano-methylene-cyclopenta-dicyclopentadiene) (PCNCY) in which two cyclopentadiene rings are connected by a dicyanomethylene group. Trends in structural properties indicate that the lower band gap in the cyano substituted polymers is accompanied by greater charge delocalization in the aromatic or trans-cisoid forms and by greater charge localization in the quinoid or cis-transoid forms in comparison to

their parent polymers. Other important factors that contribute to band gap lowering are maximum planarity, weak interactions of the chain backbone with the bridging groups, enhanced π character of the highest occupied and lowest unoccupied bands and the additional stabilization of the conduction bands due to the charge transfer phenomena. The comparison of the heats of formation for the compounds indicates that polymers in *planar-anti* conformation are more stable than those in *twisted-syn* conformation.

Acknowledgment

I like to thank my supervisor Dr. Jolanta B. Lagowski for her continuous encouragement, support and guidance. I also wish to express my sincere appreciation to Dr. Peter Pickup, Dr. Uli Salzner, Dr. Raymond Poirier for their valuable help and stimulating discussions at every stage of this project.

I would like to thank Memorial University of Newfoundland for awarding a Graduate Fellowship and offering me a Teaching Assistantship.

I am grateful to members in conducting polymer group, members of condensed matter group in the Department of Physics, MUN for providing support and encouragement. I also like to thank the system administrators Fred Perry and Chris Stevenson for their immense computational support.

Finally, I would like to thank my husband, Mr. Vembu Subramanian, who deserves my warmest appreciation for understanding and timely help.

Table of Contents

List of Tables

List of Figures

List of Abbreviations

αT_6	α-sexithiophene
A	Aromatic or s-cis or trans-cisoid
A1	Aromatic unit cell type 1
A2	Aromatic unit cell type 2
AM1	Austin Model 1
AVE	All-valence Electron
BW	Band Width
BZ	Brillouin Zone
CB	Conduction Band
CMS	Cluster Model for Solids
EA	Electron Affinity
E_g	Energy Gap or Band Gap
E_{el}	Electrochemical Gap
E_{op}	Optical Gap
H_f	Heat of Formation
ΔH_f	Average Heat of Formation
HF	Hartree-Fock
HOMO	Highest Occupied Molecular Orbital
IP	Ionization Potential
LUMO	Lowest Unoccupied Molecular Orbital
MNDO	Modified Neglect of Diatomic Overlap
NDDO	Neglect of Diatomic Differential Overlap
PA	Polyacetylene
PAni	Polyaniline
PCY	Polycyclopentadiene
PFv	Polyfulvene
PM3	Parametric Method 3
PPY	Polypyrole
PT	Polythiophene
PCNTH	Poly-(dicyano-methylene-cyclopenta-dithiophene)
PCNCY	Poly-(dicyano-methylene-cyclopenta-dicyclopentadiene)
PCNFv	Poly-(dicyano-methylene-cyclopenta-difulvene)
Q	Quinoid or s-trans or cis-transoid
Q1	Quinoid unit cell type 1
Q2	Quinoid unit cell type 2
VB	Valence Band
VEH	Valence Effective Hamiltonian

Chapter 1

Introduction

1.1 Conducting Polymers

In general, synthetic polymers are large macromolecules that are made of repeating units called monomers. In this work we study a special class of synthetic polymers called **conducting polymers (CP's)**. CP's are conjugated, often organic, linear, unbranched chains of atoms covalently bonded. CP's are increasingly becoming important because of their many industrial applications such as conducting fabrics, conducting fibers, electronic membranes, field effect transistors etc. [1, 2, 3, 4]. The many uses in the electronic and optical industries arise from their properties and characteristics such as greater strength, compatibility and ease of synthesis in comparison to the conventional metals and semiconductors. Examples of extensively studied CP's are shown in Fig. 1.1.

CP's can be metals or semiconductors. Possessing a finite band gap, E_g, means that a polymer is a semiconductor. Most of the undoped CP's are semiconductors that exhibit intrinsic conductivity when valence electrons are thermally or photonically excited

from the highest filled band into the lowest unfilled band. Thus, one of the desirable properties of CP's is a small intrinsic band gap in order to achieve readily intrinsic conductivity. It is the main goal of this work to identify CP's with small band gaps. Having a small band gap is also important for the doped CP's (which are not studied in this thesis). This can be shown as follows. Roughly, in a simple metal, the electrical conductivity, σ, decreases almost linearly with temperature T [5]. In non metals conductivity increases with T. according to the activation law

$$\sigma = n(T)|e|\mu_0 = \sigma_0 e^{(\frac{-2E_g}{kT})}. \tag{1.1}$$

By definition, σ is proportional to the concentration n of charge carriers with the (mean) mobility μ_0. In Eq. 1.1 e is the electronic charge and k the Boltzmann constant. In a simple semiconductor (such as some of the doped CP's), the charge number density, n, ($n_{electrons}$ or n_{holes}) produces the activation of conductivity, σ, ($\sigma_{electrons}$ or σ_{holes}). In Eq. 1.1. we note that σ also depends exponentially on the ratio E_g/kT indicating that smaller E_g will result in larger extrinsic conductivity for given temperature T and charge carrier concentration.

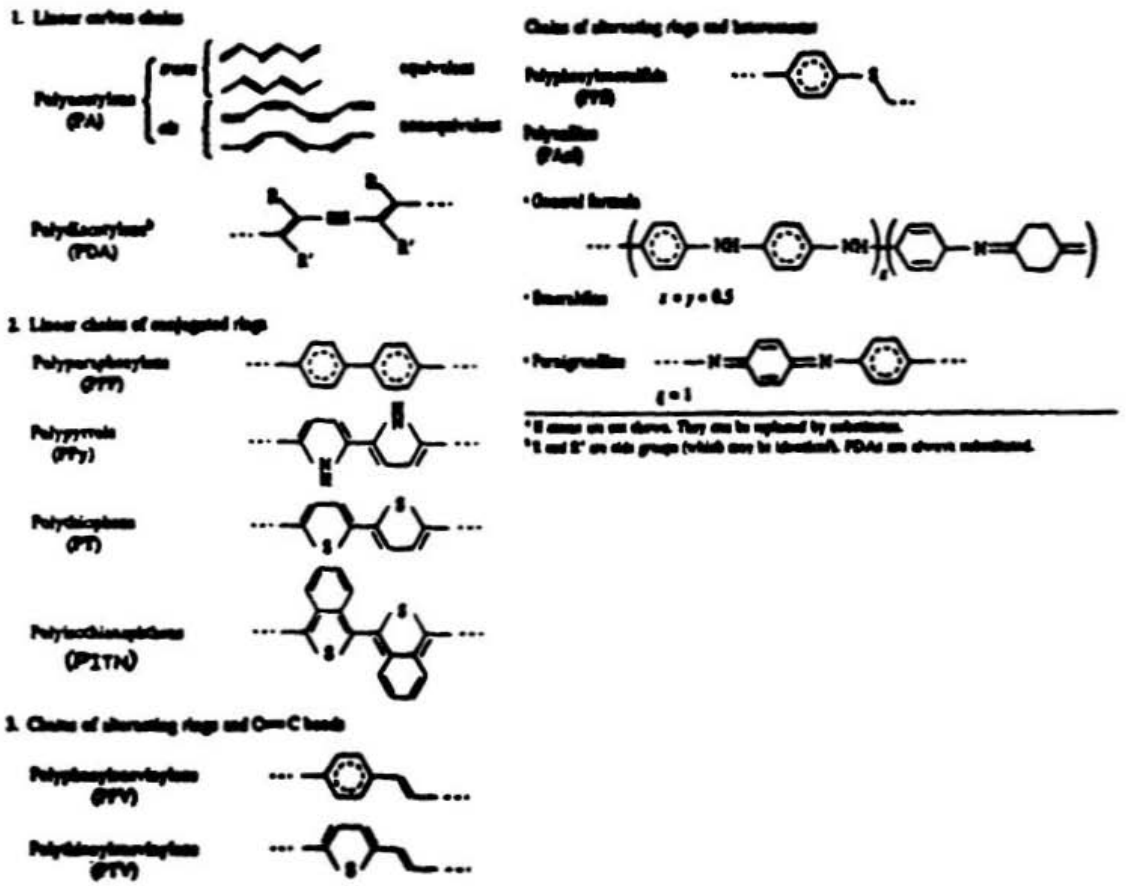

Figure 1.1: Common conjugated polymers. This figure is taken from [6].

1.2 Literature Review

The field of CP's has experienced phenomenal growth over the past few years. Interest in the theory of conjugated molecules, particularly the polyenes made of alternating single and double bonds, for instance hexatriene (H-CH=CH-CH=CH-CH=CH-H) dates back to the early days of quantum chemistry and in the 1960's [7, 8, 9] reached a high level of understanding. This was immediately followed by formulation of theoretical framework for the study of conjugated polymers.

On the other hand, a key development in the evolution of the CP area is the discovery of polyacetylene (PA), which was synthesized by Natta et al., in the late 1950's [10], using Ziegler-Natta catalysts and observed at room temperature, to have a conductivity of the order of 10^{-6} S/cm. Later in 1970's [11] Natta's synthesis was modified yielding self standing fibrillar films with metallic luster. Another decisive discovery was that PA could be *doped* with electron-acceptors and electron-donors. This process is universally known as "doping". (Shirkawa [12] has made a polymer PA that was highly conducting ($\approx$ 50 to 500 S/cm) by exposing it to strong acceptors such as I_2.) It was then shown that doping can also be produced electrochemically, whereby, for instance, ClO_4^- ions are intercalated to compensate for the positive charges injected into the Shirkawa PA chains, with resultant conductivities of about 10^3 S/cm [13].

Table 1.1: Relationship between experimental and theoretical routes for investigating conducting polymers.

	Experimental	Theoretical
Preparation	Chemical, Electrochemical, Synthetic Routes	
Geometric Structure	X-ray, Electron Diffraction	Quantum or Classical Models
Frequency Distribution	Raman, NMR Spectra	Force Calculation
Electronic Structure	Absorption or Emission (Ultra Violet,Visible) Spectra	Band Structure, Density of States

A significant breakthrough occurred in 1979 with the discovery [14] that polyparaphenylene, (PPP), could be doped to conductivity levels quite comparable to those obtained in the PA system. This discovery was important in that it demonstrated the non uniqueness of the PA system and paved the way for the discovery of a number of polyaromatic based CP systems. These polyaromatics now include polypyrole(PPY), polythiophene(PT), polyaniline(PAni). Even more important, it opened the way to a general preparation method of the electrochemical polymerizations of pyrrole by anodic oxidation [15, 16] which produced smooth, highly conducting doped (100 S/cm) films. The same method was then used to prepare PT (with similar results [17]) for which the electrochemical band gap (E_{el}) was measured from the difference between onset of oxidation and reduction potentials using cyclic voltommograms [18].

Once the interest in CP was established several strategies were tried to improve the processibility while keeping (most of) the conductivity. All materials mentioned in Fig. 1.1 are neither soluble nor fusible. They are generally poorly ordered and non compact films, whose morphology is determined by the chemical or electrochemical growth conditions. An exception is PAni [19] which is soluble in few solvents and strong acids [19]. Earlier few attempts were made to generate CP from a soluble precursor polymer. But this was hardly a general method. Later in 1986, the first soluble alkyl-substituted polythiophene was synthesized [20]. Its electronic properties were similar to those of PT and high quality films were easily formed from solution. This is. a fairly general method. The bulkiness of most substituents had structural consequences, which in turn affected their electronic properties.

CP's are rarely "crystalline" polymers in that they always contain an amorphous fraction $\geq$ 50% of the total volume. Typically the crystalline fraction may be $\leq$ 10% of the volume. It is the latter that is selected in 'structural studies', but the amorphous phase may often dominate the physical properties. The same material depending on synthesis method can be either crystalline or amorphous. For example, electrochemical PT is amorphous [17], whereas the chemically prepared polymer is partly crystalline [21]. Unfortunately, their amorphous nature has prevented X-ray determination of their structure and only a few X-ray scattering data [21, 22] are available at present.

Diffraction methods and work in the reciprocal space are prominent techniques used in

determining atomic positions. However, in poorly ordered materials such as CP's the amount of structural information that can be obtained from a typical X-ray, neutron or electron diffraction experiments is minimal. Real space methods, such as scanning electron microscopy (SEM), scanning tunneling microscopy (STM) are major sources of information about morphology of these systems at mesoscopic scales, mainly of surface regions. On the Angstrom scale, NMR has been used to measure CC bond lengths accurately without a complete structure determination. On the scale of 10 to 100 $\AA$, resonance raman spectroscopy (RRS) is generally used to infer conjugation lengths, deduced from a measure of the extent of spatial order along the CP chains [23, 24].

Spectroscopic methods such as X-ray, ultra violet, visible gives pertinent information about energy gap. The photo induced absorption, emission and luminescence spectra are widely used for determining the mid-gap states. With soft X-ray photons (XPS), for example, both electrons in the atomic core levels and valence electrons can be studied. With ultra violet (UPS) and visible photo electron spectra only the valence electrons can be studied, but with certain resolution and cross sections that are better than those obtained with XPS. The most important point is that there is a one-to-one correspondence between the distribution of electron energy states in the sample and the kinetic energy distribution of the photo electrons in photo electron spectra.

The visible absorption spectra of all CP's shows a broad and intense band. Its threshold is anywhere between 12,500 $\AA$ (or 1 eV) for polyisothionapthene [25] to 4000 $\AA$ (or 3

eV) for PPP [26], and at 8000 to 9000 $\AA$ (or 1.35 eV to 1.5 eV) in *trans*-PA, depending on the preparation conditions [27]. The absorption band is usually well separated from further absorption at higher energies. The corresponding transition is assigned to the π electrons. In polymers this refers to direct transition of π electrons from π band to π^* band which is measured from the threshold of the intense absorption. In oligomers this transition corresponds to the energy of maximum absorption [28]. This measurement is often referred as *optical gap* (E_{op}). From electro absorption spectra of films of PT [29] and its hexamer, α-sexithiophene (αT_6), [28] the optical gaps were calculated to be 2.1 eV and 2.78 eV respectively. The absorption threshold differed approximately by 0.7 eV which indicates that in PT conjugation extends over more than six monomers.

Naturally solid-state theory otherwise called electronic band structure theory could be used for studying polymers. This theory is the application of the Hartree-Fock one electron approximation to solids based on the assumption that the solids have translational symmetry underlying their atomic level structure. Although solids can have symmetry elements other than translational invariance, it is the translational symmetry that leads to the characteristic classification of the energy levels and eigenfunctions. The wave functions describing the electronic states in the bands extend throughout the solid, unlike the atomic orbitals, which are localized around particular atoms, and decay exponentially away from those atoms. In this sense, we refer to solid wave functions as *delocalized orbitals*. The concept of electronic charge delocalization is an important

one. It is responsible for most of the electronic transport phenomena in solids, for example, the conductivity and non-linear optical properties. The picture of electronic levels broadening can be understood from the Fig. 1.2 given below.

For example, consider a free lithium atom: the electron moves in a potential well, as shown in Fig. 1.2(a). The electronic energy levels are denoted by 1s, 2s, 2p. The lithium atom contains 3 electrons, two of which occupy the 1s subshell (completely full), and the third the 2s subshell. Now consider the situation in which two lithium atoms assemble to form the lithium molecule Li_2. The potential "seen" by the electron is now the double well shown in Fig. 1.2(b). Each atomic level-that is the 1s, 2s, 2p, splits into two closely spaced levels called molecular levels. Each molecular level can accommodate at most two electrons, of opposite spins. The Li_2 molecule has 6 electrons; four occupy the 1s molecular levels and the other two the lower level of the 2s molecular level.

The above considerations may be generalized to polyatomic Li of an arbitrary number of atoms. The lithium solid may then be viewed as the limiting case in which the number of atoms has become very large. What happens to the shape of the energy spectrum? Each of the atomic levels is split into N closely spaced sublevels, where N is the number of atoms in the solid. Since N is very large (order of 10^{23}) the sublevels are extremely close to each other so they coalesce and form an *energy band.* Thus 1s, 2s, 2p levels give rise, respectively, to the 1s, 2s, 2p bands, as in Fig. 1.2(c). The

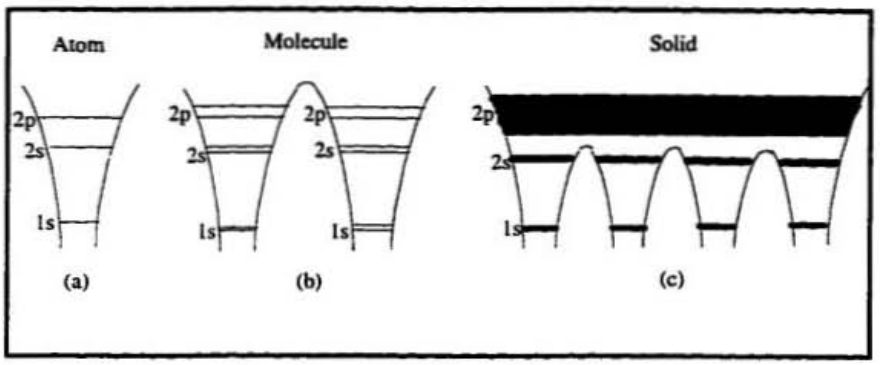

Figure 1.2: For example energy levels of lithium: (a) atom, (b) molecule, (c) solid.

intervening regions separating the bands are *energy gaps*, E_g, i.e. regions of forbidden energy which cannot be occupied by electrons. This broadening of discrete levels into bands is one of the most fundamental properties of solid.

Band structure of a solid determines most of its electronic properties. As shown in Fig. 1.3 no conduction can take place in an empty band because it contains no electrons. Conduction is also impossible in a full band because the total population of electrons in such a band can have no net motion. A metal is a material with partially filled band, where the electrons can be given a net velocity by shifting some of them to infinitesimally higher energies within the band. An insulator has only completely filled bands and completely empty ones, with a large $E_g \geq 2$ eV between them. A semiconductor has a band structure much like that of an insulator but has some mobile charge carriers. The carriers can be introduced by impurities, by defects, by excitation

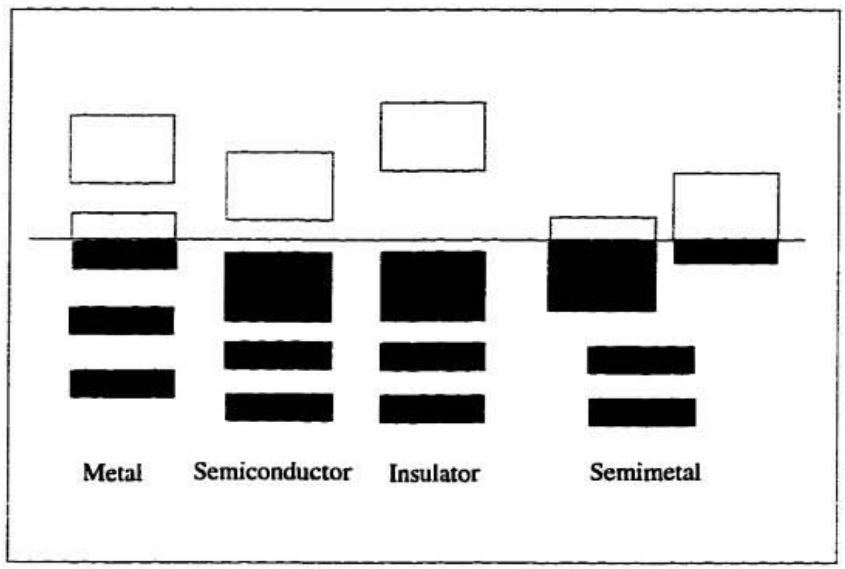

Figure 1.3: Difference between metal, semiconductor, insulator and semimetal. The shaded portion represents the filled levels and unshaded portion the unfilled levels.

of electron from the highest filled band (the valence band) to the lowest empty one (the conduction band). What distinguishes a semiconductor from an insulator is that the E_g is comparatively small in semiconductor. In a semimetal the valence band is filled and the conduction band is empty, but these bands overlap in energy. As a result electrons redistribute themselves to create two partially filled bands.

The electronic structure of the parent (undoped, unsubstituted) polymers is now known fairly well. Many different experimental and theoretical techniques have been applied to the various conjugated polymers, with varying degrees of success in predicting, for

example, electron affinity (EA), ionization potential (IP), band gap or energy gap (E_g), band width (BW). The band width at least in a qualitative sense gives some indication of the extent of electron delocalization in the system and suggests how mobile the carriers will be once produced (e.g. by the ionization process). The IP is important, since it determines whether or not a particular electron-acceptor is capable of ionizing the polymer chain. Iodine, for example, will ionize PA to produce a conducting complex, but has little effect on the conductivity of PPP [30]. This result is due to the fact that iodine is a relatively weak electron-acceptor and PPP has a higher IP than PA.

If the CP is a purely one-dimensional polymer, say linear PA (whose bonds are all equal), that contributes one electron per lattice site, and then it should be a metal. However, the linear PA transforms into a semiconductor. The linear PA becomes semiconductor because of the lattice or Peierls distortions [31, 32, 33]. Lattice distortions in 1D systems arises because of the modulations of the electronic densities [34] and vibration of the ions in the lattice. Due to this modulation electronic states may be degenerate and they may interact with a vibrational mode. That is, the electronic states may be coupled with the phonon causing the lattice to distort from the original configuration and thus splitting the degeneracy. The distortion opens a gap in the incompletely filled band forming the valence and the conduction bands. This splitting of the band is produced by the net lowering of the electronic energy. Thus the bond alternate structures are created. The bond alternation may be in phase or out of phase

depending on the orientation of the bonds in the respective mesomers. Thus in the CP's after lattice distortion the resulting mesomers can be degenerate (e.g. PA) or non-degenerate (PPY, PT, PPP, PAni).

Typically theoretical calculations may be performed at the *ab initio* or semiempirical level. In the case of conjugated molecules or polymers the large number of atoms per unit cell precludes the use of *ab initio* methods. The most successful technique developed to date for general applicability is the Valence Effective Hamiltonian (VEH) technique [35, 18]. In fact, many VEH calculations have shown a close agreement between the theoretical density of states and experimental X-ray photo electron spectra [36]. The semiempirical methods which is computationally efficient, is also used by many workers [37, 38, 39] to study the topology of bands and density of states. The results predicted with this method were in close agreement with the VEH method. Also the IP and E_g values were in agreement with the experimental results. Therefore, in practice, to understand the qualitative aspects of the solids as pertaining to their band structures and the charge transfer phenomena, the semiempirical approach appears to be valid and hence we have chosen it for our calculation. Further validation of our results was carried out with *ab initio* molecular orbital calculations on the stable mesomers for the oligomer systems.

1.3 Current Research

The work, in this thesis, focuses on identifying low band gap organic polymers with thiophene and cyclopentadiene as the initial building blocks of their backbones. Specifically, we investigate the geometric and electronic properties of the following systems, polythiophene (PT), polycyclopentadiene (PCY), polyfulvene (PFv), poly-(dicyano-methylene-cyclopenta-dithiophene) (PCNTH), poly-(dicyano-methylene-cyclopenta-dicyclopentadiene) (PCNCY) and poly-(dicyano-methylene-cyclopenta-difulvene) (PCNFv) (see Fig. 1.4 for the corresponding monomeric units). The compound which has not been studied previously either theoretically or experimentally is PCNFv which consists of two PFv rings which are bridged by a dicyano group as seen in Fig. 1.4.

The above polymers are of interest because historically the π conjugated polymers, polythiophene and polypyrole, have been shown to be promising (i.e. having small intrinsic band gaps) organic CP's (see the discussion in the previous section). Recently [40]. it has been shown that enhanced conductivity can be obtained in polymers containing both electron-donating and accepting groups which form charge transfer complexes. Accordingly, compounds containing fulvene and/or cyano groups are of special interest. In 1978, Mizuno et al., [41] first reported that bis(ethylenedithio)-tetrathiafulvalene (BEDT-TTF) (of a fulvene origin) is a superconducting organic compound. In this molecular system an electron-donor unit TTF is attached to an electron-acceptor unit

BEDT forming a charge transfer complex. This work was followed by the synthesis of small band gap polymers such as polysquaraines and polycroconaines [42] that were formed by attaching an electron-donating and/or an electron-withdrawing groups to the conjugated backbones. Before this, in 1973, Ferraris et al., [43] produced organic charge transfer material tetrathiafulvalene-tetracyanoquinolone (TTF-TCNQ) with the conductivity of 10^2 Scm^{-1} which is in the range of conductivity of graphite. Again in 1991, Ferraris and group synthesized [44] a polymer PCDM (referred to as poly-4-dicyanomethylene-4H-cyclopenta [2,1-b;3,4-b']dithiophene in his work and PCNTH in our work) whose band gap was measured with the use of absorption spectroscopy and found to be 0.8 eV. Recently, theoretical polymer calculations were performed for PCNTH [45] and PCNCY [46] (called PDICNCY in [46]). In these cases, the geometrical (fully optimized) structures were obtained using semiempirical AM1 (Austin Model) approach which was followed by electronic band structure calculations that employed the pseudo-potential method, VEH [47, 35]. The band structure calculations predicted a band gap of 0.56 eV for PCNTH and 0.16 eV for PCNCY polymers. The discrepancy between the experimentally and theoretically determined values for the band gaps can be attributed in part to the fact that in the computations polymers are treated as pseudo one-dimensional systems, neglecting their inherent three dimensional nature and their intermolecular interactions that are present in the solid-state.

In this work, we focus on examining the geometries as well as the band structures

of the polymers listed above. All calculations are performed using the semiempirical solid-state cluster method [48, 49] as implemented in MOPAC93 [50]. In this method, polymers are considered as infinite pseudo one-dimensional systems. We have used both AM1 and MNDO(Modified neglect of Diatomic Overlap) methods for geometry optimizations and BZ (Brillouin Zone) functionality in MOPAC93 for band structure calculations. Both the space group symmetry and periodic boundary condition are employed in the solid-state cluster calculation [49]. The cluster method works best for clusters that are large enough so that the influence of the end groups on the bulk is negligible. For our systems, the optimum cluster size is an octamer [51] for the systems with smaller monomeric units such as PT, PCY and PFv and tetramer for the polymers with larger repeat units such PCNTH, PCNCY and PCNFv. However for consistency only the results obtained for tetramers (with unit cells containing four monomers) are reported in this work.

For the systems considered in this work, the size of the unit cell which is a fundamental part of the cluster must be determined with care. Typically, in the molecular calculations one monomer (e.g. one ring in PT) is considered to be the fundamental unit of the polymer. However, in the solid-state computations the symmetry arguments alone dictate that a unit cell should contain at least two monomers if the long range translational symmetry and *planarity* of the whole systems is to be maintained. To assess the importance of this, calculations were carried out on systems with two monomers and

one monomer per unit cell. The main finding of these computations is that with two monomers per unit cell one obtains a planar structure [52, 53] (with the rings pointing in the opposite directions [52, 53] i.e. *anti* conformation) whereas with one monomer per unit cell one obtains a twisted structure [54] since the rings in this case point in the same direction i.e. *syn* and steric interactions prevent the formation of a planar structure. The extended. twisted structure would form a narrow helix in the infinite chain.

In addition, in the case of having two monomers per unit cell, we investigated the importance of applying symmetry constraints (other than the translational symmetry) in the geometry optimizations and solid-state calculations. We have found that for the parent polymers [55] PT, PCY and PFv the full band structure calculations gave the same results for band gaps irrespective whether the additional symmetry constraint were used or not. The reason for this is that the unconstrained geometry optimized stable structures already exhibited most of the point group symmetries included in the symmetry constraint computations. Thus, for large systems such as PCNTH, PCNCY and PCNFv we did not impose symmetry constraint in their geometry optimizations and consequently in the full band structure calculations.

From our previous discussion on lattice distortion it is clear that the polymers studied can exist in two mesomeric forms. In PT and PCNTH either aromatic(A) or quinoid(Q) mesomeric forms [56, 57] have been observed. That is, they are aromatic when the

monomeric units are connected by longer (referred to as "single") bonds and quinoid when they are connected by shorter (referred to as "double") bonds (see Fig. 4.12). The PCY, PFv, PCNCY and PCNFv can also exist in two forms, the trans-cisoid(A) and cis-transoid(Q) [46]. S-cis form has a "single" bond between the monomers and s-trans form has a "double" between the monomers [18].

The extensive semiempirical calculations have been followed by all-electron, molecular orbital calculations using Gaussian94 at a level of 3-21G*/RHF basis set for a selected set of polymers. That is, *ab initio* calculations have been performed on the most stable mesomeric forms for short oligomers (dimers) [6] with chemical compositions corresponding to all polymers studied. In the oligomer calculations hydrogen atoms were used as end groups and compounds were kept *planar* by constraining dihedral angles to values 0° or 180°.

In this thesis, chapter 2 outlines the Hartree-Fock self-consistent methodology and semiempirical methods. In chapter 3, we concentrated mainly on the solid-state theoretical aspects. The first section of this chapter reviews briefly solid-state theory, application of Bloch's theorem and brief description of energy spectra. The cluster model is outlined in section 2 of this chapter. The geometry of a conducting polymer can have a marked effect on the band structure. It is for this reason that chapter 4 is used to analyze the structure of model compounds in their mesomeric forms both in *syn* and *anti* orientations. In chapter 5, the band structures, the dispersion of π

bands and wave functions of the valence and conduction bands are discussed. Also, their structural features are correlated with their electronic properties and the trends in the E_g, IP, EA and band structures for the two mesomeric forms of the polymers are discussed in chapter 5. In chapter 6 we summarize our conclusions.

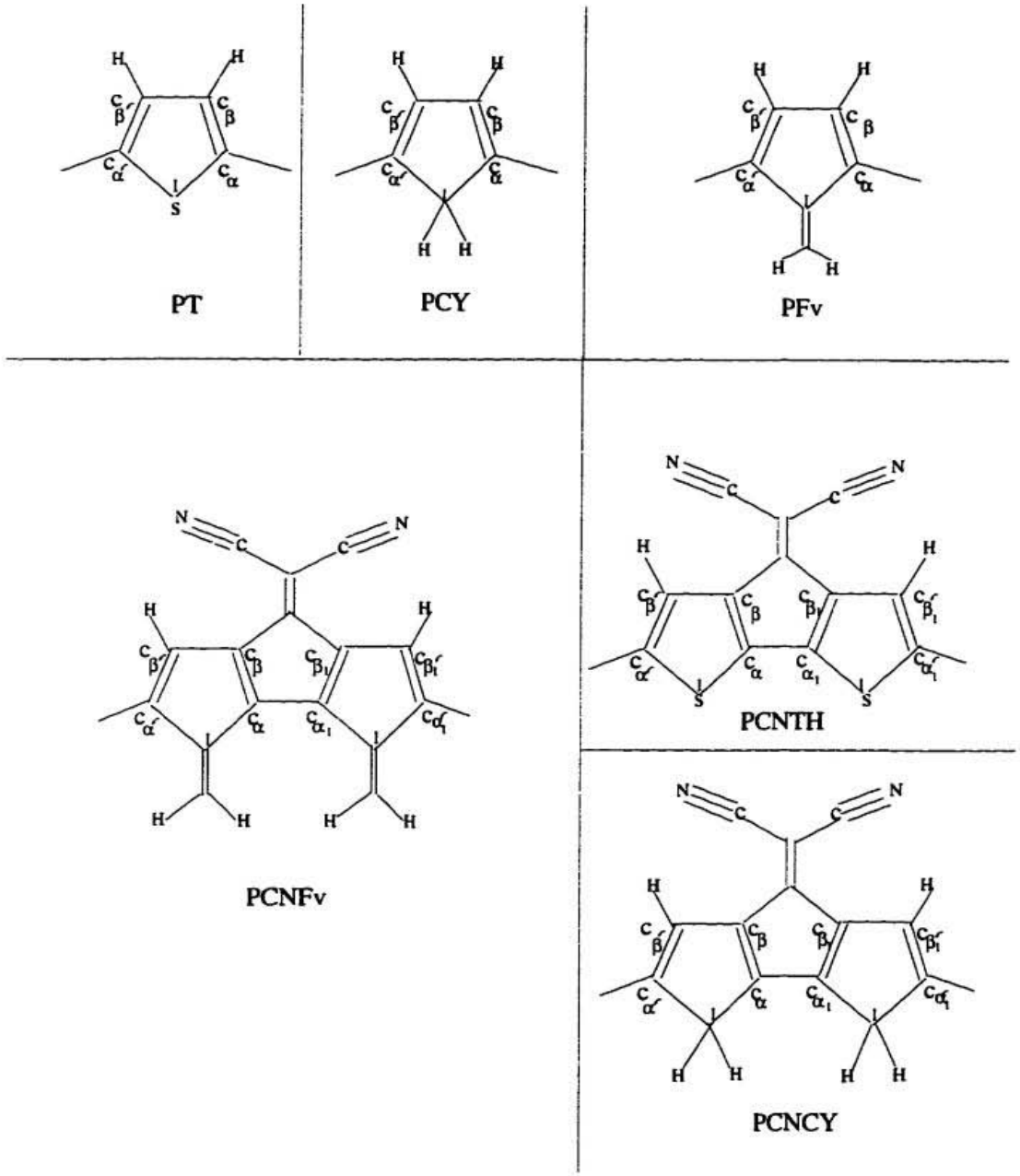

Figure 1.4: Conjugated polymer systems studied.

Chapter 2

Hartree-Fock (HF) Method in Semiempirical Models

Quantum chemical methods use the principles of quantum mechanics to determine the various properties of atoms, molecules and solids. One group is concerned with purely non-empirical methods (often called *ab initio* methods) while the second group is concerned with semiempirical methods, i.e. calculational methods that utilize an additional posteriori information. In the present chapter, we briefly discuss the main features of the semiempirical methods. We summarize the evolution of semiempirical methods as derived from the exact formulation of the linear combination of atomic/molecular orbitals, LCAO/MO, method within the Hartree-Fock (HF) approximation.

2.1 Hartree-Fock Approximation

The central equation in quantum mechanics is the Schröedinger equation Eq. 2.1

$$\hat{H}\Psi = E\Psi, \tag{2.1}$$

For systems larger than H_2^+ it is difficult to solve this equation exactly and certain approximations must be introduced in the exact quantum mechanical theory. The solutions, Ψ, of Eq. 2.1 are functions of the space and spin coordinates of all particles. They are called wave functions of the states with eigen energies E.

The motion of nuclei is relatively slow compared to that of electrons. This leads to Born-Oppenheimer approximation. In this approximation the Hamiltonian in Eq. 2.1 is treated to be non-relativistic and time independent with nuclei assumed to be stationary [58]. In general, for many-body system containing N nuclei and $2n$ electrons the electronic Hamiltonian (in atomic units) is given by

$$\hat{H}_{el} = -\sum_{i}^{2n} \frac{1}{2}\nabla_i + \sum_{i<j}^{2n}\sum^{2n} \frac{1}{|\vec{r}_i - \vec{r}_j|} - \sum_{A=1}^{N}\sum_{i=1}^{2n} \frac{Z_A}{|\vec{r}_i - \vec{R}_A|}. \tag{2.2}$$

We define $\Psi_{el}(\vec{r}, m_s; \vec{R})$ as a solution of the Schrōedinger equation given by

$$\hat{H}_{el}\Psi_{el}(\vec{r}, m_s; \vec{R}) = E_{el}(\vec{R})\Psi_{el}(\vec{r}, m_s; \vec{R}). \tag{2.3}$$

In Eq. 2.3 $E_{el}(\vec{R})$ is the potential energy which represents the electronic energy for a fixed set of nuclear co-ordinates. Thus, the total energy E_t is defined as the sum of the electronic energy, $E_{el}(\vec{R}_0)$, calculated for the given nuclear geometry R_0 and the

nuclear interaction energy:

$$E_t = E_{el}(\vec{R}_0) + \sum_{A<B}^{N}\sum^{N}\frac{Z_A Z_B}{R_{AB}}. \tag{2.4}$$

Considering that electrons are indistinguishable particles, their fermionic character requires that they satisfy Pauli exclusion principle. i.e. the total many-electron wave function is antisymmetric (with respect to the electrons interchange of the electrons' quantum numbers.) To satisfy the Pauli exclusion principle the wave function is written in the form of Slater determinant [59] in HF approximation as follows

$$\Psi(\vec{r}, m_s) = \frac{1}{\sqrt{2n!}}\begin{vmatrix} \psi_1(1)\alpha(1) & \psi_1(2)\alpha(2) & ..... & \psi_1(2n)\alpha(2n) \\ \psi_1(1)\beta(1) & \psi_1(2)\beta(2) & ..... & \psi_1(2n)\beta(2n) \\ ..... & ..... & ..... & ..... \\ \psi_n(1)\alpha(1) & \psi_n(2)\alpha(2) & ..... & \psi_n(2n)\alpha(2n) \\ \psi_n(1)\beta(1) & \psi_n(2)\beta(2) & ..... & \psi_n(2n)\beta(2n) \end{vmatrix}. \tag{2.5}$$

The elements of the above determinant are spin orbitals Φ_i which are given by the product of a function of electron space coordinates, $\psi_i(\vec{r}_i)$, and one of the two possible $\pm\frac{1}{2}$ spin functions

$$\Phi_i(\vec{r}_i, m_{si}) = \psi_i(\vec{r}_i)\zeta(m_{si}) \tag{2.6}$$

where $\zeta(m_{si}) = \alpha$ for $m_{si} = +\frac{1}{2}$ and $\zeta(m_{si}) = \beta$ for $m_{si} = -\frac{1}{2}$. In the HF approximation, it can be shown [58] that the spin orbitals are eigenfunctions of single electron Hamiltonians,

$$\hat{H}^{eff}(i)\Phi(i) = E_i\Phi(i). \tag{2.7}$$

2.1.1 Basis Set Expansions

Basis set expansions are used to approximate ψ_i. For example, each molecular orbital ψ_i can be expanded as a linear combination of atomic-like orbitals χ_ν [1]

$$\psi_i = \sum_{\nu=1}^{N} c_{\nu i}\chi_\nu \tag{2.8}$$

where the atomic-like orbitals called basis functions χ_ν constitute the basis set for the calculation and the molecular orbital expansion coefficients $c_{\nu i}$ can be determined from the variational principle [59].

2.1.2 The Electronic Energy

The electronic energy is determined by the expectation value as obtained from the equation. $E = \frac{<\Psi|\hat{H}|\Psi>}{<\Psi|\Psi>}$, where Ψ is given in Eq. 2.5 and $\hat{H} = \hat{H}_{el}$ is given in Eq. 2.2.

[1] In semiempirical methods Slater type orbitals (STO) are used as basis functions.

After dividing the electronic Hamiltonian into one electron and two electrons contributions and performing the integrations over space coordinates and the spin summations according to rules explained elsewhere [58], the total electronic energy is given by

$$E = 2\sum_{i=1}^{n} < i|\hat{h}^N|i > + \sum_{i}^{n}\sum_{j}^{n}(2J_{ij} - K_{ij}) \tag{2.9}$$

where

$$< i|\hat{h}^N|i >= \int \psi_i^*(1)\hat{h}^N\psi_i(1)dv_1 = H_{ii}^N \tag{2.10}$$

are the one electron integrals that consist of first and third terms of Eq. 2.2 and $\hat{h}^N$ is called the one electron operator. There are two types of two electron integrals: the coulomb and the exchange integrals. The coulomb integral can be represented as

$$J_{ij} = \int \psi_i^*(1)[\int \psi_{\mathbf{j}}^*(\mathbf{2})\frac{\mathbf{1}}{\mathbf{r_{12}}}\psi_{\mathbf{j}}(\mathbf{2})\mathbf{dv_2}]\psi_i(1)dv_1 \tag{2.11}$$

and exchange integral can be represented as

$$K_{ij} = \int \psi_i^*(1)[\int \psi_{\mathbf{i}}^*(\mathbf{2})\frac{\mathbf{1}}{\mathbf{r_{12}}}\psi_{\mathbf{j}}(\mathbf{2})\mathbf{dv_2}]\psi_j(1)dv_1. \tag{2.12}$$

Similarly the terms inside the brackets can be identified in the above integrals as the coloumb operator, $\hat{J}_{ij}$, and the exchange operator $\hat{K}_{ij}$ respectively.

2.1.3 The Variational Principle

The variational principle states that an arbitrary function Ψ', (which, in the basis set expansion approximation depend on the particle co-ordinates and numerical parameters $c_{\nu i}$) used in calculations to approximate the exact eigenfunction Ψ of the lowest energy eigenstate of a given system satisfies the following condition for the eigenvalue E' corresponding to Ψ'

$$E' \geq E \tag{2.13}$$

where E is the exact energy (refer Eq. 2.9) eigenvalue of state Ψ (true ground state). It follows from this inequality (Eq. 2.13) that the **best** approximation of E' to the eigenvalue E will be obtained when ψ_i (refer Eq. 2.8) will be adjusted to minimize the expectation value of the energy E' i.e.,

$$\frac{\delta E'}{\delta \psi_i} = 0 \qquad (for\ all\ i) \tag{2.14}$$

where

$$\frac{<\Psi'|\hat{H}'|\Psi'>}{<\Psi'|\Psi'>} = E' \geq E. \tag{2.15}$$

After substituting Eq. 2.9 into Eq. 2.15 E' is varied with respect to ψ_i. Performing the unitary transformation which diagonalizes the matrix of Lagrangian multipliers leads to eigenvalue equations called Hartree-Fock integro-differential equations of the form

$$[\hat{h}^N(1) + \sum_{j=1}^{n}(2\hat{J}_j(1) - \hat{K}_j(1)]\psi_i(1) = \epsilon_i\psi_i(1) \tag{2.16}$$

where i=1.2.3.....n or equivalently

$$\hat{H}^{HF}\psi_i = \epsilon_i\psi_i. \tag{2.17}$$

To provide the physical interpretation of the Lagrangian multipliers, ϵ_i, we multiply Eq. 2.16 by ψ_i^* and integrate over electron coordinates, then

$$\epsilon_i =< i|\hat{h}^N(1)|i > + \sum_{j=1}^{n} < i|2\hat{J}_j(1) - \hat{K}_j(1)|i >=< i|\hat{H}^{HF}|i > \tag{2.18}$$

where $\hat{H}^{HF}$ is called 'Hartree-Fock Hamiltonian' [60] or the effective one electron 'Fock

operator' [58] defined as

$$\hat{H}^{HF} = \hat{h}(i) + \sum_{j=1}^{n}(2\hat{J}_j(i) - \hat{K}_j(i)), \tag{2.19}$$

2.1.4 The Hartree-Fock Roothan (HFR) Equations

Introduced by Roothan [61] in 1951 the substitution of Eq. 2.8 into Eq. 2.16. and addition of an arbitrary function φ (orthogonal to all basis function) and multiplying both sides by χ_μ^* and integrating over the coordinates we transform the integro-differential equations into algebraic ones

$$\sum_\nu c_{\nu i}[H_{\mu\nu}^N + \sum_{\lambda,\sigma} P_{\sigma\lambda}(<\mu\nu|\lambda\sigma> - \frac{1}{2} <\mu\sigma|\lambda\nu>)] = \sum_\nu c_{\nu i}\epsilon_i <\mu|\nu> . \tag{2.20}$$

We define subsequent integrals that are part of the above equation as follows:

$$P_{\lambda\sigma} = 2\sum_j^{occ} c_{\lambda j}c_{\sigma j}^* \tag{2.21}$$

$$S_{\mu\nu} =<\mu|\nu> \tag{2.22}$$

$$F_{\mu\nu} = [H_{\mu\nu}^N + \sum_{\lambda,\sigma}(<\mu\nu|\lambda\sigma> - \frac{1}{2} <\mu\sigma|\lambda\nu>)] \tag{2.23}$$

$$= H_{\mu\nu}^N + G_{\mu\nu}$$

$$H_{\mu\nu}^N = (\chi_\mu^*(1)|[\frac{1}{2}\nabla_1 - \sum_{A=1}^{N}\frac{Z_A}{r_{A1}}]|\chi_\nu(1)). \tag{2.24}$$

This allows us to write down the above set of equations in a more compact form as follows

$$\sum_{\nu} c_{\nu i}(F_{\mu\nu} - \epsilon_i S_{\mu\nu}) = 0, i = 1, 2, ...n. \tag{2.25}$$

These are the algebraic HF equations (with basis functions χ_ν), the so-called Hartree-Fock-Roothan (HFR) equations. $P_{\lambda\sigma}$, $S_{\mu\nu}$ and $F_{\mu\nu}$ can be treated as elements of square matrices: **P** (the charge density matrix), **S** (the overlap matrix) and **F** (the Fock matrix containing one and two electron integrals) respectively, with dimensions equal to that of the basis set χ_ν. HFR equation can be written in the abbreviated form as

$$\mathbf{FC} = \mathbf{SC}\epsilon \tag{2.26}$$

C is a square matrix, the i^{th} column of which are the MO coefficients $c_{\nu i}$ obtained via matrix diagonialization. The basis functions are orthogonal and upon unitary transformation of the basis functions will produce molecular orbitals. That is we proceed as follows:

$$\begin{aligned} \mathbf{S}^{(-1/2)}\mathbf{F}\mathbf{S}^{(-1/2)}\mathbf{S}^{(1/2)}\mathbf{C} &= \mathbf{S}^{(1/2)}\mathbf{C}\epsilon \qquad (2.27) \\ \mathbf{F}'\mathbf{V} &= \mathbf{V}\epsilon \end{aligned}$$

In the HF method the total electronic energy is given by Eq. 2.9. Expanding the integrals H_{ij}^N, J_{ij} and K_{ij} in terms of the basis functions we obtain the electronic energy in the HFR method as:

$$E_{el} = \frac{1}{2}\sum_{\mu,\nu} P_{\mu\nu}(H_{\mu\nu}^N + F_{\mu\nu}). \tag{2.28}$$

2.1.5 Self-Consistent Procedure

The following steps are common to all self-consistent field molecular orbital calculations:

(1) Calculate the integrals for **F**, **S**.

(2) Diagonalize **S**.

(3) Form the Fock matrix **F**.

(4) Form F' as in Eq. 2.27.

(5) Diagonalize F' for the MO eigenvalues ϵ.

(6) Back transform **V** to obtain the MO coefficients.

(7) Form the density matrix **P**.

(8) Check **P** for convergence. If **P** for the n^{th} cycle agrees with **P** for the previous cycle within a given tolerance, stop. If not, extrapolate a new **P** matrix and repeat from step (3) until a self-consistent field (SCF) (step 8) is satisfied.

2.2 History of Semiempirical Methods (SEM)

Prior to 1965 only qualitative π HMO methods existed. Originally Hückel Molecular Orbital (HMO) method was limited to the π system. Later it was extended to the σ framework, this gave rise to the extended Hückel method (EHMO). With the exception of these two methods, *ab initio* methods had an automatic claim to respectability since they were nominally fundamental and gave (in most cases) accurate predictions. It was clear from the beginning that ab initio methods would be impractical for the study of large molecular systems.

From the form of the HFR equations derived above (refer. Eq. 2.25), the calculation of several integrals are required with an assumed set of basis functions. In its non-empirical form the HFR method is conceptually simpler but it becomes impractical for the study of large polyatomic systems. Attempts were made to use empirically determined data to approximate the complicated integrals (refer. Eq. 2.23) used in the *ab initio* theory. All of the difficult three- and four-centre integrals were ignored, and one- and two-centre terms were approximated using a mixture of functions based on atomic spectra and on formal theory. (Refer Appendix A for the nomenclature). Procedures of this type, which had both experimental and theoretical components, are called semiempirical methods (SEM). Usually the derivation of semiempirical equation

involves two steps. The first step involves additional approximations to the HFR equation and the second step involves the calculation of non-empirical integrals (integrals which are evaluated numerically using basis set functions, typically done for valence electrons only in the semiempirical approach).

2.2.1 All-Valence Electron (AVE) Approximation

In SEM the molecular electrons comprise two subsets: subset A which consists of the inner shell electrons of all atoms in the molecule and subset B which consists of the atomic valence shell electrons (we assume that these subsets are separable). Thus the total molecular wave function can be written as

$$\Psi = X[\Psi_A \Psi_B] \tag{2.29}$$

where X is an antisymmetrization operator. The separability of wave functions corresponding to the subsets A and B is obtained when the so-called strong-orthogonality condition

$$\int \Psi_A^*(\vec{r}_1, \vec{r}_2, ...)\Psi_B(\vec{r}_1', \vec{r}_2' ...) = 0 \tag{2.30}$$

is fulfilled. For the above equation if subset A comprises of σ-type electrons and subset B comprises of π-type electrons, Eq. 2.30 is automatically satisfied on the symmetry

grounds. With this approximation for all electrons of a given system one can derive variational equation analogous to HF equations (refer Eq. 2.16) assuming the separability of subsets A and B.

Experiments indicate that inner shell electrons are relatively inert in typical chemical processes. Moreover, Ψ_A should not depend on the state of valence shell electrons. Thus inner shell electrons represent only a source of electrostatic potential and simply screen the nuclear charges. These electrons may be effectively eliminated by substituting the atomic core charges Z_k' for the corresponding nuclear charges Z_k. Then the one electron operator $h^N(1)$, defined previously can be replaced by the core Hamiltonian h^c

$$h^c(1) = \frac{1}{2}\nabla_i - \sum_{k=1}^{N} \frac{Z_k'}{r_{1k}} = \frac{1}{2}\nabla_1 - \sum_{k=1}^{N} V_k(1). \tag{2.31}$$

According to Eq. 2.31 the core Hamiltonian $h^c(1)$ represents the total energy operator for an electron moving in the field of N atomic cores with charges Z_k'. The elimination of direct reference to inner shell electrons forms the basis of the so-called all-valence electron (AVE) approximation.

2.2.2 Neglect of Diatomic Differential Overlap (NDDO) Approximation

Moreover, there are additional approximations involved in the HFR equations and they are classified according to the degree and range of assumptions. Historically, the first in

the series of zero differential overlap (ZDO) method was the simple π electron method due to Hückel [62] in 1931. In the early 1950's the Pariser-Parr-Pople (PPP) model [63], a true SCF model was developed. In 1965, Pople and his co-workers introduced a series of ZDO approximations that generalized the π--electron PPP scheme to all-valence electrons [64].

To start with, in neglect of diatomic differential overlap (NDDO) scheme the differential overlap of atomic orbitals on different atoms is neglected in both overlap and two electron integrals, leading to the following conditions

$$S_{\mu_A\nu_B} = \delta_{\mu_A\nu_B} \tag{2.32}$$

where μ, ν refers to individual orbitals and A, B C and D refers to atomic centres

$$(\mu_A\nu_B|\lambda_C\sigma_D) = (\mu_A\nu_A|\lambda_C\sigma_C)\delta_{AB}\delta_{CD}. \tag{2.33}$$

Due to this approximation the matrix element $\mathbf{F}$ will not contain three-, four-centre two electron integrals entering via the element $G_{\mu\nu}$ in Eq. 2.23. The latter element will have $G_{\mu_A\nu_B}$ with $A = B$ becoming $G_{\mu_A\nu_A}$ and similarly $G_{\mu_C\nu_D}$ with $C = D$ becoming $G_{\mu_C\nu_c}$ thus involving only one- and two-centre terms. Thus, the matrix elements of

HFR operator in the NDDO approximation are given by

$$\begin{aligned} F_{\mu_A\nu_A} &= H^c_{\mu_A\nu_A} + \sum_{\lambda_A\sigma_A} P_{\lambda_A\sigma_A}[(\mu_A\nu_A|\lambda_A\sigma_A) - \frac{1}{2}(\mu_A\lambda_A|\mu_A\sigma_A) \\ &\quad + \sum_{B\neq A}\sum \lambda_B\sigma_B P_{\lambda_B\sigma_B}(\mu_A\nu_A|\lambda_B\sigma_B). \\ F_{\mu_A\nu_B} &= H^c_{\mu_A\nu_B} - \frac{1}{2}\sum_{\lambda_A\sigma_B} P_{\lambda_A\sigma_B}(\mu_A\lambda_A|\nu_A\sigma_B) \text{ for } A \neq B. \end{aligned} \tag{2.34}$$

The introduction of NDDO approximations to the matrix elements of core operator is an another problem. Let us rewrite the core Hamiltonian in Eq. 2.31 as

$$\hat{h}^c(1) = \frac{-1}{2}\nabla_1 - V_A(1) - \sum_{C\neq A} V_C(1) \tag{2.35}$$

and then

$$H^c_{\mu_A\nu_A} = U_{\mu_A\nu_A} - \sum_{C\neq A}(\mu_A|V_C|\nu_A) \tag{2.36}$$

where the one-centre one electron integral is defined as

$$U_{\mu_A\nu_A} = (\mu_A|\frac{-1}{2}\nabla - V_A|\nu_A). \tag{2.37}$$

2.2.3 Choice of Empirical Parameters in SEM

The formal reduction of HFR equations for non-empirical schemes must be followed by replacement of some non-empirical quantities by appropriate parameters.

The introduction of numerical parameters into semiempirical schemes is advantageous, providing these parameters are of sufficient generality. Such parameterization both compensates for the intrinsic inaccuracies and errors of the simplified scheme and reduces the computational effort by replacing certain types of integrals. We can distinguish two different types of quantities appearing in the equations. (i) atomic or molecular integrals calculated theoretically from known atomic orbitals. (ii) empirical parameters whose values are fixed by direct reference to experimental data. Each specific semiempirical realization of the approximate HFR method can be completely characterized as follows:

(A) The form of the assumed AO basis.

(B) The determination of the one-centre one electron integral parameters $U_{\mu_A\mu_A}$.

(C) The determination of one-centre two electron integrals.

(D) The calculation or approximation of two electron Coulomb integrals.

(E) The calculation or approximation of resonance integrals $\beta_{\mu_A\nu_B}$ for two-centre core integrals.

(F) The calculation or approximation of the core-core repulsion energy C_{AB}.

2.2.4 MNDO, AM1 Schemes

The first practical NDDO method was introduced by Dewar and Thiel in 1977 [48] called MNDO. This method is superior over other semiempirical schemes because this takes into account the lone pair-lone pair interactions (i.e. interactions between two pairs of unshared electrons) and parameterization of integrals is performed from experimental molecular geometries, heats of formation, dipole moments and ionization potentials.

The Fock matrix in MNDO has the form of Eq. 2.34. The orbital exponents, core integrals are regarded as empirical parameters and to be determined by fitting procedures. The core-core repulsion energy term was made as function of the electron-electron repulsion integral. The atomic parameters $U_{\mu_A\mu_A}$ are derived from atomic spectral data using transition energies between different atomic configurations, ionization potentials and electron affinities using the formulae of Oleari et al., [65].

MNDO is superior than other schemes but it is poor in predicting the hydrogen bond [48]. Shortcomings in the MNDO model has led to reexamination of the model and thus AM1 [66] scheme was developed. In the AM1 approximation each atom was assigned a number of spherical gaussians which were intended to mimic accurately the repulsions at van der Waals distances. Recent development in the SEM is the Parametric Model 3 (PM3) scheme by [67]. This scheme is still being tested, thus our calculations were

performed with MNDO and AM1 schemes.

In 1983 the first MOPAC program [68] was written and contained MNDO models. In 1985 AM1 code was implemented and present model contains MNDO, AM1 and PM3. The accuracy of these three schemes in reproducing experiments has been examined in considerable detail [48, 50, 68]. The average errors in predicting heats of formation, IP, EA, dipole moments etc. are discussed in details in [69].

The more useful quantity is the standard enthalpy of formation or simply heat of formation H_f of a substance. It refers to the amount of heat absorbed in a reaction that produces one mole of a compound in its standard state (i.e. in the gas phase, at 298 K), from elements in their standard states. For large molecules or polymers H_f is determined from the energies required to ionize the valence electrons of the atoms involved (calculated using semiempirical parameters), $E_{isol}(A)$, and the heats of atomization, $E_{atom}(A)$, which are then added to the electronic and the nuclear energies [70, 60]. This yields the following equation

$$H_f = E_{el} + E_{nuc} + \sum_A E_{isol}(A) + \sum_A E_{atom}(A). \tag{2.38}$$

In the above equation, the sum of the first and second terms constitutes the total energy of the large molecule or polymer which can be obtained from a self-consistent electronic calculation (refer Eq. 2.4). The remaining two terms relate the energies of

the isolated atoms, i.e their ionization potential energies and average bonding energies to the total energy of the molecule or polymer.

At the present time, SEM are evolving with increased accuracy, and the study of ever larger systems is their target (refer chapter 3). The data for the parameterization have often been from experiments. Increasingly, parameters for semiempirical methods are also derived using *ab initio* results (e.g. PM3). Also semiempirical Hamiltonians have always been the testing ground for new theories, and they are used increasingly to generate the input data (geometries and trial MO coefficients) for high level calculations. Moreover, it can be seen from our calculations, that SEM offer a good qualitative description of the problem, and even a quantitative one in some cases before the more expensive calculations are performed.

Chapter 3

Theory of Electronic Structure of Solids: Solid-State vs Molecular Approach

In Chapter 2, the Hartree-Fock theory has been summarized. HF approximation can be employed in quantum mechanical calculations for atoms, molecules or solids. The actual implementation of the HF theory depends largely on the system studied. In this thesis, we study extended systems such as polymers. Polymers are long chains of covalently bonded atoms. Since synthetic polymers are formed from repeating units, there are two types of approaches that can be used to study their electronic properties: (1) pseudo one-dimensional solid-state approach that employs the translational invariance; (2) molecular approach that applies molecular orbital calculations to oligomers that are large enough to accurately simulate bulk properties of the polymers. Both methods should lead to the similar results and conclusions. Yet another way is to retain certain features of (1) and (2) and thus form the basis for the cluster solid-state approach. We will summarize the main, fundamental concepts used in solid-state physics in section 3.1. In section 3.2 we will make a connection between solid-state concepts and the molecular orbital picture. In section 3.3, a hybrid solid-state cluster method will be

discussed. Finally, in section 3.4 technical details of the hybrid method as implemented in MOPAC93 are briefly discussed.

3.1 Solid-State/Band Theory

The study of electronic structures of solids is really the study of the energy bands and the distributions of electrons in real and in momentum space. The fundamental theorem underlying the formalism of solid-state theory for periodic crystals is the **Bloch's Theorem** (Bloch, 1928) [71].

3.1.1 Lattice Vectors

The essential aspect of a periodic lattice is its regular arrangement of atoms. A crystal lattice is defined mathematically by specifying three noncoplanar vectors $\vec{a}_1$, $\vec{a}_2$ and $\vec{a}_3$ (called *primitive vectors*). Starting from some arbitrary point, all points in the lattice can be generated from it by performing translations with vectors, $\vec{l}$, that are linear combinations of $\vec{a}_1$, $\vec{a}_2$, $\vec{a}_3$ (thus creating an infinite array of points)

$$\vec{l} = l_1\vec{a}_1 + l_2\vec{a}_2 + l_3\vec{a}_3 \tag{3.1}$$

where l_1, l_2, l_3 are integers. The volume of the parallelogram whose sides are the primitive vectors $\vec{a}_1$, $\vec{a}_2$, $\vec{a}_3$ is called the *fundamental or primitive unit cell* of the lattice. If

such a cell is translated by all the lattice vectors the infinite lattice, sometimes called *Bravais lattice*, is constructed.

3.1.2 Periodic Functions

In order to develop a physical model of a crystal structure with its underlying translational symmetry we often need to consider *periodic functions*, $f(\vec{r})$ such that

$$\begin{aligned} f(\vec{r}+\vec{l}) &= f(\vec{r}+l_1\vec{a}_1+l_2\vec{a}_2+l_3\vec{a}_3) \\ &= f(\vec{r}). \end{aligned} \tag{3.2}$$

In real space, $f(\vec{r})$ could be an electron number density $\rho(\vec{r})$ or an electronic potential $V(\vec{r})$ etc.

Beginning with a lattice in the three dimensional space, whose primitive vectors are $\vec{a}_1$, $\vec{a}_2$, $\vec{a}_3$, we can define set of wave vectors $\vec{b}_1$, $\vec{b}_2$, $\vec{b}_3$ such that the resultant plane waves will have the periodicity of a given Bravais lattice, thus generating the *reciprocal lattice* (in Fourier space). A general vector of reciprocal lattice has the following form

$$\vec{g} = g_1\vec{b}_1 + g_2\vec{b}_2 + g_3\vec{b}_3 \tag{3.3}$$

where g_1, g_2, g_3 are integers. Vectors $\vec{b}_1$, $\vec{b}_2$, $\vec{b}_3$ are called the *reciprocal lattice vectors.*

From an elementary vector analysis, we can verify that the direct and the reciprocal lattice vectors will satisfy following relations:

$$\vec{b}_j \cdot \vec{a}_i = 2\pi\delta_{ij} \tag{3.4}$$

where $\delta_{ij} = 1$ if i=j and $\delta_{ij} = 0$ if $i \neq j$ and

$$\vec{g} \cdot \vec{l} = (g_1\vec{b}_1 + g_2\vec{b}_2 + g_3\vec{b}_3) \cdot (l_1\vec{a}_1 + l_2\vec{a}_2 + l_3\vec{a}_3) = 2\pi \times \text{integer} \tag{3.5}$$

and

$$e^{i\vec{g}\cdot\vec{l}} = 1. \tag{3.6}$$

3.1.3 Bloch's Theorem

Bloch's theorem describes the general form of wave function of one electron Hamiltonian for periodic systems such as single crystals or stereo-regular polymers. Independent electrons, each of which obeys a one electron Schrödinger equation with a periodic potential, are known as *Bloch electrons* (in contrast to free electrons). The periodicity of the lattice as expressed by the periodic potential, $V(\vec{r}) = V(\vec{r} + \vec{l})$, requires that electronic properties such as the electronic charge density are also periodic. The periodicity of the electronic charge density can be used to obtain a general form of the

Bloch's wave function.

In quantum mechanics we can define a translational operator $\tau(\vec{l})$ that has the the following property

$$\tau(\vec{l})\psi(\vec{r}) = \psi(\vec{r}+\vec{l}) = \lambda(\vec{l})\psi(\vec{r}) \tag{3.7}$$

where $\lambda(\vec{l})$ is the eigenvalue of $\tau(\vec{l})$ [1]. Since the electronic charge density $\rho(\vec{r})$ must be periodic we must have

$$\rho(\vec{r}) = |\psi(\vec{r})|^2 = \rho(\vec{r}+\vec{l}) = |\psi(\vec{r}+\vec{l})|^2 \tag{3.8}$$

which requires that

$$|\lambda(\vec{l})|^2 = 1. \tag{3.9}$$

The condition in Eq. 3.9 can be satisfied if

$$\lambda(\vec{l}) = e^{i\vec{k}\cdot\vec{l}}. \tag{3.10}$$

The vector $\vec{k}$ characterizes a particular eigenfunction, and determines the eigenvalue

[1] Detailed proof of Bloch's theorem can be seen elsewhere [5].

for every translation $\vec{l}$ in the Bravais lattice. That is, substituting Eq. 3.10 into Eq. 3.7 the following phase relation between the solid-state orbitals can be obtained:

$$\psi(\vec{k}, \vec{r} + \vec{l}) = e^{i\vec{k}\cdot\vec{l}}\psi(\vec{k}, \vec{r}) \tag{3.11}$$

The above equation is one type of statement of Bloch's theorem. An alternative (but equivalent) form of Bloch's theorem states that the Bloch function $\psi(\vec{k}, \vec{r})$ in Eq. 3.11 can be written as a product of periodic function, $u(\vec{k}, \vec{r})$ such that $u(\vec{k}, \vec{r}) = u(\vec{k}, \vec{r} + l)$ and a plane wave $e^{i\vec{k}\cdot\vec{r}}$ or

$$\psi(\vec{k}, \vec{r}) = e^{i\vec{k}\cdot\vec{r}}u(\vec{k}, \vec{r}) \tag{3.12}$$

or more generally as

$$\psi_n(\vec{k}, \vec{r}) = e^{i\vec{k}\cdot\vec{r}}u_n(\vec{k}, \vec{r}) \tag{3.13}$$

where the index n will be discussed in the next section.

3.1.4 Periodic Boundary Condition

The wave vector $\vec{k}$ is a quantum number characterizing the electron wave function. In principle, we could specify the allowed values of $\vec{k}$ by imposing some boundary condition on the lattice potential. However, most solids are large in comparison to atomic dimensions (a solid sample of 1 cm^3 contains $\approx 10^{23}$ atoms), and surface conditions are quite diverse. Thus, in order to simplify the solid-state formalism, the periodic boundary conditions [5] are invoked. The periodic boundary implies that the crystal repeats itself in all respects after translations and surface effects are discarded. It can be shown that the application of periodic boundary conditions means that the general form for allowed Bloch wave vectors is

$$\vec{k} = \sum_{i=1}^{3} \frac{m_i}{N_i} \vec{b}_i \tag{3.14}$$

where m_i are integers and N_i is of order $N^{1/3}$ with N being the total number of primitive unit cells in the crystal.

Furthermore we note that if the eigenfunction $\psi(\vec{k}, \vec{r})$ has a wave vector $\vec{k}$ associated with it such that

$$\vec{k}' = \vec{k} + \vec{g} \tag{3.15}$$

where $\vec{g}$ is some reciprocal lattice vector then $\psi(\vec{k},\vec{r})$ and $\psi(\vec{k}',\vec{r})$ are said to be equivalent since $\vec{k}'$ and $\vec{k}$ are equivalent. This is clearly true when one notes that the phase factor in Bloch's theorem (see Eq. 3.11) obeys the following

$$e^{i\vec{k}'\cdot\vec{l}} = e^{i\vec{k}\cdot\vec{l}} \times e^{i\vec{g}\cdot\vec{l}} = e^{i\vec{k}\cdot\vec{l}} \tag{3.16}$$

and $\psi(\vec{k}',\vec{r}) = \psi(\vec{k}+\vec{g},\vec{r}) = \psi(\vec{k},\vec{r})$. Consequently, the wave functions $\psi(\vec{k},\vec{r})$ and $\psi(\vec{k}',\vec{r})$ have the same eigenvalue λ for all lattice translations. The solution of Schrödinger equation (with $\vec{r}$ and $\vec{k}$ being restricted to a single primitive cell of the crystal) results in an infinite spectrum of eigenvalues for a wave vector $\vec{k}$. These different solutions are labeled by an index n. Thus, the eigenvalues of the states with wave vector $\vec{k}$ are denoted by $\epsilon_n(\vec{k})$ or

$$\hat{H}\psi_n(\vec{k},\vec{r}) = \epsilon_n(\vec{k})\psi_n(\vec{k},\vec{r}) \tag{3.17}$$

where $\hat{H}$ is the Hamiltonian. The function $\epsilon_n(\vec{k})$ is referred to as an energy band and $\psi_n(\vec{k},\vec{r})$ is called a *Bloch function*. The function $\epsilon_n(\vec{k})$ is a continuous and differentiable function of $\vec{k}$.

Table 3.2: Molecular vs solid-state terminology

Molecules	Solid-State
Hückel LCAO-MO method	Tight Binding method
Molecular Orbital	Crystal Orbital
Highest Occupied Molecular Orbital (HOMO)	Valence Band (VB)
Lowest Unoccupied Molecular Orbital (LUMO)	Conduction Band (CB)
HOMO-LUMO Energy Difference	Energy Gap or Band Gap (E_g)
Jahn-Teller Distortion	Peierls Instability

3.2 Qualitative Aspects of Band Theory

Thus far the fundamentals of closed shell HF molecular orbital and solid-state theories were briefly described in the previous chapter and above sections. Polymers can be treated as closed shell molecular systems as well as solid-state (pseudo one-dimensional) infinite systems. In order to develop a qualitative picture of the band energies for polymers we apply the molecular orbital methodologies to very large molecular systems and discuss how the solid-state concepts arise from this extrapolation. It is illustrative to do this using the Hückel Molecular-Orbital (HMO) approximation [72, 73] [2]. Approximate analogs between molecular and solid-state terminologies are listed in Table. 3.2

[2]The HMO method is a simple and an useful tool for explaining the stabilities and physical properties of organic π systems. Full discussion of HMO method can be seen elsewhere [73, 74, 8]

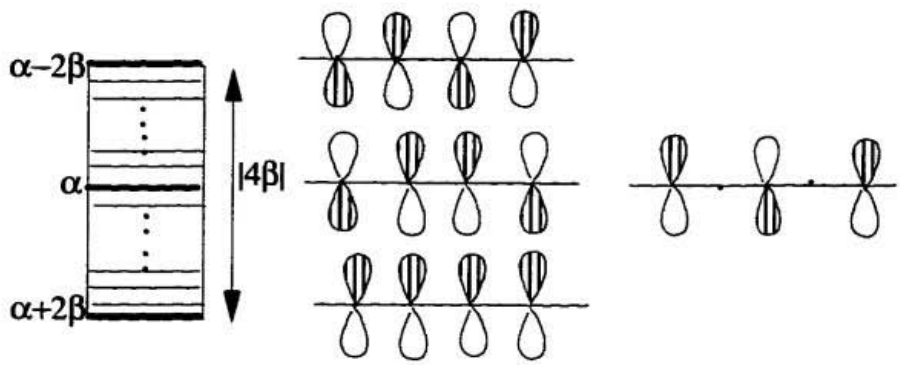

Figure 3.5: Electronic levels spreading into a band (as for example in Hückel calculation).

3.2.1 Energy Bands

Simple Hückel theory [73] cites an analytical expression for the energy of orbitals of linear polyenes whose j^{th} level for an N atom chain is given by

$$\epsilon_j = \alpha + 2\beta \cos \frac{j\pi}{N+1}. \tag{3.18}$$

When N is very large, the lowest level will lie at $\epsilon_1 = \alpha + 2\beta$ where there are bonding interactions between all adjacent atom pairs and the highest level will be at $\epsilon_N = \alpha - 2\beta$ and it contains antibonding interactions between all adjacent atom pairs (see Fig. 3.5). Between them lies a continuum of orbital energy levels usually referred to as an energy band with an energy spread of $|(\alpha - 2\beta) - (\alpha + 2\beta)| = 4\beta$. In the middle of this stack of levels one of ϵ_j's satisfies the equality $\epsilon_{1<j<(N+1)} = \alpha$. α level corresponds to a

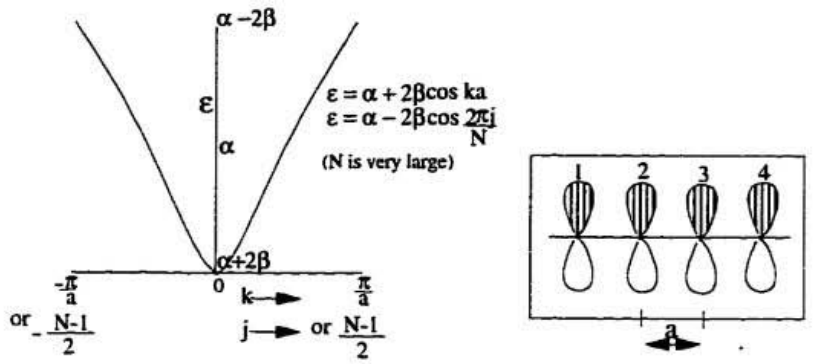

Figure 3.6: One π orbital per unit cell in one-dimensional polymer.

number of nonbonding molecular orbitals (see for example Fig. 3.5).

If the polymer is treated as a very large molecule then within the molecular orbital picture this molecule would be represented by a very large number of orbital energy levels. How can we handle this "infinite" collection of orbitals? The answer is we can make use of the solid-state concepts such as periodic boundary condition and primitive unit cell. In order to illustrate how these concepts are applied to polymers we discuss two cases: (1) one-dimensional chain with monoatomic unit cell and (2) one-dimensional chain with diatomic unit cell.

Case 1

As shown in Fig. 3.6 assume that the atoms in a very long one-dimensional system can be described by a single orbital per atom and the system behaves as if the atoms

were embedded in a very big ring (to satisfy the periodic boundary condition). Given the above approximations we can assume that the system correspond to an analogous macroscopic "bulk" system. Again from HMO analogy for cyclic systems the energy of the j^{th} level can be given by

$$\epsilon_j = \alpha + 2\beta \cos \frac{2\pi j}{N} \tag{3.19}$$

where j=0, ± 1, ± 2, ... Since N is large we can rewrite the Eq. 3.19 using the variable $k = \frac{2\pi j}{Na}$ as follows

$$\epsilon(k) = \alpha + 2\beta \cos ka \tag{3.20}$$

The value of k ranges between 0 and $\pm\frac{\pi}{a}$ or equivalently the value of j ranges between 0 and $\pm\frac{(N-1)}{2}$ (similarly to the case for finite system). One important difference between finite and infinite cases, of course, is that the use of k allows us to treat energy as function of a continuous variable whereas in the finite system with j increasing in discrete steps the energy is also a discrete function. In both finite and infinite cases, we note that ϵ_j (for the finite system) with $|j| > \frac{(N-1)}{2}$ and $\epsilon(k)$ with $|k| > \frac{\pi}{a}$ (for the infinite system) lead to redundant information. In the solid, the region of k between $\pm\frac{\pi}{a}$ is referred to as the first Brillouin Zone (BZ). The points $k = \pm\frac{\pi}{a}$ are called the

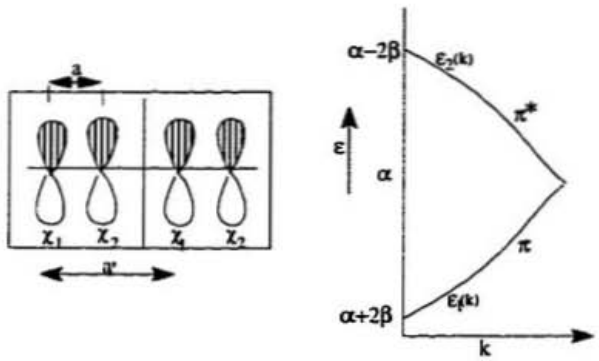

Figure 3.7: Two π orbitals per unit cell in one-dimensional polymer.

zone edges and k=0 is called the zone center. Since the Fig. 3.6 has a mirror symmetry about k=0 it will be sufficient just to use one-half of the first BZ (we choose the right half in our discussion). As explained before, the index k is called the wave vector and the variation of energy as a function of k is called the dispersion of the band.

Case 2

Consider a case as shown in Fig. 3.7 where the unit cell contains two atoms (thus, we have a lattice with a basis) each with one electron represented by a single molecular orbital and the lattice constant is $a' = 2a$; how does the qualitative picture described in the Case 1 change? First we note that the BZ will range from $\frac{-\pi}{2a}$ to $\frac{\pi}{2a}$, as shown in Fig. 3.7. Consequently, the energy spectra will differ from those given in case 1. In the Hückel approximation all the non-nearest neighboring interactions are neglected.

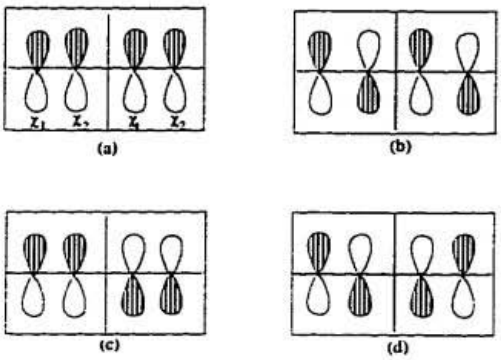

Figure 3.8: Inter-cell and intra-cell interactions in regular one-dimensional polymer chain. Unit cell possesses two π orbitals.

Solving the secular determinant in this case will result in the eigenvalues given by

$$\epsilon(k) = \alpha \pm 2\beta \cos \frac{ka'}{2}. \tag{3.21}$$

The π orbitals that correspond to the lowest energy point in the π band will combine as shown in Fig. 3.8(a) thus result in intra-cell and inter-cell bonding. At the same time π^* orbitals that correspond to the highest energy point in the π^* band will combine as shown in Fig. 3.8(b) thus contribute to antibonding between cells and within cells. At $k = \frac{\pi}{a'}$ the combination of π orbitals as shown in Fig. 3.8(c) results in intra-cell bonding but inter-cell antibonding. Similarly in Fig. 3.8(d) the π^* combination results in intra-cell antibonding but inter-cell bonding. Clearly molecular orbital arrangements corresponding to Fig. 3.8(c) and (d) have the same energy (we have a degeneracy at

this point) and the top of the π band and bottom of the π^* band touch at this point. And since we have an even number of electrons (in contrast to the case 1), each state in the π band is filled with two electrons. Thus in the ground state the π band is full and the π^* is empty. The material is still metallic due to the presence of the degeneracy at the BZ edges (see Fig. 3.7).

Next we discuss the general form of single electron wave functions for the cyclic chain consisting of N unit cells in the limit of N being very large. As described in Eq. 2.8 chapter 2, we can let χ's be the basis functions which form the basis set for the Bloch single electron wave functions. That is the Bloch function, $\psi(k,\vec{r})$, shown in Eq. 3.13 can be expanded in terms of single atomic orbitals, $\chi_\mu(r-d_p-l_\nu)$ (LCAO), (which are centered on the p$^{\text{th}}$ atom in the ν^{th} unit cell) as follows:

$$\psi_j = \sum_{\nu=1}^{N}\sum_{\mu=1}^{K} c_{\nu j} b_{j\mu}\chi_\mu(r-d_p-l_\nu) = \frac{1}{\sqrt{N}}\sum_{\nu=1}^{N}\sum_{\mu=1}^{K}[e^{\frac{2\pi ij(\nu-1)}{N}}]b_{j\mu}\chi_\mu(r-d_p-l_\nu) \quad (3.22)$$

Substitution of $k=\frac{2\pi j}{Na}$ leads to expression

$$\psi_k = \frac{1}{\sqrt{N}}\sum_{\nu=1}^{N}\sum_{\mu=1}^{K} b_{k\mu}[e^{ik(\nu-1)a}]\chi_\mu(r-d_p-l_\nu) \quad (3.23)$$

or

$$\psi_k = \frac{1}{\sqrt{N}} \sum_{\nu=1}^{N} \sum_{\mu=1}^{K} b_{k\mu} [e^{ikl_\nu}] \chi_\mu (r - d_p - l_\nu). \tag{3.24}$$

Thus ψ_k can be thought of as symmetry adapted linear combination of atomic orbitals that has been acted on by the translation operator. The wave functions in Eq. 3.24 are orthogonal to each other for different k values. Also at zone center ($k = 0$) the wave functions are in phase and at zone boundary ($k = \pi/a$) they are out of phase and in between the wave function is complex [50, 75, 5].

We shall now show that the *number of orbitals (corresponding to the allowed values of* k*) in a band inside the first BZ is equal to the number of unit cells in the crystal.* The requirement of a periodic boundary condition means that the only allowed values of k are

$$k = \frac{2\pi}{L} \tag{3.25}$$

where L is the length of the system. The number of states inside the first BZ, whose length is $\frac{2\pi}{a}$, is equal to

$$\frac{\frac{2\pi}{a}}{\frac{2\pi}{L}} = \frac{L}{a} = N \tag{3.26}$$

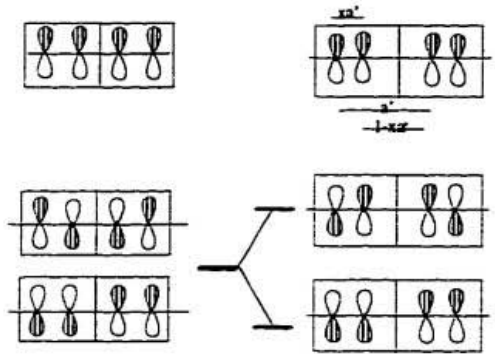

Figure 3.9: Inter-cell and intra-cell interaction in distorted one-dimensional polymer chain. Unit cell possesses two π orbitals.

where N is the number of unit cells. Thus each band has N states inside the first zone. Since each state can accommodate at most two electrons (which must be of opposite spins in accordance to Pauli exclusion principle) it follows that the maximum number of electrons that may occupy a single band is $2N$. With a given number of electrons in the solid the bands, doubly occupied, will be filled to a certain energy level ϵ_F, called the *Fermi level*. *Fermi level* corresponds to a specific value $k = k_F$. This result will be used in later chapters to establish the criterion for predicting whether a solid is going to behave as a metal or an insulator.

3.2.2 Distortions in One-Dimensional Systems

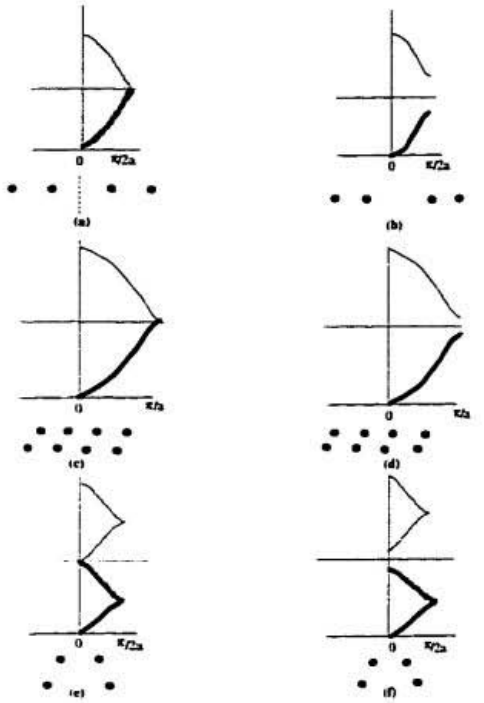

Figure 3.10: Metallic (on the left), semiconductor (on the right) behavior of linear, one-dimensional polymer chains. Bands near Fermi surface are shown in the reduced zone scheme. Solid dark line indicates the filled band. Dotted (horizontal) line indicates the Fermi surface.

Case 3

In the previous cases it has been shown that a regular linear chain with one or two electrons per lattice site is a conductor. Whereas, as we shall see, this is not so for the chain with unequal bond lengths (often referred as the alternating bond lengths). As explained in the introduction, lattice distortion are common in the quasi one-dimensional and linear systems. As shown in case 2 if the lattice with a basis has two atoms, the

bands are folded and BZ ranges from $\frac{-\pi}{2a}$ to $\frac{\pi}{2a}$. Since there are two orbitals per lattice site, the π band is full and Fermi surface crosses from the $\frac{-\pi}{2a}$ to $\frac{\pi}{2a}$ points (Refer. Fig. 3.10(a)). Due to the lattice instabilities (see Fig. 3.10(b)) the degeneracy at the BZ edges is lifted in the case of two atoms per unit cell. Also the filled π band is pushed down in energy due to intra-cell bonding and π^* band is pushed up in energy due to intra-cell antibonding. Thus the folded band is separated, that is, a forbidden region is formed between π and π^* bands. In the case of one atom per unit cell a band gap appears at the Fermi level. The formation of the band gap in either case signals the transition from a metallic to a semiconductor state for a linear chain.

Case 4

The polymeric material such as PA as shown in Fig. 3.10(c) with one π orbital per atom has a π band structure. In this case the primitive cell contains two atoms and the lattice constant is a, so that the BZ ranges from $\frac{-\pi}{a}$ to $\frac{\pi}{a}$. Since we have two electrons per primitive cell π band is full. Similarly to the case 2, there exists some degeneracy of the orbitals so that the bands stick at the zone edges (effectively doubling the size of the BZ). Hence the PA will be metallic if all bond lengths are equal in the polymer. Now consider the lattice distortion occurring in this system. The regular PA will exhibit bond alternation as shown in Fig. 3.10(d). In contrast to the previous case 2, here the lattice constant is not doubled but the glide plane is lost due to the

reconstruction. Note the primitive unit cell has still two atoms, hence two electrons per lattice site. Due to this reconstruction, the degeneracy of the Bloch orbitals for k points equal to $\frac{-\pi}{a}$ and $\frac{\pi}{a}$ is lifted and a gap opens at the zone edges.

The electronic structure of regular PT, PCY, PFv are essentially similar to that of PA. Owing to the extension of the unit cell from two to four or more carbon atoms, a folding of the bands takes place. The BZ extends from $\frac{-\pi}{2a}$ to $\frac{\pi}{2a}$ in the reduced zone scheme (refer Fig. 3.10(e) for doubly folded band). In order to understand this more complex problem it is easier if the bands are unfolded (i.e. consider the extended zone scheme). Then the two bands π and π^* will stick together at $\frac{-\pi}{a}$ and at $\frac{\pi}{a}$ due degeneracy of these Bloch orbitals. This extended zone is called Jones zone [76]. Moreover the electrons fully occupy the lower π band in this zone and upper π^* band is completely empty thus conduction can take place. Lattice distortion will cause the formation of alternate mesomeric forms as shown in Fig. 3.10(f). Due to this alternate structure, degeneracy in the middle of Jones zone is lifted and a gap is formed. Again in the reduced zone scheme. the bands are refolded so that the direct band gap appears at the center of the BZ [33, 77, 76]. Note the Bloch functions at the zone boundary are degenerate, (i.e. sticking at the zone edges) as a consequence of screw axis (rotation followed by translation operation) symmetry [76]. Hence although the regular (with equal bond lengths) chain behaves as conductor, the lattice distortion and the formation of stable mesomeric forms give rises to semiconducting polymers for practical purposes.

3.3 Solid-State Calculation in Semiempirical Models

As described in the previous chapter, the basic idea of molecular quantum chemical calculation is the usage of LCAO approximation. A direct application of LCAO approximation to an extended systems such as solids leads to a problem of solving a very large number of single electron, self-consistent equations for the nearly infinite number of atomic orbitals. One way of overcoming this problem is to use the full solid-state methodology (as described above). However, due to the low symmetry involved in cases such as polymeric solids a pure solid-state approach is also very cumbersome. Another way is to use the so called cluster or the large-molecule approach to simulate the bulk properties of solids. Cluster solid-state approach is a hybrid method that uses concepts from molecular as well as from solid-state theories. The large-molecule or cluster approach was first described in the early 1950's by Inui et. al [78]. During 1970's cluster calculations for studying vacancies and defects in semiconductor solids were carried on by Messmer et. al [79, 80] for HMO. The above approach faced difficulties due to the neglect of surface effects and the two electron interaction terms in the Hamiltonian. Then in late 1970's the above problems were rectified in the so called cluster model for solids (CMS) by appropriate semiempirical schemes that included the two electron interactions and some solids state aspects that allowed for the neglect of the surface effects (by making the cluster large enough so that it becomes a good approximation

for a solid). In this section, we give a very brief discussion of cluster approach as it is used to study solid-state properties and its implementation in MOPAC93.

Traditionally quantum mechanical, electronic structure calculations for polymers are performed in two ways. One involves the use of oligomers (short chain segments with end groups) and other is a solid-state type of approach with the appropriate boundary conditions. In order to simplify the calculation of polymers, CMS has been adapted in conjunction with MNDO Hamiltonian. In this approach, the cluster unit cell (CU) is taken as the multiple of the primitive unit cells in order to accurately represent the bulk properties of the polymer chain. If the translational vector or the size of CU is large enough, the nature of the bands in the BZ will not change significantly at the zone edges. Thus a sufficiently large cluster unit cell would allow the use of only one k point (obviously Γ point) to represent the entire BZ. Clearly, if the primitive unit cell is small, several k points may be needed in order to obtain a good representation of the band.

From the previous sections on qualitative aspects of band theory explained using HMO methods for cyclic polyenes we have obtained ϵ_j where j=1 gives the lowest and j=N gives the highest π eigenvalues. These limiting values are to be identified with the "solid-state" values at Γ and X point of the π band in the BZ. The following paragraphs explains how the eigenvalues are generated for a cluster of atoms that are used to produce the corresponding band structure.

Consider a one-dimensional cluster consisting of N primitive unit cells. The cluster basis set will be generated by $\sum_{j=1}^{N} \tau_j \chi$ where τ is the translational operator which can translate the basis set χ over j primitive unit cells along one translational axis. For the time being assume that the translational symmetry of such a one-dimensional system is the only symmetry that the system has. Because of N translational operations there will be N irreducible representations. Suppose that if we consider j^{th} representation in l^{th} translation then since the group is Abelian the character of the representation will be equal to $e^{\frac{ijl2\pi}{N}}$. The effect of time reversal is to replace i by -i in the characters of all the representations.

As a consequence of time induced degeneracy, any linear combination of eigenfunctions related by time reversal are also eigenfunctions of the Hamiltonian i.e. the time reversal operator T^{-1} commutes with the Hamiltonian. Then

$$T^{-1}|\chi_j >= |\chi'_j > \tag{3.27}$$

$$\psi_j = \alpha\chi_j + \beta\chi'_j$$

$$\psi'_j = \beta\chi_j - \alpha\chi'_j.$$

We can calculate the phase of a function χ^p_ν in one primitive unit cell from that in the

adjacent unit cell using Bloch's theorem

$$\theta_p|\chi_\lambda^p >= \theta_{p-1}|\chi_\lambda^p > e^{\frac{2\pi ij}{N}}. \tag{3.28}$$

Now because of mixing of the wave functions χ_j and $\chi_{j'}$ we have, in general,

$$\begin{aligned} \theta_p &= [\alpha e^{\frac{2\pi ij}{N}} + \beta e^{\frac{-2\pi ij}{N}}]\theta_{(p-1)} \\ \theta'_p &= [\beta e^{\frac{2\pi ij}{N}} - \alpha e^{\frac{-2\pi ij}{N}}]\theta'_{(p-1)}. \end{aligned} \tag{3.29}$$

However, cluster calculations yield only real numbers, α and β are constrained to those values which give rise to real phase factors. If ψ_j, $\psi_{j'}$ are real then, the eigenvectors calculated by any LCAO calculation on a cluster leads to two eigenvalue equations related to two points in the real space.

Then the back transformation of cluster eigenvector coefficients obtained from these two equations yield k-points that are generated from the relation

$$\begin{aligned} C_1 &= \alpha \\ C_2 &= \beta \\ C_3 &= \alpha\cos(\frac{2\pi j}{N}) + \beta\sin(\frac{2\pi j}{N}) \\ C_4 &= \beta\cos(\frac{2\pi j}{N}) - \gamma\sin(\frac{2\pi j}{N}) \end{aligned} \tag{3.30}$$

$$j = \frac{N}{2\pi}\cos^{-1}\left(\frac{C_1C_3 + C_2C_4}{C_1^2 + C_2^2}\right) \tag{3.31}$$

3.4 MOPAC93 – Software Description

MOPAC93 [50] software has many utilities. Among them MAKPOL is used for building Z-matrices, BZ is used for producing band structures upon introducing space group operations. DENSITY is used for plotting wave functions and calculating total electron density of the system. The part of MOPAC that performs HF molecular-orbital calculations is the part that is used in our investigation. As described in section 3.3 phase functions are introduced in MOPAC and cluster coefficients are created from this calculations.

3.4.1 Cluster Method in MOPAC93

Unlike more conventional methods, MOPAC93 does not normally uses the fundamental unit cell or samples the BZ in order to produce the electronic structure. Instead, it uses a large unit cell called "cluster" and applies the boundary conditions.

If a unit cell supplied by the user called central unit cell (CUC) is large enough (which can be represented in terms of translational vector), then a single point in *k-space*, the $\Gamma-$point is sufficient to specify the BZ. The secular determinant for this point is setup by adding together the Fock matrix for the central unit cell plus those for

the adjacent unit cells. The periodic boundary conditions are required to be satisfied. Diagonalization of the secular determinant yields the correct cluster coefficients and from the density matrix the Γ point is constructed. The contribution to the Fock matrix arising from the orbitals which are more than half the translational vector away are ignored.

The optimizations on polymeric cluster usually produces equilibrium geometries. These geometries refer to the optimum arrangement of nuclei corresponding to given electronic distribution. When the energy gradients vanish

$$-\frac{\partial H_f}{\partial r} = 0. \tag{3.32}$$

this means the geometry optimization is completed.

In our calculations, during the geometry optimization the gradients calculated are not zero since the Cartesian energy derivatives for an atom in a unit cell is sum of forces on that atom due to all of the atoms in that unit cell. The Cartesian derivatives do not include the terms from the surrounding unit cells. This is why, at the cell boundaries, energy is likely to have finite (larger) derivatives. By choosing large translational vectors this adverse behavior can be minimized [50]. Numerically the condition of vanishing energy gradients is satisfied to within a certain convergence criteria. A tight convergence criteria is setup by choosing a cutoff value of 10^{-11}. Typically in our

calculation we used Eigenvector Following, EF, optimization method [50].

3.4.2 MOPAC93 and Brillouin Zone Outputs

The output generated by MOPAC93 usually contains information needed to run the Brillouin Zone, BZ, calculation. The BZ utility provides the information needed for studying band structures of solids. MOPAC93 calculations generate the *cluster* Fock matrix from which the Fock matrix of the *fundamental unit cell* is produced. The cluster coefficients are then used to generate the eigenvalues in the k-space. Then the band structures are readily constructed by joining the points in the order in which they are generated. In general, the bands of different symmetries are allowed to cross. But by simply joining the k-points generated as stated above bands will not be allowed to cross.

The symmetrization of Fock matrices, done by means of modified cluster technique, is performed by the Brillouin Zone utility program [50]. For this BZ needs to know how the Fock matrix is organized, and MERS=(nx,ny,nz) keyword gives the number of unit cells in each direction. For a polymer, the BZ consists of a line, for a layered structure, a surface and for a solid, a three-dimensional shape. The Fock matrix representing the interaction of the fundamental unit cell with the other neighboring unit cells are stored in a large matrix. The cluster theory assumes that the interaction matrix relating two unit cells which are separated by more than half the distance of the translation vector is

vanishingly small. Although this Fock matrix does include the point group symmetries it lacks in the space group or non-primitive group symmetry operations such as screw axis or glide plane symmetries. The non-primitive or space group operations are supplied by the user and the Fock matrix is further symmetrized. Since the cluster Fock matrix generated by MOPAC93 will not exhibit the high symmetry of the associated (infinite) polymer the band structure generated using cluster method will be almost, but not quite, identical to the one generated by the fully symmetrized band structure calculation.

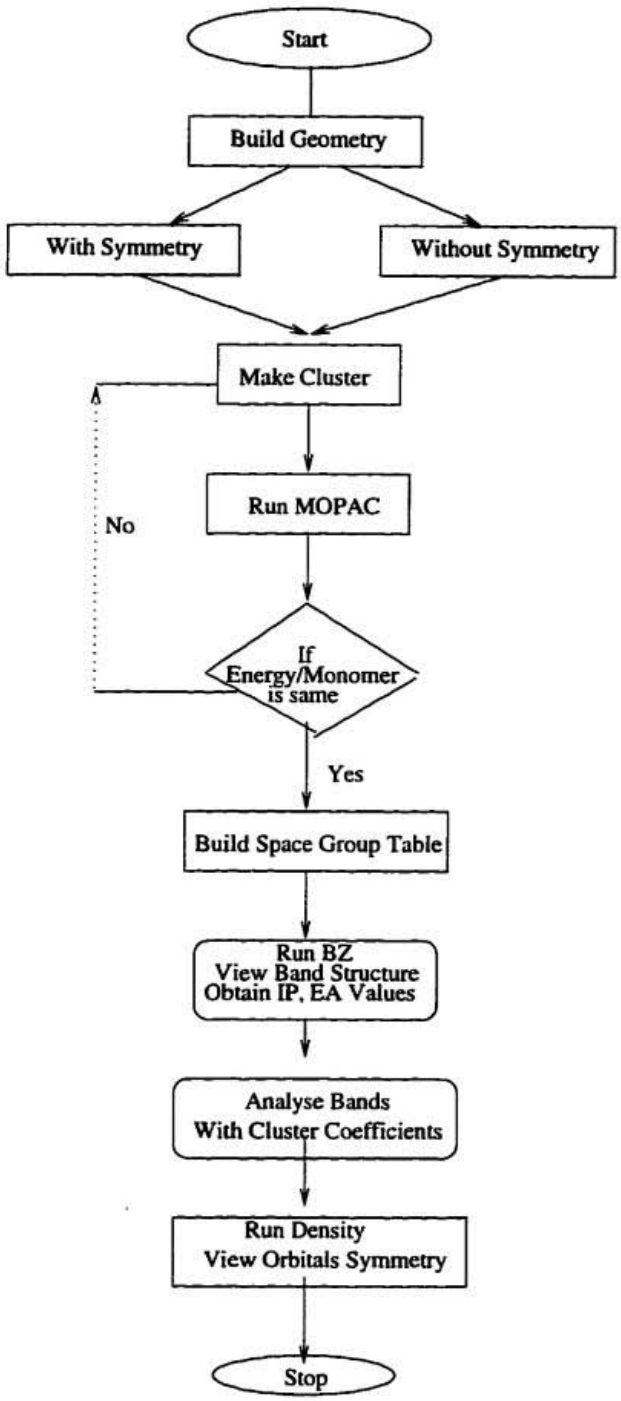

Figure 3.11: Sequence for investigating geometric and electronic properties of a polymer using MOPAC93 semiempirical model.

Chapter 4

Geometric Structure Investigation

Owing to their potential environmental stabilities conjugated polymers containing cyclic repeat units (phenyl, thiophene, furan, etc) have recently become major targets of studies in the field of CP's. The ground state of the CP's corresponds to the mesomeric conformation [81] that possesses the lowest energy. Some CP's such as polydiacetylene and *trans*-PA, pernigraniline (see Fig. 1.1 and 4.12) have degenerate ground states. In these cases two mesomeric forms can be present in a single chain with the accompanied formation of a soliton [82]. Most CP's, known today, have non-degenerate ground states. However, for a given ground state mesomeric conformation, most CP's can exist in a number of torsional isomers.

Many structural studies conducted in the solution have shown that free rotation around the inter-thiophene linkages is a prevailing factor determining the mean molecular conformation in oligothiophenes. In these systems the tendency to coplanarity can be hindered by intramolecular steric interactions such as those created by bulky groups. Typically monomers associated with the non-degenerate ground state can be in the true *anti* or *syn* or *anti-like* or *syn-like* orientations (see Fig. 4.13). For instance, the

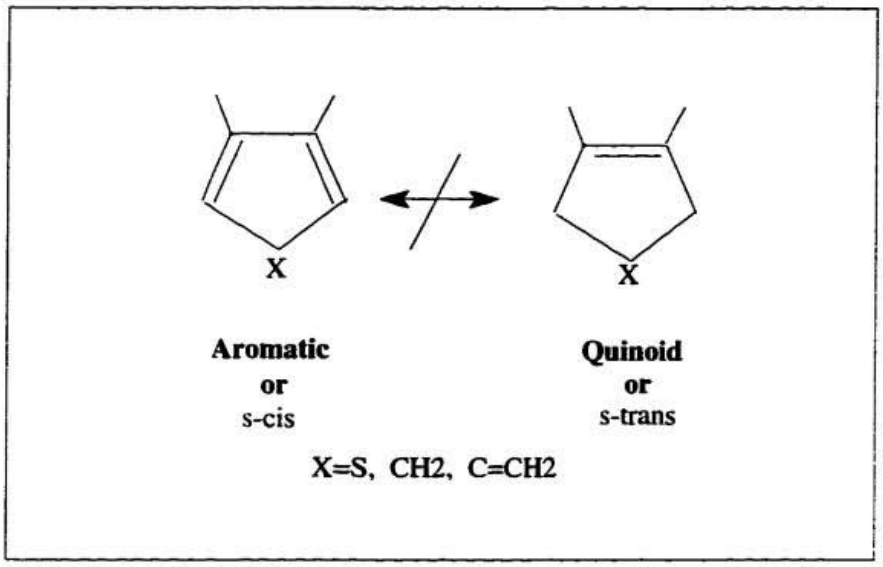

Figure 4.12: The non-degenerate ground state geometries of five membered ring systems.

structure of bithiophene, which may be envisaged as a simple model for PT, is well known in the gas phase [83] and in the crystal form [84] from X-ray diffraction results. In the gas phase, the two rings are nonplanar with a torsional angle of 146°, whereas a planar arrangement is found in the crystal with the two rings in the *anti* orientation. On the other hand ^{13}C-NMR results [24] for bithiophene in liquid crystal solvents indicated the existence of both the *anti* and *syn* orientation at the room temperature and predicted a rotational barrier of 5 ± 2 kcal/mole between them. For unsubstituted quarterthiophene (four monomers) there is no crystallographic data found as of yet. But studies on ^{13}C-CPMAS (cross polarization magic angle spinning) on even and odd oligothiophenes indicated that terthiophene (three monomers) possess high torsional

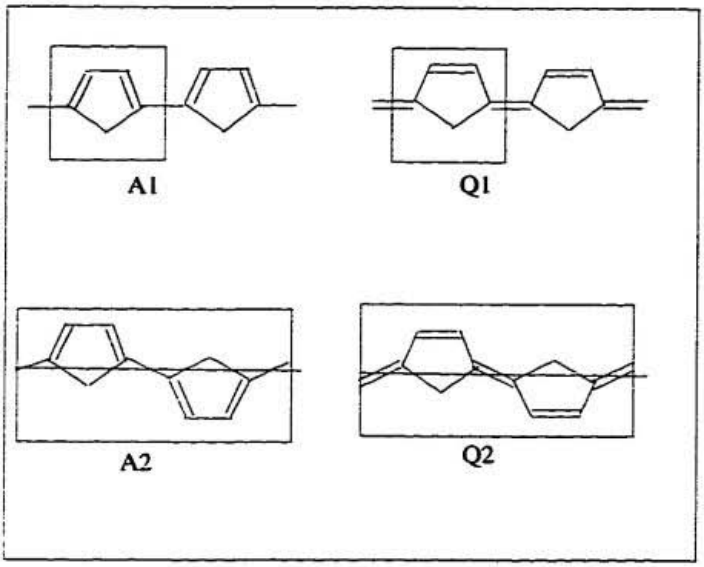

Figure 4.13: One monomer per repeat unit in *syn* orientation (A1, Q1) and two monomers per repeat unit in *anti* orientation (A2, Q2).

mobility [85]. For larger oligomers, as well as their substituted compounds, the crystal structure data show an *anti* conformation [86, 3, 28], whereas in the chloroform ^{13}C-NMR measurements show an *anti-like* conformation is found [87, 88, 89]. Recently substituted polythiophenes have been investigated using infrared, NMR spectroscopies [90]. The results again indicated the presence of twisted as well as planar conformations for the substituted polymers. The ability of polymers to exist in two or more torsional isomeric states results in the optical phenomena referred to as thermochrometry (color change). Thus far, for other polymers and their respective oligomers we have not found many crystallographic and/or theoretical results that would enable us to characterize

their conformations.

We can summarize the above discussion by noting that amorphous nature of the polymers prevents an accurate determination of their structure from say the X-ray diffraction patterns that require that polymers form crystals. For example, oligothiophenes are difficult to crystallize and only in recent years X-ray structure determinations have been reported for a number of oligothiophenes such as bi-[91], ter-[92] and sexithiophenes [86] [93]. These studies confirmed that single crystals of oligothiophenes prefer *planar*, *anti* orientations in the crystalline packing. Their geometries are aromatic, thus ensuring that the ground state is non-degenerate as expected for these systems.

The few theoretical calculations related to conformational studies of polythiophenes as modeled by bithiophenes and their derivatives, provide a description of the torsional potential energy surface for the different rotational isomers. The recent ab initio calculations [94] confirmed the existence of *syn-like* and *anti-like* conformations in bithiophene in agreement with experimental observations. Also single stranded polymer films examined under scanning probe microscopes in association with theoretical calculations using AM1 (MOPAC93) [95] indicated the existence of *syn-like* conformation in vacuum. Following this, our investigation of geometric structure of polymers was extended to include both the *syn-like* and *anti-like* conformations of polymers. The first step in this analysis involves the determination of the most stable mesomer and for each mesomer we, in turn, determine the lowest energy rotational isomer. In the

second stage, solid-state optimizations were performed with two types of unit cells for *syn* and *anti* orientations. Different unit cells were chosen since in accordance with the translational symmetry, the *syn* or *anti* ordering will result depending on the size of the unit cell. Thus the clusters are classified according to the following scheme: **Aromatic unit cell type one (A1)**, **Quinoid unit cell type one (Q1)**, **Aromatic unit cell type two (A2)** and **Quinoid unit cell type two (Q2)** (See Fig. 4.13). In agreement with experimental and theoretical calculations our results show that there are rotational defects in the polymeric systems when symmetry constraints are relaxed. The polymers in the A2 or Q2 orientations are coplanar and symmetrical with distortions of less than 1° arising from the monomers at the end. On the other hand, the investigation of the geometrical properties of polymers in A1 or Q1 conformation leads to the generation of pronounced rotational defects in polymers in order to relieve conformational strain due to the steric hindrances.

In this chapter initial geometries for PT are taken from the gas phase electron diffraction data on bithiophene [83]. For PCY the input geometry was chosen from the AM1 optimized values [46]. The input geometries for the remaining polymers are estimated from data obtained for PT and PCY. Heat of formation values are used for determining cluster size, comparative stability of mesomers and rotational isomers (the results are discussed in section 4.1). Geometries are fully optimized for clusters and the corresponding geometrical parameter values for tetramers are presented in section

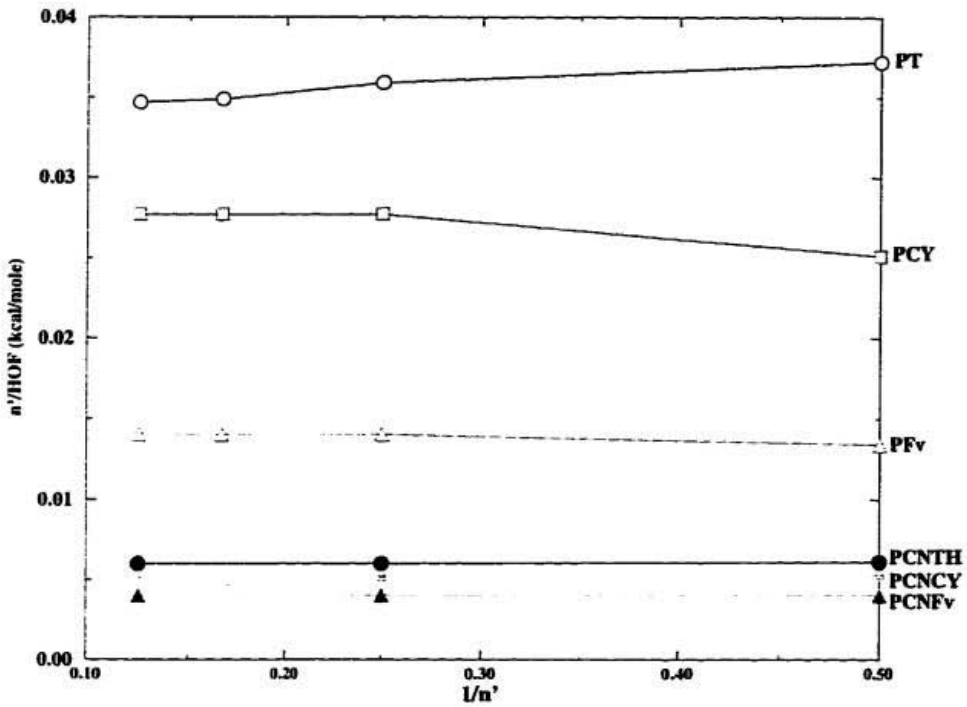

Figure 4.14: The inverse of the heat of formation per monomer ($\frac{n'}{H_f}$) plotted as a function of the inverse conjugation length ($\frac{1}{n'}$), n' is the conjugation length or the number of monomers.

4.2.

Table 4.3: Heat of formation H_f (in kcal/mole) calculated in the AM1 scheme for the polymers in A2 forms are given.

POLYMER	PT	PCY	PFv	PCNTH	PCNCY	PCNFv
Dimer	53.821	79.685	149.081	326.570	378.805	499.620
Tetramer	111.548	144.554	285.883	660.737	758.371	999.340
Hexamer	171.881	216.461	428.833	-	-	-
Octamer	230.700	288.330	571.359	1342.467	1525.408	2008.829

Table 4.4: Inverse of the heat of formation per monomer ($\frac{n'}{H_f}$) and inverse conjugation length ($\frac{1}{n'}$) (n' is the conjugation length or the number of monomers) are given. Values are calculated in the AM1 scheme for polymers in A2 form.

POLYMER	$\frac{1}{n'}$	PT	PCY	PFv	PCNTH	PCNCY	PCNFv
Dimer	0.5000	0.0372	0.0251	0.0134	0.0061	0.0053	0.0040
Tetramer	0.2500	0.0359	0.0277	0.0140	0.0060	0.0052	0.0040
Hexamer	0.1667	0.0349	0.0277	0.0140			
Octamer	0.1250	0.0347	0.0277	0.0140	0.0060	0.0052	0.0040

Table 4.5: AM1, MNDO heats of formation (H_f) (in kcal/mole) for polymeric clusters in A1, Q1, A2, Q2 forms.

MNDO	Dimer			Tetramer			
Polymer	A1	A2	Q2	A1	Q1	A2	Q2
PT	54.46	49.23	63.42	96.00	165.81	97.14	116.64
PCY	67.45	69.11	60.28	123.21	281.72	122.78	114.29
PFv	113.42	138.51	134.72	216.45	287.94	267.95	262.16
PCNTH	296.73	298.04	308.03	595.63	643.16	599.64	614.29
PCNCY	328.71	328.71	300.20	657.50	774.07	657.50	600.24
PCNFv	421.91	445.78	420.18	854.49	918.78	892.08	840.69
AM1	Dimer			Tetramer			
Polymer	A1	A2	Q2	A1	Q1	A2	Q2
PT	51.06	53.82	65.53	112.28	-	111.55	154.28
PCY	82.35	79.69	72.36	145.10	292.456	144.55	135.19
PFv	135.40	149.08	141.31	263.29	296.094	285.88	273.26
PCNTH	326.40	326.57	332.63	663.89	-	660.74	717.83
PCNCY	378.81	378.81	346.81	758.37	857.559	758.37	693.62
PCNFv	486.98	499.62	463.25	984.92	1074.365	999.34	926.98

- indicates the geometries for which converged results have not been obtained.

4.1 Heats of Formation – Cluster Size and Conformational Stability

As stated in the introduction, the values of heat of formation play a dual role in our calculations. Firstly, they are used to determine the optimum cluster size [96]. Little or no change in the value of the heat of formation per monomer (also called the average heat of formation) ΔH_f, indicates that the cluster is sufficiently large [96] to simulate bulk properties of polymers (see Fig. 4.14 and Tables 4.3 and 4.4). In our computations, cluster size was increased in steps of two monomers (N=2, 4, 6, 8) per unit cell. Very small changes (of the order of less than 1 kcal/mole) have been observed in the values for ΔH_f between the tetramers and octamers) for a selected sample of systems (see Tables 4.3 and 4.4). This fact and the large size of the repeat unit for some of the polymers meant that the full analysis of geometry optimizations were performed for tetramers only. Secondly, heats of formation, H_f, are also used to determine the relative stability of the mesomers (aromatic versus quinoid) and rotational isomers (*syn* versus *anti*) of the polymers. The two mesomeric forms were found by performing non-rigid energy scans with respect to the distances between the monomers in the dimer. That is, total energies were determined as a function of an inter-cell distances, ranging from 1.30 $\AA$ to 1.48 $\AA$, using AM1 scheme. Fig. 4.16 shows local minima located near inter-cell distances 1.34 $\AA$ and 1.45 $\AA$ (for most of the polymers) and there seems to be a large rotational barrier approximately $\approx$ 10 kcal/mole per unit cell for PT, PCY and

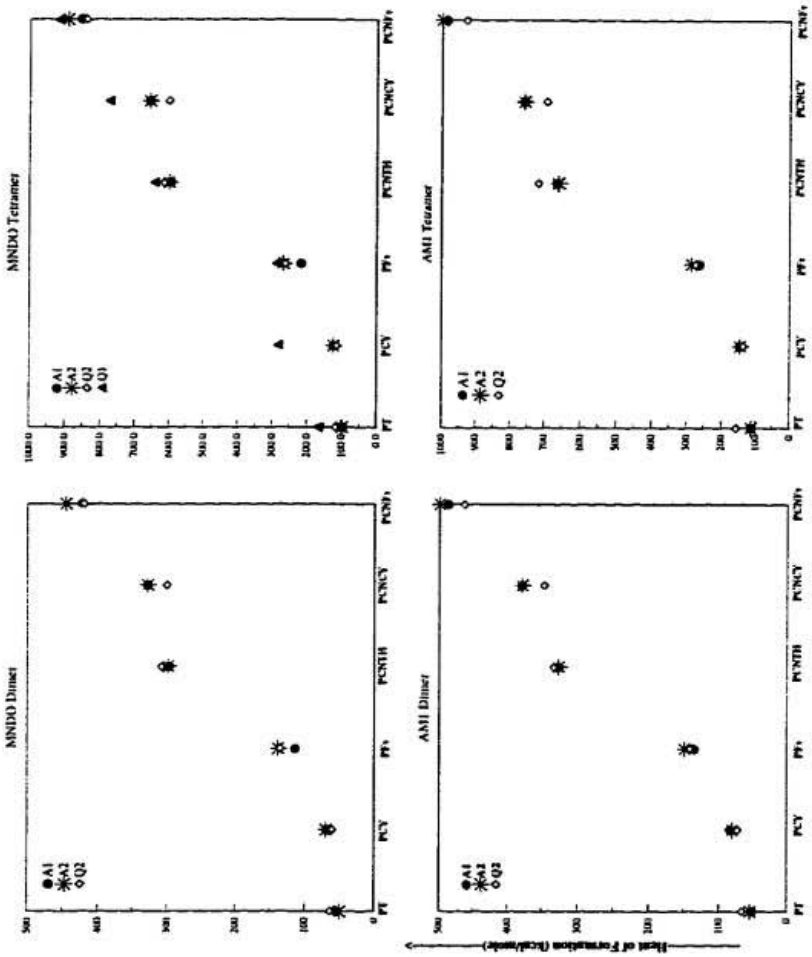

Figure 4.15: Stable mesomers of the polymers.

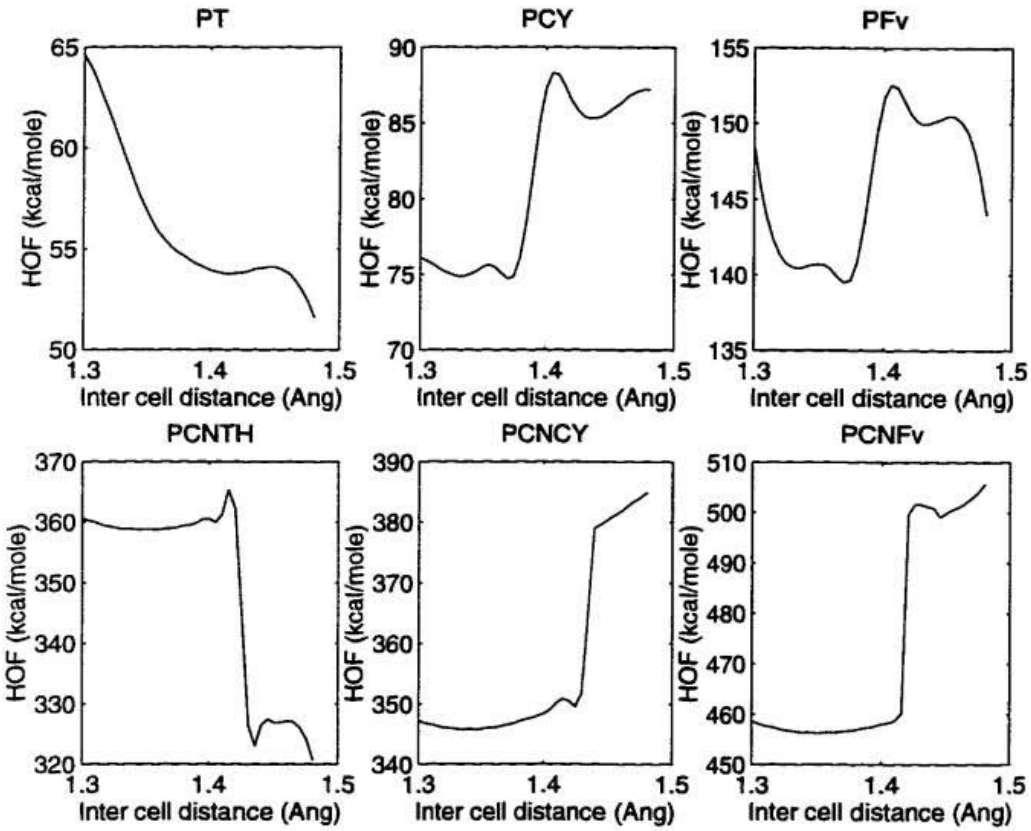

Figure 4.16: Scan of inter-cell distance in a dimer using AM1 scheme.

PFv and $\approx$ 40 kcal/mole per unit cell for PCNTH, PCNCY and PCNFv. The former minimum (at 1.34 $\AA$) corresponds to the *planar* quinoid or s-trans form (Q2) and the latter to the *planar* aromatic or s-cis (A2) form. Complete geometry optimization beginning with the two local minimum structures is then performed.

Predicting the most stable conformation for the mesomers in polymers considered in this work is a subject of many ongoing investigations in the field of CP's. The AM1, MNDO H_f values for A2 and Q2 forms are listed in the Table 4.5. For completeness and comparison, the dimer values are also given since our initial geometry optimizations were performed on dimers. However, it should be noted that tetramers produce the more accurate data and the following discussion (unless otherwise stated) will focus primarily on the results for tetramers. As expected from the previous works [83, 56, 37], PT(A2) is more stable than PT(Q2) by 19.5 kcal/mole in MNDO and by 42.7 kcal/mole in AM1 calculation. For comparison purposes we noted that for dimers PT(A2) is more stable by 14.2 kcal/mole (MNDO) (see Table 4.5, by 14.4 kcal/mole from solid-state calculation [37] and by 16.1 kcal/mole from molecular calculation [56] that used end groups instead of T_v. Also, PCNTH(A2) is more stable than PCNTH(Q2) by 14.6 kcal/mole in MNDO and by 57.1 kcal/mole in AM1 calculation. In contrast to PT and PCNTH, for PCY [46], PCNCY [46], PFv and PCNFv, the Q2 (corresponding to quinoid) forms are more stable. For PCY and PFv, the Q2 forms are more stable by approximately 10 kcal/mole in both the AM1 and MNDO calculations. For PCNCY

and PCNFv, the H_f for their two forms differ by more than 50 kcal/mole (see Table 4.5), again in both the AM1 and MNDO calculations.

Rotations around inter-cell bonds are also possible in CP's. That is, the varying of the corresponding inter-cell dihedral angle leads to the rotation of one monomer with respect to the another. Plots of total energy as a function of central dihedral angle in the dimer unit cells of PT, PCY, PFv, PCNTH, PCNCY and PCNFv mesomers showed that *anti-* and *syn-like* conformations are possible for these systems. That is, by increasing the dihedral angle and optimizing at each value of the angle we have found the A1 *(syn-like) conformations in addition to the A2 and Q2 (*anti-like) conformations for dimers. Polymers in the A1 orientation do not belong to the point group C_{2h} because of the coil like twisting of the polymer monomeric units.

A comparison of the heat of formation values for the A1 and A2 forms illustrates that some polymers are more stable in A1 conformation or are nearly degenerate with the A2 conformation (see Table 4.5 and Fig. 4.15). For dimers, the A1 conformation is more stable for PT (by $\sim$ 3 kcal/mole), PFv and PCNFv (both by $\sim$ 15 kcal/mole) and is degenerate with the A2 conformation for PCNTH and PCNCY for the AM1 approximation. The MNDO calculations agree with these findings with the exception of PT and PCY where they predict that A2 conformation is more stable for PT and A1 conformation is more stable for PCY. For the PCY this discrepancy is not very critical since both AM1 and MNDO calculations show that the most stable conformation

for the dimer of this polymer is Q2. Given these initial results for dimers, we have then attempted to obtain stable *syn* A1 conformation for tetramers. The results of these calculations have been summarized in Table 4.5 and Fig. 4.15. First we note that complete geometry optimization using the dimer results as our initial (input) geometries does not result in an all *syn* conformations for tetramers, instead segments undergo inter-cell rotations. The net result is: the dihedral angle between the central monomers is approximately 180° but it is approximately 0° inside the dimer units of the tetramer. Due to this the tetramer of these polymers has *syn* orientation at the edges and *anti* in the middle which makes the orientation of the monomers to be *planar* in some cases. Given this arrangement it is seen that PFv and PCNFv are more stable in the A1 conformation relative to the A2 conformation in the AM1 calculation (PCNCY the two conformations give the same energies). The dihedral angles in these polymers are around 150° with the relative energy difference of approximately 20 kcal/mole in PFv and 8 kcal/mole in PCNFv. MNDO also predicts that the A1 conformation is more stable for PFv and PCNFv (by approximately 20 kcal/mole) relative to the A2 conformation and that there is a degeneracy or near degeneracy in PT, PCY, PCNTH and PCNCY (in most cases the energy differences are less than 1 kcal/mole). Summarizing this rotational analysis, we see that the A1 conformation is more stable than the A2 conformation for PFv and PCNFv however for the remaining polymers A1 and A2 conformations have nearly the same energies.

The trend in the relative stabilities of A1 versus Q1 forms is different from the one for A2 versus Q2 *planar* forms. Unlike *planar* forms, MNDO calculations (see Table 4.5 show that the A1 (aromatic or s-cis) mesomers are more stable (by a large amount, typically larger than 50 kcal/mole) than Q1 (quinoid or s-trans) mesomers for all of the polymers. The AM1 calculations for PCY, PFv, PCNCY and PCNFv also support this observation. This result is not surprising since typically, a rotation of single bond takes less energy than a corresponding rotation of a double bond. We note that for some polymers indicated with – in the table we have not been able to obtain stable Q2 conformations (for tetramers) with the AM1 calculations. We suspect that this is due to the fact that, in PT and PCNTH the *syn* conformation for quinoid mesomers is not stable.

Further *ab initio* Hartree-Fock calculation using 3-21G* basis set on PFv(A1) (dimer-oligomer) also confirms that A1 conformation is more stable. The dihedral is around 0° and pure *syn* conformation is energetically favorable by 7 kcal/mole relative to PFv(A2). Finally comparing the A1, A2, Q2 conformations for PFv and PCNFv we note that PFv prefers A1 and PCNFv prefers Q2 conformation.

In summary we point out that when all conformations are considered, the following trend emerges: A2 conformation is the most stable one for PT and PCNTH, Q2 is the most stable one for PCY, PCNCY and PCNFv and A1 is the most stable one for PFv.

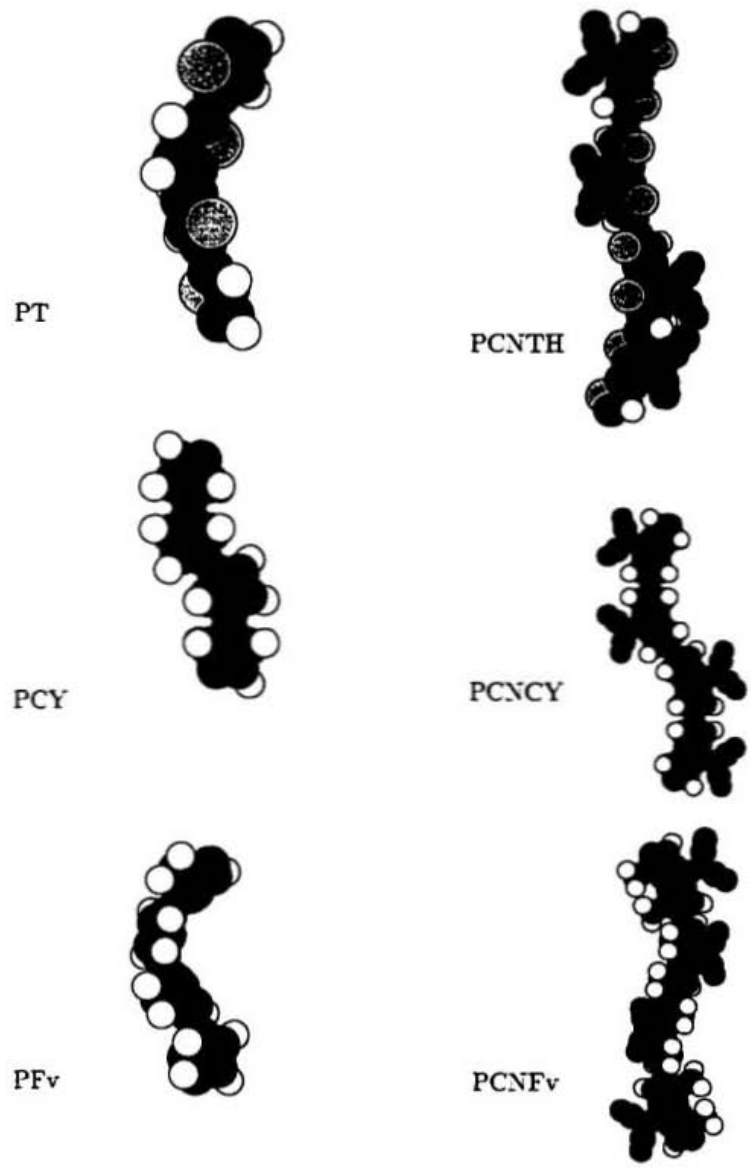

Figure 4.17: AM1 optimized geometries of *syn* conformations of the polymers in the aromatic or s-cis (A1) form (tetramers).

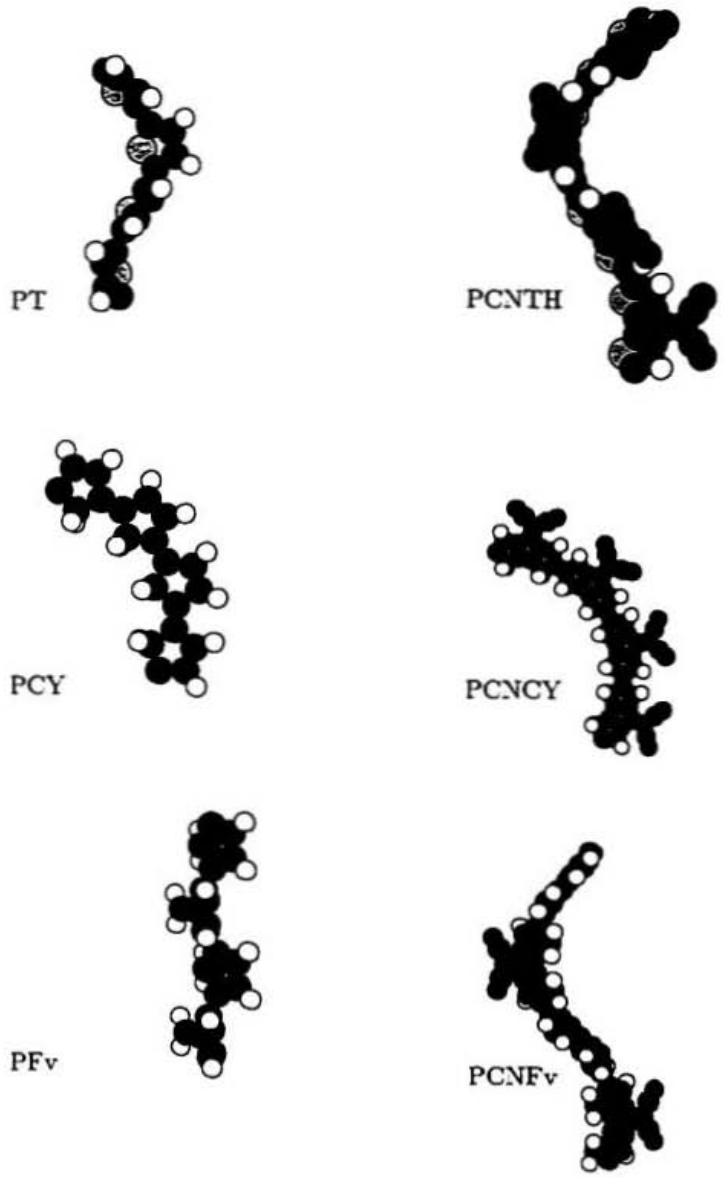

Figure 4.18: MNDO optimized geometries of *syn* conformations of the polymers in the quinoid or s-trans (Q1) form (tetramers).

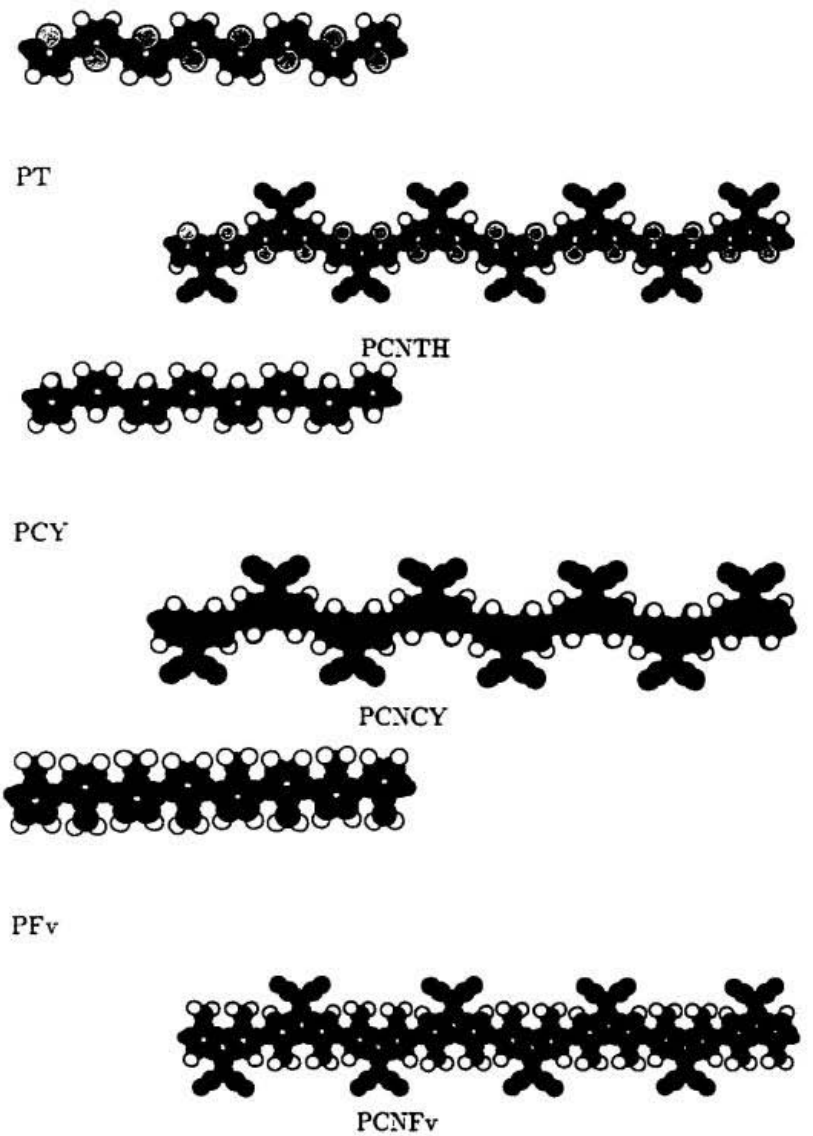

Figure 4.19: AM1 optimized geometries of *anti* conformations of the polymers in the aromatic or s-cis (A2) form (octamers).

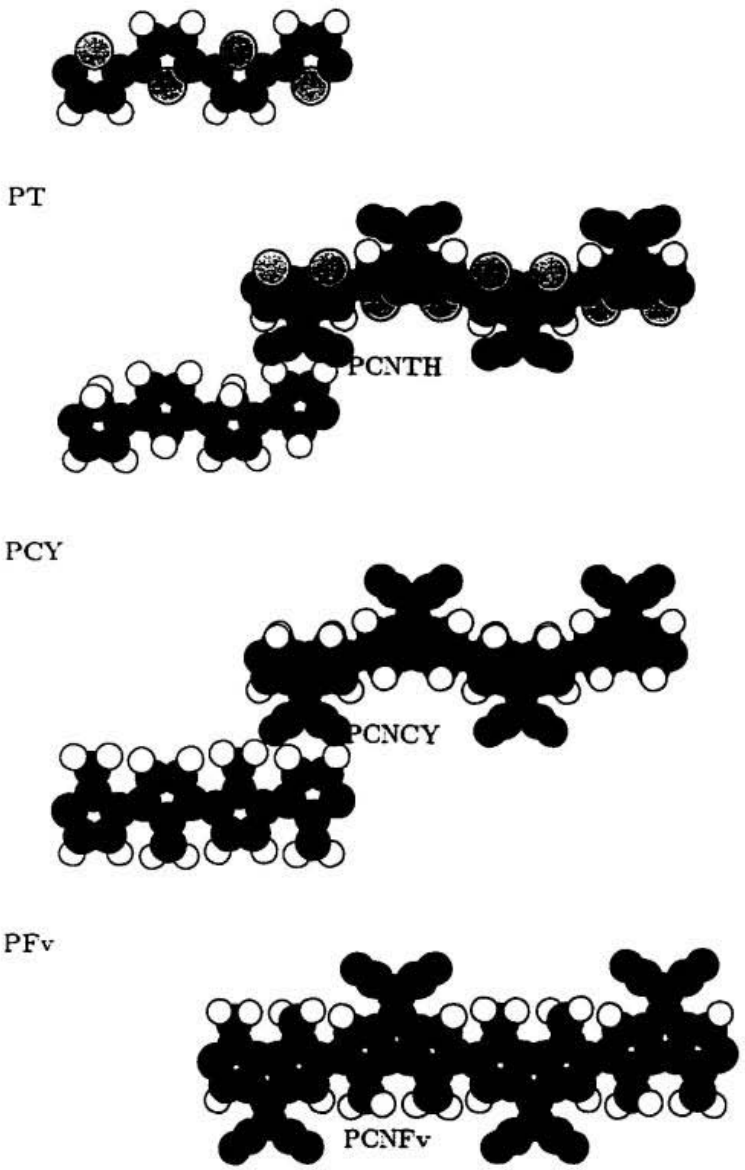

Figure 4.20: AM1 optimized geometries of *anti* conformations of the polymers in the quinoid or s-trans (Q2) form (tetramers).

4.2 Optimized Geometries

The full geometry optimizations (using both AM1 and MNDO methods) were performed with the use of the translational vector (T_v). In the solid-state cluster approach translational vector defines the size of the cluster (not the size of the unit cell which is the more conventional use of this term). Thus, in this work, the translational vector is closely related to the size of the cluster. Also in the geometry optimizations the value of T_v is subject to the optimization procedure (i.e. it is allowed to vary). The optimized values of T_v for tetramers are given in Tables 4.3 and 4.4. The T_v ranges from 15 to 30 $\AA$ (unit cells are half this length for tetramers). Large translational vectors (T_v) are needed [49] for the solid-state cluster calculations in order to minimize the edge effects on the monomers in the center of the cluster. A decrease in T_v indicates a switch from aromatic or s-cis (A1 or A2) to quinoid or s-trans (Q1 or Q2) mesomeric form of the compound.

The optimized geometries for the tetramers in A1, Q1, A2 and Q2 conformations are displayed in Fig. 4.17, 4.18, 4.19 and 4.20 respectively. In Tables 4.6 and 4.7 the geometric structure parameters are given. Bonds are labeled as indicated in Fig. 1.4. The average bond length alternation, δr, which is the signature of the given geometry will the focus of the discussion below.

The main structural feature of the polymers in the A1 and Q1 (*syn* or *syn-like*) conformations is that they form twisted coil-like structures which may possess C_2 point group symmetries (most often they belong to the C_1 point group). As noted above the geometry optimization of tetramers in the A1 and Q1 conformations resulted in *syn-like* structures whose dihedral angles between the monomers in the inner and outer portions of the polymers are not the same. It was suggested [54, 95] that these *syn-like* (twisted) conformations are due to the steric hindrance between the sulfur atoms in PT and PCNTH and between hydrogen atoms in the other tetramers located on the β, β' positions as well as between the bridging groups (such as the cyano groups) in the cyano substituted polymers. For example, in PCY the A1 or Q1 geometries constrained to be planar would result in the distance between the non-bonded hydrogens to be less than 1.5 $\AA$ which in the (relaxed) fully geometry optimized structure is approximately near 3 $\AA$ in(A1) forms and 2 $\AA$ in (Q1) forms both in (AM1 and MNDO). In other words, there is strong electrostatic repulsion between the hydrogens which in turn results in the rotation (twist) around the bond resulting in the formation of *syn-like* or *anti-like* conformations. Tetramers of PT, PFv, PCNTH and PCNFv belongs to C_2 point group and PCY and PCNCY belong to C_1 point group.

The inter-cell bond distances and bond length alternation δr values are discussed next for the A1 and Q1 conformations. Only the MNDO values are discussed since they are available for all tetramers. We note that the inter-cell distances for the A1 conformation

in PT, PCY and PFv approximately range from 1.45 $\AA$ to 1.46 $\AA$ (in PFv) which do not change significantly in the cyano substituted compounds (with the exception of PCNFv where this value decreases to 1.43 $\AA$). Similarly, the inter-cell and/or intra-cell distances range from 1.36 to 1.35 $\AA$ in all the tetramers in the Q1 conformation. In addition, we note that δr is of the order of -0.08 $\AA$ in A1 conformation for PT, PCY and PFv and -0.05 $\AA$ for PCNTH, PCNCY and PCNFv. In the Q1 conformation δr is approximately 0.12 $\AA$ for PT, PCY and PFv and approximately 0.14 $\AA$ for PCNTH, PCNCY and PCNFv. Thus bond length alternation decreases in the cyano compounds in the aromatic or s-cis forms but it increases in the the cyano compounds in the quinoid or s-trans forms relative to the unsubstituted tetramers.

Next we analyse the geometry optimized results for A2 and Q2 conformations. Since the most stable conformations are the A2 or Q2 rotational isomers they will be discussed in greater details than the corresponding A1 or Q1 isomers. We consider the inter-cell distance in PT which from the electron diffraction experiment [83] in bithiophene was determined to be 1.480 $\AA$. In PT(A2) this distance is equal to 1.447 $\AA$ (MNDO) which agrees with the value found in [36] but is smaller than the experimental value. AM1 calculation also underestimates this distance (equal to 1.424 $\AA$). This significant lowering is due to poor parameterization of sulphur in the MOPAC93 [97] in the AM1 method. For the remaining discussion, only AM1 results for the geometrical parameters for A2 and Q2 conformations will be discussed. In PT(Q2) the inter-cell distance is

1.345 $\AA$ which agrees with the computational findings of [37] and [36]. Using the AM1 bond lengths we determine that the δr is -0.03 $\AA$ for PT(A2) and 0.13 $\AA$ for PT(Q2) clearly differentiating between PT's aromatic and quinoid forms (see Fig. 5.43).

The AM1 geometrical structure for PCY is similar to the one obtained by [46]. The inter-cell bond distance obtained for the s-cis form is 1.424 $\AA$ (AM1) and for the s-trans form it is 1.339 $\AA$ (AM1). These values are relatively close to the corresponding values found in PT (see Table. 4.7). This is also reflected in their δr values (see Table. 4.7 and Fig. 5.43) which are -0.07 $\AA$ for the PCY(A2) and 0.12 $\AA$ for the PCY(Q2) in the AM1 calculation. However, it can be seen from the increased absolute value for δr (by 0.04 $\AA$) that, in PCY(A2), its aromaticity is decreased relative to PT(A2). In other words the replacement of sulphur with carbon leads to greater charge localization.

The structure of PFv is even more similar to PCY (than PCY to PT structure) as can be seen from the values of δr. The average bond length alternation for PFv(A2) is -0.08 $\AA$ (also agrees with [38]) and for PFv(Q2) it is 0.11 $\AA$ [98] which are very close to the corresponding values in PCY (see Fig. 5.43). A closer look at the magnitudes of the bond lengths reveals that there are some structural differences between PFv and PCY, for example, in both of the mesomeric forms, the inter-cell distances (1.442 $\AA$ (AM1) in PFv(A2) and 1.357 $\AA$ (AM1) in PFv(Q2)) are consistently longer (by 0.02 $\AA$) than the respective values in either PT or PCY. However, overall, the addition of the vinylene group to PCY does not lead to significant changes in its structure and

electronic properties.

Next we consider the cyano substituted systems. In the following discussion we will focus on the trends in the values of the outer ($C_{\alpha'}$-$C_{\beta'}$, $C_{\alpha'}$-C_1, inter-cell) and inner (C_α-C_β, C_α-C_1, intra-cell) bonds (the values of bond length alternations, δr will be discussed in chapter 5). as obtained in the AM1 and MNDO calculations (see Table. 4.7). Our first observation is that the presence of the cyano group distorts the thiophene rings in such a way that the inner bonds such C_α-C_β become longer than outer bonds of the type $C_{\alpha'}$-$C_{\beta'}$ by approximately 0.02 $\AA$. At the same time, the inner bonds of the type C_α-C_1 become shorter than the outer bonds of the type $C_{\alpha'}$-C_1 by approximately 0.03 or 0.04 $\AA$. Similarly, the intra-cell distances are shorter than inter-cell distances. In general the outer bonds (further from the cyano group) are closer in value to the corresponding bonds in their parent polymers (see Table. 4.7) than the inner bonds (closer to the cyano group). In other words, the electron-withdrawing effects of the cyano group on the structure of these compounds are localized to the central (inner) part of the monomer. Bonds of the type C_β-$C_{\beta'}$ remained relatively unaltered between the cyano substituted and unsubstituted compounds (C_β-$C_{\beta'}$ slightly decreases in cyano derivatives, typically less than 0.01 $\AA$). Similar observations have been made by Toussaint et al., [45] for PCNTH and PCNCY.

Table 4.6: Comparison of the fully optimized solid-state geometrical parameters (for tetramers) of the polymers as indicated in the mesomeric forms with one monomer/unit cell. The bond distances are in $\AA$. The intra-cell distances in PT, PCY, PFv are same as the inter-cell distances thus the space is left blank in column six.

POLYMER		DISTANCE ($\AA$)							
		$\alpha-\beta$	$\beta-\beta'$	$\beta'-\alpha'$	Inter cell	Intra cell	T_v	δr^*	$H(\beta-\beta')$
PT(A1)	MNDO	1.383	1.446	1.384		1.450	13.78	-0.065	3.844
	AM1	1.389	1.423	1.389		1.428	13.37	-0.043	3.781
PT(Q1)	MNDO	1.480	1.356	1.480		1.361	13.58	0.121	2.486
	AM1								
PCY(A1)	MNDO	1.374	1.470	1.374		1.453	12.96	-0.088	3.910
	AM1	1.371	1.461	1.370		1.423	12.93	-0.072	3.985
PCY(Q1)	MNDO	1.478	1.362	1.478		1.357	11.48	0.119	2.459
	AM1	1.460	1.360	1.468		1.339	11.07	0.115	2.408
PFv(A1)	MNDO	1.373	1.469	1.373		1.463	13.06	-0.093	3.817
	AM1	1.369	1.469	1.370		1.453	12.71	-0.092	3.812
PFv(Q1)	MNDO	1.477	1.358	1.477		1.346	11.93	0.125	2.571
	AM1	1.486	1.350	1.485		1.368	11.98	0.123	2.180
PCNTH(A1)	MNDO	1.392	1.435	1.419	1.442	1.452	28.41	-0.036	3.763
	AM1	1.396	1.408	1.396	1.440	1.438	28.34	-0.028	3.723
PCNTH(Q1)	MNDO	1.482	1.359	1.505	1.356	1.364	25.66	0.134	2.326
	AM1								
PCNCY(A1)	MNDO	1.379	1.460	1.401	1.447	1.455	27.48	-0.065	4.638
	AM1	1.379	1.444	1.437	1.439	1.423	27.19	-0.030	4.975
PCNCY(Q1)	MNDO	1.489	1.363	1.505	1.349	1.359	23.49	0.139	2.390
	AM1	1.473	1.355	1.509	1.341	1.342	22.93	0.143	2.371
PCNFv(A1)	MNDO	1.379	1.447	1.416	1.440	1.429	27.36	-0.043	3.354
	AM1	1.386	1.443	1.442	1.440	1.464	27.32	-0.033	3.936
PCNFv(Q1)	MNDO	1.485	1.350	1.515	1.353	1.354	25.11	0.148	2.106
	AM1	1.484	1.355	1.514	1.349	1.350	24.53	0.146	2.140

* δr is average bond length alternation. For PT, PCY, PFv it is calculated as $((C_{\alpha'-\beta'})$-$(C_{\beta'-\beta})+(C_{\beta-\alpha})$ -$(C_{\alpha-\alpha'}))/2$ [38, 99] and for cyano substituted ones δr is $((C_{\alpha'-\beta'})$-$(C_{\beta'-\beta})+(C_{\beta-\alpha})$- $(C_{\alpha-\alpha_1})+(C_{\alpha_1-\beta_1})$-$(C_{\beta_1-\beta_1'})$ +$(C_{\beta_1'-\alpha_1'})$-$C_{\alpha_1'-\alpha'})/4$.

Table 4.7: Comparison of the fully optimized solid-state geometrical parameters (for tetramers) of the polymers as indicated in their two mesomeric forms with two monomers/unit cell. The bond distances are in Å. The blank spaces in column three indicate that α'-1 and 1-α (in column four) distances are the same in PT, PCY and PFv. Also since the intra-cell distances in PT, PCY and PFv are same as the inter-cell distances the space is left blank in column eight.

POLYMER		DISTANCE (Å)								
		α'-1	1-α	α-β	β-β'	β'-α'	Intra-cell	Inter-cell	T_v	δr[a]
PT(A2)	MNDO		1.686	1.389	1.441	1.389		1.447	15.520	−0.055
	AM1		1.668	1.399	1.417	1.394		1.424	15.291	−0.026
PT(Q2)	MNDO		1.705	1.476	1.361	1.476		1.358	15.227	0.117
	AM1		1.719	1.459	1.354	1.459		1.345	15.123	0.110
PCY(A2)	MNDO		1.532	1.374	1.466	1.374		1.452	15.162	−0.085
	AM1		1.514	1.371	1.470	1.371		1.424	14.867	−0.070
PCY(Q2)	MNDO		1.530	1.479	1.361	1.479		1.356	14.947	0.120
	AM1		1.511	1.468	1.359	1.468		1.339	14.696	0.119
PFv(A2)	MNDO		1.524	1.376	1.455	1.376		1.472	15.500	−0.088
	AM1		1.508	1.373	1.454	1.373		1.442	15.207	−0.075
PFv(Q2)	MNDO		1.522	1.476	1.356	1.477		1.376	15.278	0.110
	AM1		1.504	1.468	1.354	1.468		1.357	15.012	0.113
PCNTH(A2)	MNDO	1.695	1.649	1.419	1.431	1.399	1.441	1.447	30.851	−0.028
	AM1	1.682	1.627	1.437	1.404	1.401	1.439	1.422	30.649	0.002
PCNTH(Q2)	MNDO	1.713	1.670	1.501	1.363	1.482	1.353	1.362	30.631	0.131
	AM1	1.725	1.670	1.498	1.355	1.460	1.360	1.353	30.599	0.123
PCNCY(A2)	MNDO	1.541	1.502	1.402	1.457	1.384	1.446	1.453	30.218	−0.061
	AM1	1.524	1.487	1.412	1.442	1.380	1.437	1.421	29.895	−0.039
PCNCY(Q2)	MNDO	1.538	1.489	1.506	1.362	1.489	1.349	1.359	29.721	0.139
	AM1	1.520	1.486	1.510	1.355	1.473	1.343	1.341	29.448	0.144
PCNFv(A2)	MNDO	1.522	1.483	1.406	1.448	1.388	1.463	1.468	30.656	−0.060
	AM1	1.508	1.470	1.413	1.437	1.387	1.447	1.434	30.240	−0.039
PCNFv(Q2)	MNDO	1.502	1.468	1.508	1.352	1.480	1.355	1.356	30.168	0.135
	AM1	1.519	1.484	1.505	1.358	1.490	1.358	1.376	29.790	0.140

[a] δr is average bond length alternation. For PT, PCY, PFv it is calculated as $((C_{\alpha'-\beta'})$-$(C_{\beta'-\beta})+ (C_{\beta-\alpha})$-$(C_{\alpha-\alpha'}))/2$ [38, 99] and for cyano substituted ones δr is $((C_{\alpha'-\beta'})$-$(C_{\beta'-\beta})+(C_{\beta-\alpha})$ -$(C_{\alpha-\alpha_1})+(C_{\alpha_1-\beta_1})$-$(C_{\beta_1-\beta_1'})$ +$(C_{\beta_1'-\alpha_1'})$-$(C_{\alpha_1'-\alpha'}))/4$.

Chapter 5

Electronic Structure Analysis

As was stated in the introduction the main goal of this research is to identity properties and characteristics of CP's that would produce small band gaps. First we must determine which polymers have small band gaps which in turn means that we must study the electronic structure of CP's. In this work, CP's are treated as quasi one-dimensional systems whose electronic structure is studied using the molecular orbital theory and solid-state concepts as discussed in chapter 3. It was determined in chapter 4 that the A2 or Q2 conformation is the most stable one (relative to the A1 or Q1 conformation) for most of the polymers studied. Thus in this chapter full quasi one-dimensional band structure calculations are performed for *planar*, conjugated single polymer chains i.e. ones with unit cells that contain *two* monomers connected by an inter-ring bond. The periodic boundary conditions (underlying the translational symmetry) are used to generate the infinitely long chains. Further symmetry considerations dictate that the inter-ring bond is not parallel to the chain axis direction [100]. Specifically, we note that for our systems the primary center of symmetry is located at a half-way point on the inter-cell bond located between monomers. (A center of symmetry, if there is one,

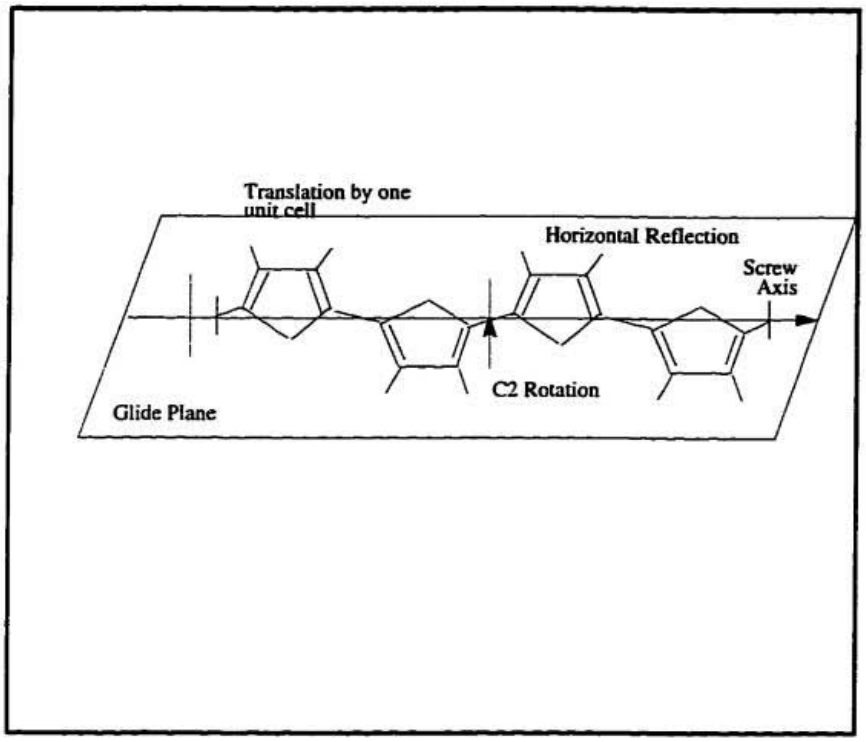

Figure 5.21: Space group operations for the polymer in the *anti* (A2) orientation.

is always at the center of gravity of a system.) Relative to this center of symmetry, all of the two-monomer unit cells could be characterized by C_{2h} point group symmetry which consists of eight symmetry operations (E, $C_2(x)$, $C_2(y)$, $C_2(z)$, i, $\sigma(yz)$, $\sigma(zx)$, $\sigma(xy)$ [49]) (refer Fig. 5.21) The full specification of the space group requires that in our symmetry considerations we have also included non-primitive translational symmetry elements such as screw axis. Polymers studied possess screw axis symmetry which are rotations followed by a translations by a half of the unit cell vector.

This chapter is organized into following sections: in section 5.1 the general features of the band structure are described; in section 5.2 the valence and the conduction bands are discussed in greater details; in section 5.3 the trends in IP, EA and E_g are analyzed; in section 5.4 the effects, as related to the presence of the donor/acceptor groups, on the band structure are briefly commented on; in section 5.5 the correlations between the electronic and geometric structures are pointed out.

5.1 Electronic Band Structures – General Features

The results for the all-valence electron, semiempirical, one-dimensional calculations for polymers in the aromatic or s-cis (A2) forms are shown in Fig's. 5.22, 5.24, 5.26, 5.28, 5.30 and 5.32. Similarly band structures for the quinoid or s-trans (Q2) forms are shown in the Fig's. 5.23, 5.25, 5.27, 5.29, 5.31 and 5.33. In all these figures, the energy is measured relative to vacuum (not to the Fermi energy levels which are designated with dashed lines). From these diagrams it can be seen that the bands are degenerate at the BZ boundaries which is due to the fact that the unit cell consists of two "identical" (at least as far as their chemical compositions is concerned) monomers. Thus, it is sometimes useful to think of these two bands (that are degenerate at the zone) as being two parts of one band [101] that would be have been produced if the unit cell were taken to consist of one monomer. That is, two bands connected at the BZ boundary arise from the folding of the respective (longer) single band when the

unit cell is doubled in size from one monomer to two monomers.

The main features of band structure calculations are summarized in Table 5.8. Since the semiempirical calculations are an all-valence electron approximation, only bands produced by valence electrons (of the constituent atoms) are shown in the above band structure figures. In addition, the Bloch functions for the valence electrons are constructed using Slater type minimal basis set. Thus, for PT pseudo one-dimensional, cluster solid-state calculations generated 24 filled bands and 20 empty bands (the number of unfilled bands is, of course, related to the size of the basis set, the bigger the basis set, the larger the number of unfilled bands). A comparison of our band structure of PT(A2) with the one obtained by Bredas et.al using non-empirical VEH calculations [102] illustrates that they are very similar in structure. For PCY and PFv, the calculations produced 24 and 28 filled bands and 24 and 28 empty bands respectively. In the case of PCY(A2) when we compare the π bands with the one generated by Hong et al., [99] the topology of the bands seemed to be similar.

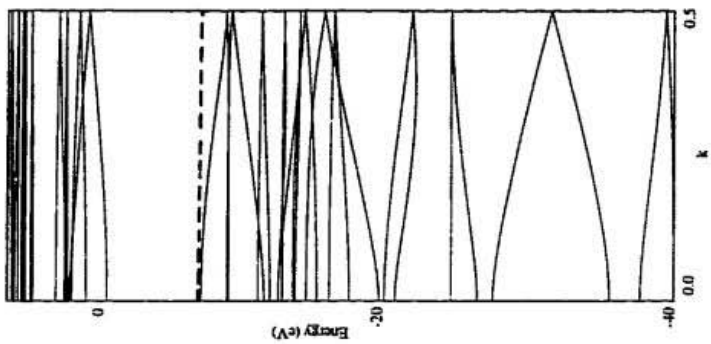

Figure 5.22: Band structure of PT(A2) cluster of tetramer from AM1 calculation.

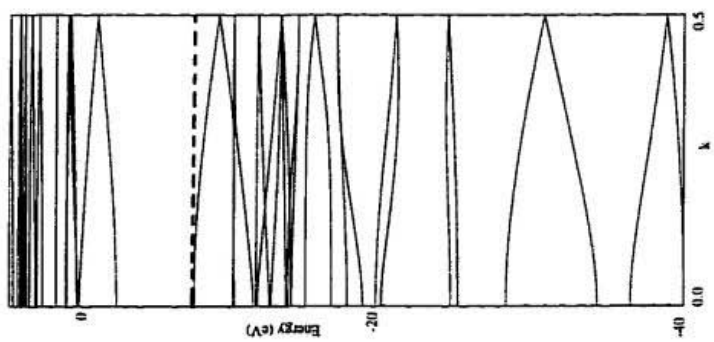

Figure 5.23: Band structure of PT(Q2) cluster of tetramer from AM1 calculation.

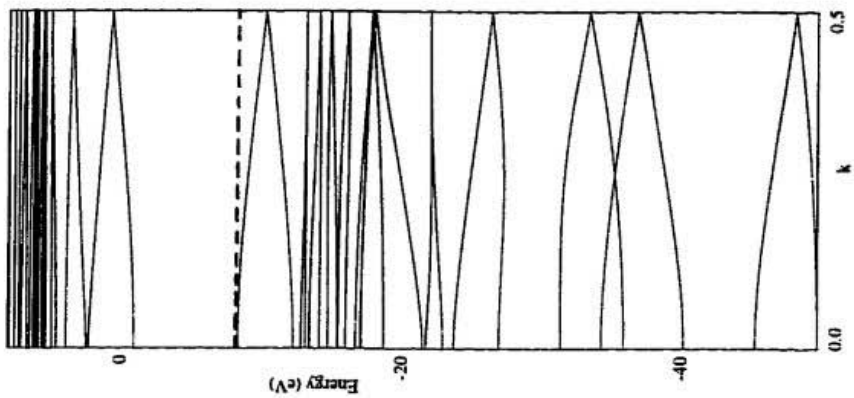

Figure 5.24: Band structure of PCY(A2) cluster of octamer from AM1 calculation.

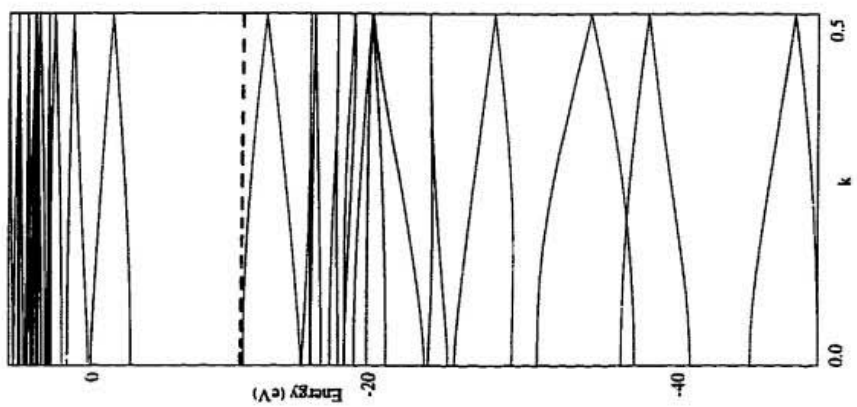

Figure 5.25: Band structure of PCY(Q2) cluster of tetramer from AM1 calculation.

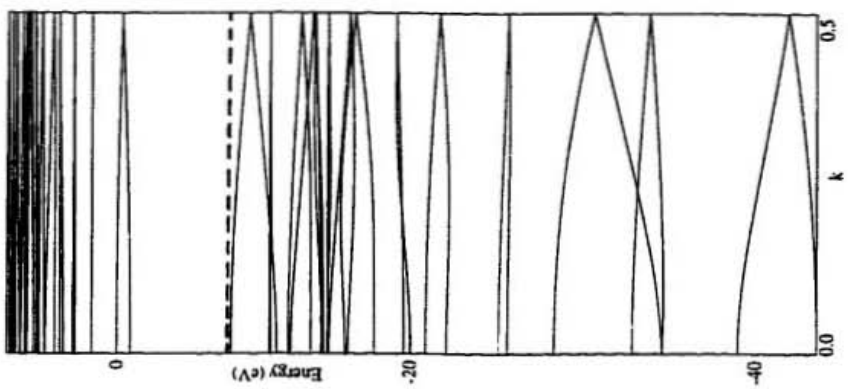

Figure 5.26: Band structure of PFv(A2) cluster of octamer from AM1 calculation.

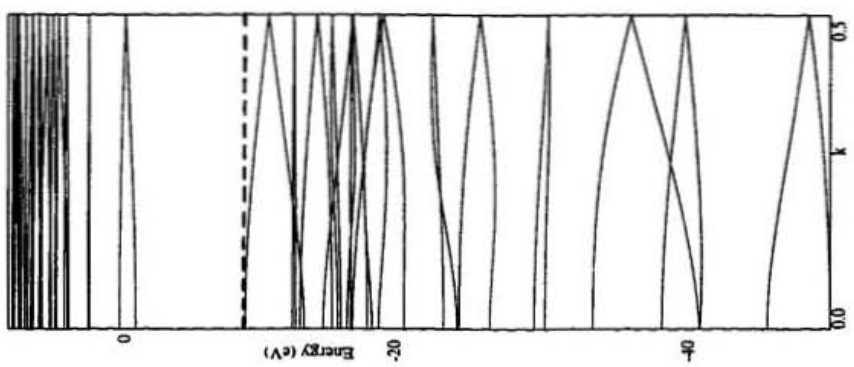

Figure 5.27: Band structure of PFv(Q2) cluster of tetramer from AM1 calculation.

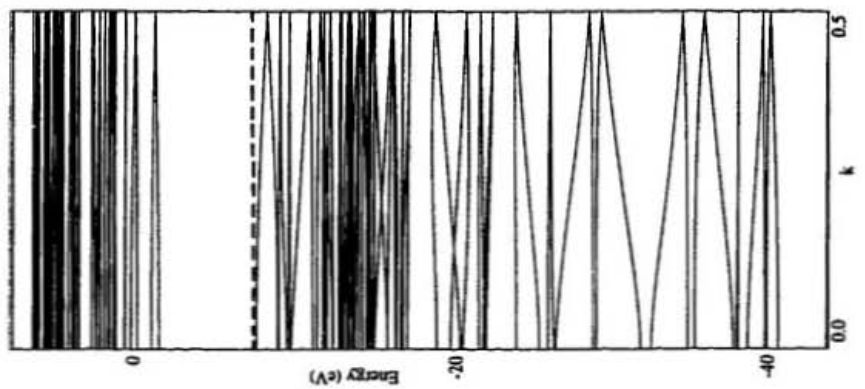

Figure 5.28: Band structure of PCNTH(A2) cluster of octamer from AM1 calculation.

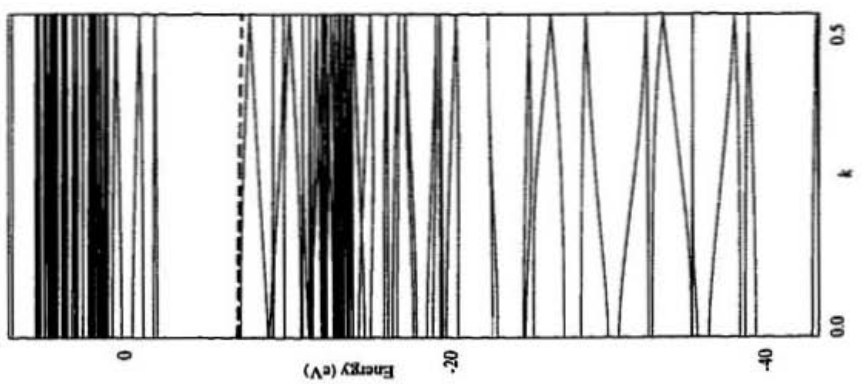

Figure 5.29: Band structure of PCNTH(Q2) cluster of tetramer from AM1 calculation.

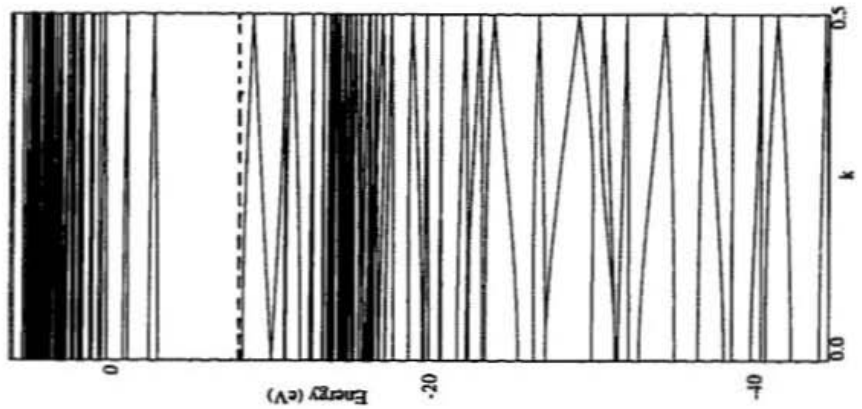

Figure 5.30: Band structure of PCNCY(A2) cluster of octamer from AM1 calculation.

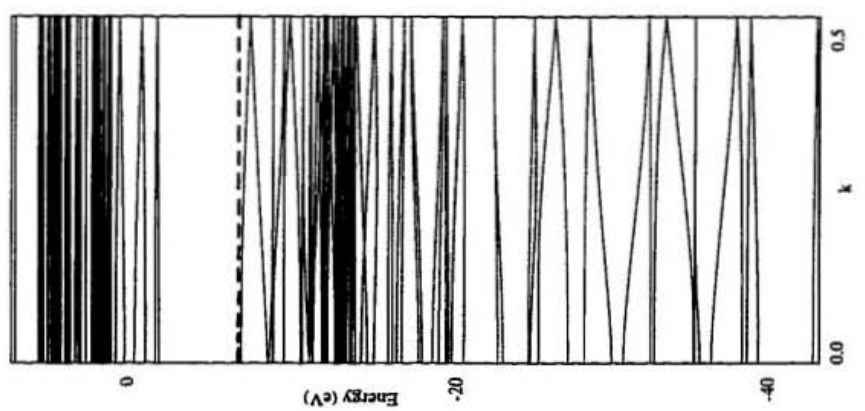

Figure 5.31: Band structure of PCNCY(Q2) cluster of tetramer from AM1 calculation.

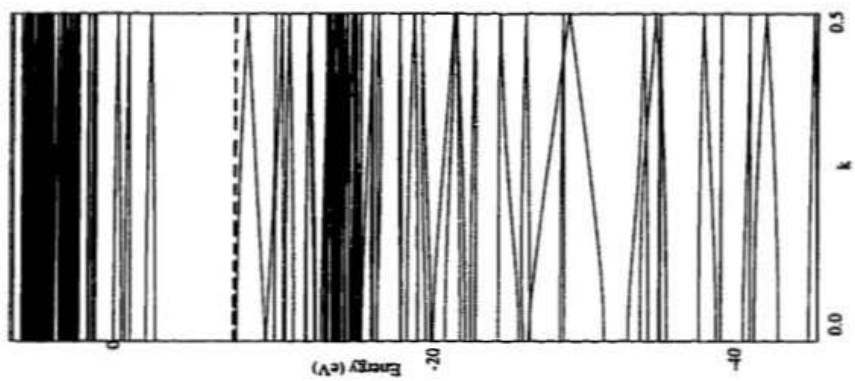

Figure 5.32: Band structure of PCNFv(A2) cluster of octamer from AM1 calculation.

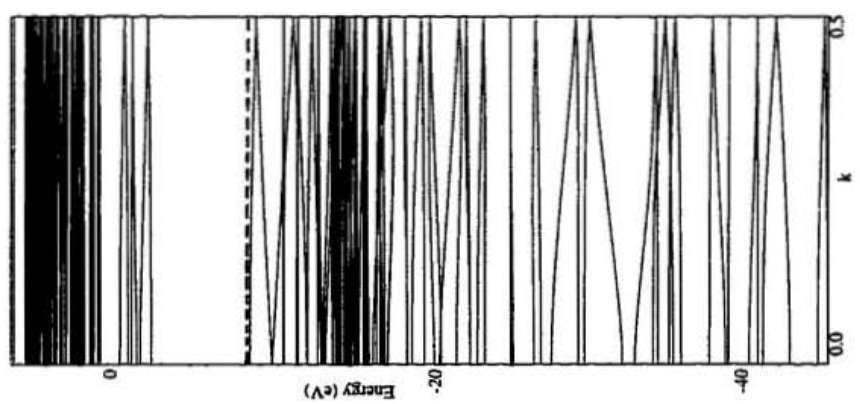

Figure 5.33: Band structure of PCNFv(Q2) cluster of tetramer from AM1 calculation.

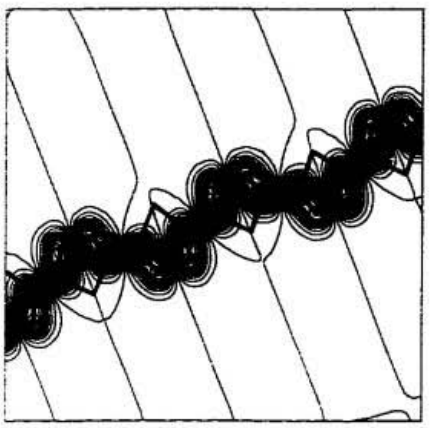

Figure 5.34: HOMO is for PT(A2). HOMO of PCY(A2), PFv(A2) and LUMO of PT(Q2), PCY(Q2), PFv(Q2) are similar.

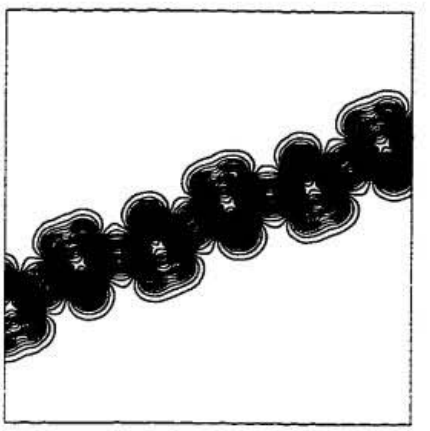

Figure 5.36: LUMO is for PT(A2). LUMO of PCY(A2), PFv(A2) and HOMO of PT(Q2), PCY(Q2), PFv(Q2) are similar.

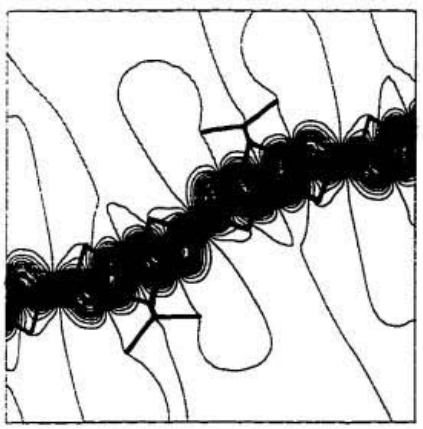

Figure 5.35: HOMO is for PCNTH(A2). HOMO of PCNCY(A2), PCNFv(A2) and LUMO of PCNTH(Q2), PCNCY(Q2), PCNFv(Q2) are similar.

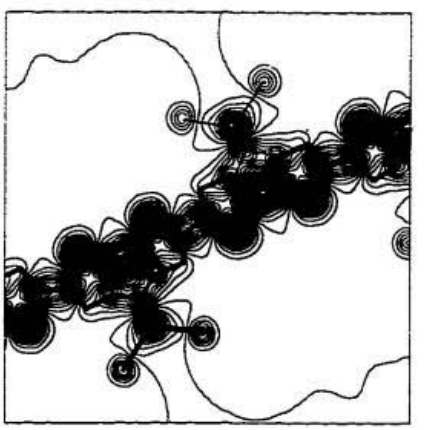

Figure 5.37: LUMO is for PCNTH(A2). LUMO of PCNCY(A2), PCNFv(A2) and HOMO of PCNTH(Q2), PCNCY(Q2), PCNFv(Q2) are similar.

Table 5.8: This table summarizes the band structure results for the polymers as indicated. The primitive unit cell of the direct lattice is a dimer containing two monomers in either A2 or Q2 mesomeric form.

	PT C8 H4 S2	PCY C10 H8	PFv C12 H8
# of valence electrons per **unit cell**	48	48	56
# of filled bands	24	24	28
# of unfilled bands	20	24	28
Total # of bands	44	48	56

	PCNTH C24 H4 S4 N4	PCNCY C24 H12 N4	PCNFv C32 H12 N4
# of valence electrons per **unit cell**	144	144	160
# of filled bands	72	72	80
# of unfilled bands	60	72	80
Total # of bands	132	144	160

The number of valence electrons increases significantly in the cyano substituted compounds hence, of course, the number of bands also increases (see Table 5.8). Another way of looking at this increase is to note that if there were no cyano group present in the unit cell we would have four monomers per unit cell (instead of two as in the parent polymers) which means that single bands that could have been obtained for one monomer per unit cell would have to be folded four times in order to account for the fact that the first BZ must correspondingly be decreased in size by a factor of four. This fourfold (instead of twofold) folding of the bands for the cyano compounds causes the bands to become flatter relative to the ones for unsubstituted polymers. This flattening of bands has also been observed by Bredas et al., for other low band gap polymers (that used emaraldine base [103]) who found that as the number of monomers per unit cell increases the corresponding bands become flatter. As shown in Table 5.8 in PCNTH, we have found 72 occupied and 60 unoccupied bands, in PCNCY, we have obtained 72 occupied and 72 unoccupied bands and in PCNFv we have found 80 occupied and 80 unoccupied bands.

5.2 Valence and Conduction Bands

As mentioned in the introduction, π_z electrons are important in defining the conducting properties of CP's. The bands formed by π orbitals are called π bands. The π

bands are identified in the process that involves extracting the cluster orbitals' expansion coefficients and phases at the k-points (k=0 or k=$\frac{\pi}{a}$) generated using solid state calculation. This process clearly identifies the pure π bands and the hybrid (π with σ) bands. Following this procedure we found that, for all the polymers in any of the mesomeric forms, the valence (the highest occupied) and conduction (the lowest unoccupied) bands are π_z bands and that they have almost identical shapes. Similar result has been found by [38] for PT, PCY, PFv polymers and by [104, 45, 46] for PCNCY, PCNTH polymers. There are five doubly folded π_z bands in PT, PCY and PFv of which three are occupied and two are unoccupied. In the cyano substituted polymers, there are eight doubly folded π_z bands of which five are occupied and three are unoccupied. The topology of the π_z bands in PCNTH, PCNCY, PCNFv differs from the ones in unsubstituted systems. As stated above, because of the larger number of the effective monomer units in the unit cell π_z bands are narrower (flatter) in the cyano substituted systems.

By examining the π_z bands in A2 structures, we note that the valence and conduction bands are formed from the orbitals whose symmetries are *bg* and *au*. That is they are formed from bonding and antibonding orbital combinations respectively. Also, in most of these sytems, there is a second π_z band that is flat and lies just below the valence band. The flattening corresponds to the states that have almost no overlap with the orbitals corresponding to the C_α and $C_{\alpha'}$ atoms. This band is present in all

polymers since the monomers are linked by the bond formed between the C_α and $C_{\alpha'}$ carbon atoms. The third π_z band is lower than the other two. In Q2 structures valence and conduction bands are formed from the *au* and *bg* combinations respectively. The splitting of the doubly folded bands in Q2 structures is comparable to the one in A2 structures. The difference in overlapping of orbitals in the Q2 structures in comparison to the corresponding overlapping in A2 structures causes the valence band to be raised or lowered in energy relative to the same band in A2 structures.

In one-dimensional infinite systems, the behavior of Bloch eigenvalues (for the valence and the conduction bands) at the zone centers (the Γ point) or at the boundaries (the X points) are important in defining the primary physical characteristics of the band structures. For example, even though the band gaps spread out over a considerable energy range, the threshold of absorption observed experimentally will often correspond to the smallest energy difference between the valence and the conduction bands. Thus it is useful to study the Bloch functions that correspond to these two points (giving the smallest energy difference) on the valence and conduction energy dispersion curves. Fig. 5.34 displays the Bloch function at the top edge of the highest occupied state which is often called HOMO (in analogy to the molecular energy levels) and Fig. 5.36 displays the Bloch function at the bottom edge of the conduction band called the LUMO. Fig. 5.34- 5.37 are contour plots of Bloch orbitals which are cross-sections in the planes of the chain backbones. The results of our calculations for HOMO and

LUMO for PT(A2), PCY(A2), PFv(A2) are in agreement with [38, 99, 45]. In this mesomeric form, the main contribution for the HOMO comes from the carbon along the chain backbone (i.e. $C_{\alpha'}$, $C_{\beta'}$, C_{β} and C_{α}) and there is no contribution from bridging atoms X_d (such as S or C_1) at the 1 position. As a result, the highest occupied band is very similar to the highest occupied band for *cis*-PA. On the other hand, the LUMO has some contributions from the X_d group for the A2 forms. The second highest π_z band in the valence region is stabilized, in contrast to the highest occupied band by a relatively large contribution from the X_d and a low contribution from C_{α} and $C_{\alpha'}$ π_z electrons.

As pointed out above, the main difference between aromatic or s-cis forms and quinoid or s-trans forms comes from interchanging the phase and the symmetry of the corresponding orbitals. This can be clearly seen from Fig. 5.34 - 5.37 where it is shown that the HOMO and LUMO of the Q2 structures are exactly the LUMO and HOMO of the A2 structures. That is, the HOMO of A2 in Fig. 5.34 becomes the LUMO of Q2 and the LUMO of A2 in Fig. 5.34 becomes the HOMO of Q2 form. This interchanging of the Bloch functions between the A2 and Q2 forms is seen in all of the polymers. The Bloch functions of cyano substituted polymers are shown in Fig. 5.35 and 5.37. In agreement with [45, 46, 104] the Bloch functions of cyano substituted polymers for the LUMO(A2) and HOMO(Q2) have large contributions from the cyano groups (see Fig. 5.37).

Theoretical calculations, such as the Hückel calculations [44] and VEH calculations [45, 46] provide us with informations regarding the wave functions of the polymer systems studied, however these calculations give different nodal characteristics from the ones we have obtained. More recently, another theoretical study [104] obtained nodal properties of the wave functions that agree with our calculations. In summary, then, in spite of different calculation producing different orbital patterns all of the calculations indicate that in A2 forms (or Q2 forms) there is no contribution from the electron-accepting cyano groups Y_a and electron-donating bridging groups X_d for the HOMO (or LUMO). And, in the case of LUMO(A2) or HOMO(Q2), there is strong contribution from the cyano and the bridging groups. Therefore the main difference between the mesomeric forms must be in the bonding patterns since the number of electrons and consequently the number of orbitals are the same in both forms. This different electron distribution also produces different band gaps for these two forms.

5.3 Trends in IP, EA and Band Gaps

The ionization potential (IP), electron affinity (EA), energy gap (E_g) and the band width (BW) are quantities that are used to describe the intrinsic, electronic properties of conducting polymers [103]. Not all of these quantities are independent. For example, the values for a direct band gap, E_g, are obtained by subtracting EA from IP or E_g = IP - EA [106, 107, 108]. This assignment is possible because the removing or

Table 5.9: A comparison of values of IP, EA and E_g (in units of eV) for A2 forms for systems as indicated in the table.

		PT	PCY	PFv	PCNTH	PCNCY	PCNFv
AM1	IP	7.79	7.46	7.51	8.24	7.79	7.72
	EA	1.36	1.26	1.66	2.54	2.68	2.94
	E_g	6.43	6.20	5.85	5.70	5.11	4.78
MNDO	IP	8.08	7.64	7.57	8.50	8.07	7.91
	EA	1.60	1.19	1.41	2.77	2.55	2.62
	E_g	6.48	6.45	6.16	5.73	5.52	5.29
THEORY	IP	4.69[a]	4.27[b]	4.68[f]	4.20[a]	3.93[b]	
	EA	3.07[a]	3.08[b]		3.64[a]	3.77[b]	
	E_g	1.62[a]	1.19[b]	0.64[d]	0.56[a]	0.16[b]	
		2.19[e]		0.87[f]		3.78[c]	
EXPT	E_g	2.10[g]			0.80[h]		

[a]Ref. [45](VEH calc.),
[b]Ref. [46](VEH calc.),
[c]Ref. [104](MNDO-AM1 calc.),
[d]Ref. [38](Huckel calc.),
[e]Ref. [100](VEH calc.),
[f]Ref. [98](VEH calc.),
[g]Ref. [105]
[h]Ref. [44]

adding of an electron from a state will not affect the equilibrium configuration of the system as explained by Koopman's theorem [109]. In turn, the values of IP and EA are determined by taking the negative of the highest occupied and lowest unoccupied Bloch function eigenvalues corresponding to k=0 point of the valence and conduction bands.

The values for IP, EA and E_g are given in Tables 5.9 5.11, 5.10 and 5.12 for the

Table 5.10: A comparison of values of IP, EA and E_g (in units of eV) for A1 forms for systems as indicated in the table.

		PT	**PCY**	**PFv**	**PCNTH**	**PCNCY**	**PCNFv**
AM1	IP	9.16	7.46	8.80	9.14	7.79	7.92
	EA	0.70	1.26	0.68	2.30	2.68	2.81
	E_g	8.36	6.20	8.12	6.84	5.11	5.01
MNDO	IP	8.67	7.64	8.73	9.07	8.07	8.15
	EA	1.11	1.19	0.59	2.50	2.55	2.51
	E_g	7.56	6.45	8.14	6.57	5.52	5.64

mesomeric forms and for AM1 and MNDO approximations. In Fig. 5.38 the band gaps are compared between A1 and A2 forms. This figure shows that A1 forms have larger band gaps than A2 forms. Similarly Q1 forms have larger band gaps than Q2 forms. This is because A2 and Q2 forms are truly planar with the monomers alternating with each other. This enhances the π_z orbital overlap to the maximum extend. Therefore the larger π_z delocalization along the chain backbone in A2 and Q2 forms lowers the band gap. In A1 and Q1 forms the π_z orbital is overlapping over only few monomers due to the rotation of one monomer with respect to another which occurs because of the steric repulsions. Thus in A1 and Q1 forms the uninterrupted π_z electron delocalization will only occur over short distances. Thus once again, the remaining part of this subsection will focus on the discussion of A2 and Q2 forms.

From the comparison with experimentally determined data [105], [44] (see Table 5.9)

Table 5.11: A comparison of values of IP, EA and E_g (in units of eV) for Q2 forms for systems as indicated in the table.

		PT	**PCY**	**PFv**	**PCNTH**	**PCNCY**	**PCNFv**
AM1	IP	6.89	7.57	7.57	7.20	8.37	8.27
	EA	2.16	1.05	1.25	3.07	2.30	2.49
	E_g	4.73	6.52	6.32	4.13	6.07	5.78
MNDO	IP	7.50	7.76	7.49	8.07	8.53	8.17
	EA	1.94	1.01	1.12	2.69	2.19	2.27
	E_g	5.56	6.75	6.37	5.38	6.34	5.90
THEORY	IP	3.98[a]	4.34[b]	4.90[c]			
	EA	3.72[a]	2.87[b]				
	E_g	0.26[a]	1.47[b]	1.80[c]			
			1.87[d]				

[a] Ref. [45] (VEH calc.),
[a] Ref. [46] (VEH calc.),
[c] Ref. [98] (VEH calc.),
[d] Ref. [38] (Huckel calc.)

one can see that semiempirical values for E_g differ by more than 4 eV (by 4.3 eV in PT(A2) and by 4.9 eV in PCNTH(A2)). This difference can be attributed to number of factors such as the fact that all calculations are performed for single chains, neglecting inter chain interactions, errors in semiempirical parameterization and the use of Hartree-Fock approximation. Thus a direct comparison of the calculated values for band gaps and ionization potentials with the corresponding experimental data exhibits large errors. However, it is our conjecture (supported by the few cases when a direct comparison is available) that these large errors are essentially system independent since as stated above they are related to the particular methodology and approximations that

Table 5.12: A comparison of values of IP, EA and E_g (in units of eV) for Q1 forms for systems as indicated in the table.

		PT	**PCY**	**PFv**	**PCNTH**	**PCNCY**	**PCNFv**
AM1	IP		8.46	7.54		8.54	8.39
	EA		1.56	0.76		2.28	2.38
	E_g		6.90	6.78		6.26	6.01
MNDO	IP	7.55	8.54	7.65	8.17	8.67	8.18
	EA	1.78	1.46	0.73	2.69	2.21	2.19
	E_g	5.78	7.08	6.92	5.49	6.46	5.99

are common to all systems studied. It is for this reason that we postulate that while the absolute values may not be accurate the trends observed in Tables 5.9 and 5.11 will compare well with experimental results. That is, we expect that the results for the trends will be more reliable than the absolute values and thus the main goal of this work is not to discuss the absolute values for E_g but to focus on their general trends.

In Table 5.9, it is shown that the values for E_g for the aromatic or s-cis form for PT, PCY and PFv are of similar magnitudes and there is a decrease of the order of 1 eV between their values and those corresponding to the cyano compounds: PCNTH, PCNCY and PCNFv (see also Fig. 5.39). The trend in this set of values for E_g indicates that PCNFv would have the potential to have the lowest band gap amongst the systems studied. Our trend is also in agreement with VEH calculations that gave the following values for E_g: 1.62 eV for PT(A2) [45], 1.19 eV for PCY(A2) [46], 0.87 eV for PFv(A2)

[98], 0.56 eV for PCNTH(A2) [45] and 0.16 eV for PCNCY(A2) [46].

In Table 5.11, the corresponding values for IP, EA and E_g are shown for the Q2 form. These values exhibit number of trends. First, the decrease in the band gap values between the PT, PCY and PFv and their corresponding cyano derivatives are not as large as for the aromatic or s-cis form (they are of the order of 0.5 eV or less instead of 1 eV). Second, while in the case of A2 form, the values of band gaps decreased continuously from PT to PCNFv, this is not the case for Q2 form. There is an increase in E_g of the order of 2 eV (AM1) (or 1 eV (MNDO)) between PT(Q2) and PCY(Q2) (PCY(Q2) and PFv(Q2) have band gaps of similar values). Also, there is an increase of the order of 2 eV (AM1) (or 1 eV (MNDO)) between PCNTH(Q2) and PCNCY(Q2) (PCNCY(Q2) and PCNFv(Q2) have band gaps of similar values). This is clearly illustrated in Fig. 5.43. Similar trends have also been observed in previous VEH calculations that determined band gaps of 0.26 eV for PT(Q2), 1.47 eV for PCY(Q2) and 1.80 eV for PFv(Q2) [98] which agree with our trends in general (in our calculations E_g for PFv(Q2) is of comparable value to that of PCY(Q2), i.e., it is not larger).

The general trend of decreasing the values of the band gap for the cyano derivatives is observed in both mesomeric forms. It is interesting to point out that the lowering of the band gaps occurs for same reason in the two mesomeric forms. It is clear from Fig. 5.39 that in both forms there are significant increases in the values for EA, typically by more than 1.0 eV for the cyano compounds. IP also increases in the

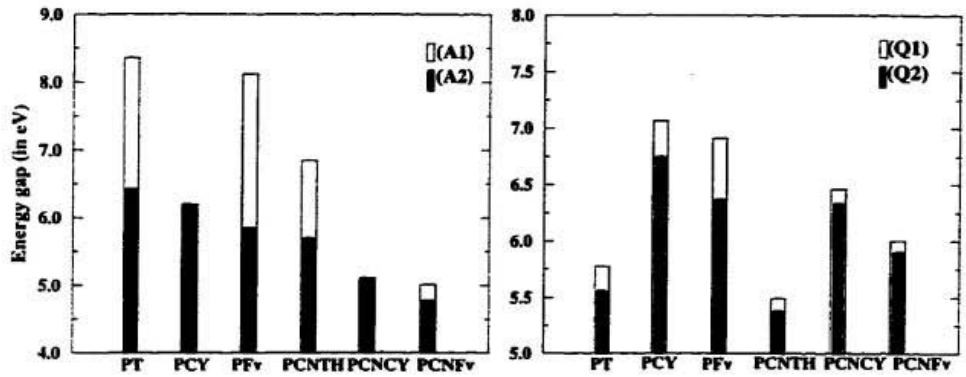

Figure 5.38: Comparison of energy gaps for the polymers in A1, A2, Q1 and Q2 forms.

cyano compounds, however, this increase is greater in the the quinoid or s-trans forms, thereby canceling more effectively the concurrent increases in EA in the quinoid or s-trans form. The net effect is that, with the exception of PT and PCNTH, the values of E_g for s-trans compounds are larger than for those in s-cis form. In PT and PCNTH, the actual values of EA and IP are increased and decreased respectively in the quinoid form relative to the corresponding aromatic form values resulting in a large decrease in E_g (by 1.6 eV in AM1 and by 0.7 eV in MNDO calculation).

As given in Fig. 5.40, if one were to relate these results to the stability of the compounds as discussed above, we note that, in all cases, lower band gaps are obtained for the less stable mesomeric form of the compounds. That is, PT(Q2) and PCNTH(Q2) have

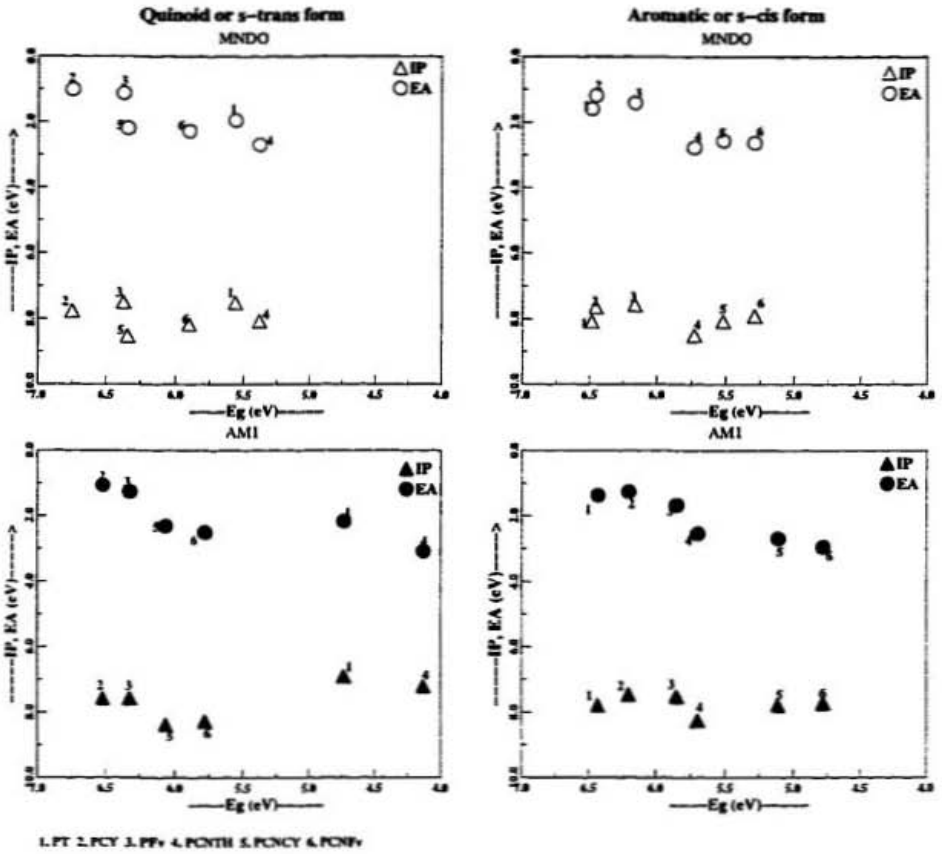

Figure 5.39: Band gaps E_g plotted as functions of IP and EA for the polymers.

lower band gaps than PT(A2) and PCNTH(A2) and PCY(A2), PFv(A2), PCNCY(A2), and PCNFv(A2) have lower band gaps than PCY(Q2), PFv(Q2), PCNCY(Q2) and PCNFv(Q2). This is may be due to the fact that electrons are more bound in the valence state in the more stable conformation. In contrast to this conclusion, however, we have found that polymers that are least stable in A1 forms have larger band gaps than in their A2 or Q2 forms. This appears to be due to smaller (discontinuous) π

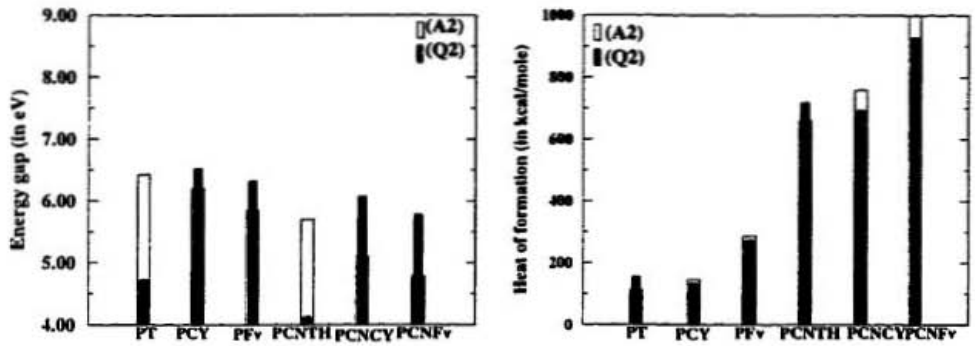

Figure 5.40: Comparison of stability vs energy gap.

electron delocalization due to nonplanar geometry (see discussion above).

Table 5.13: Values for IP, EA and E_g (in units of eV) for oligomers and polymers in their most stable forms.

	PT(A2)	PCY(Q2)	PFv(Q2)	PCNTH(A2)	PCNCY(Q2)	PCNFv(Q2)
IP[a]	7.89	7.25	7.12	7.81	7.26	7.09
IP[b]	8.08	7.76	7.49	8.50	8.53	8.17
IP[c]	7.79	7.57	7.57	8.24	8.37	8.27
EA[a]	-2.27	-3.28	-2.13	0.47	0.20	0.53
EA[b]	1.60	1.01	1.12	2.77	2.19	2.27
EA[c]	1.36	1.05	1.25	2.54	2.30	2.49
E_g^a	10.16	10.53	9.25	7.34	7.06	6.57
E_g^b	6.48	6.75	6.37	5.73	6.34	5.90
E_g^c	6.43	6.52	6.32	5.70	6.07	5.78

[a] Values for oligomers (containing two monomers) as obtained from *ab initio* calculations using 3-21G* basis set.

[b] Values for polymers (tetramers) as obtained from semiempirical MNDO scheme.

[c] Values for polymers (tetramers) as obtained from semiempirical AM1 scheme.

Table 5.14: Energy gap vs cluster size of the polymers in A2 orientation.

Polymer	Cluster	AM1 HOMO	AM1 LUMO	AM1 E_g	MNDO HOMO	MNDO LUMO	MNDO E_g
PT	Dimer	-7.85	-0.73	7.12	-8.34	-1.22	7.12
	Tetramer	-7.79	-1.36	6.43	-8.08	-1.60	6.48
	Hexamer	-7.78	-1.47	6.31	-8.05	-1.66	6.39
	Octamer	-7.78	-1.49	6.29	-8.06	-1.67	6.39
PCY	Dimer	-7.77	-1.19	6.58	-7.92	-1.03	6.89
	Tetramer	-7.46	-1.26	6.20	-7.64	-1.19	6.45
	Hexamer	-7.37	-1.29	6.08	-7.59	-1.21	6.38
	Octamer	-7.35	-1.29	6.06	-7.58	-1.21	6.37
PFv	Dimer	-8.12	-1.61	6.51	-7.97	-1.28	6.69
	Tetramer	-7.51	-1.66	5.85	-7.57	-1.41	6.16
	Hexamer	-7.42	-1.69	5.73	-7.52	-1.42	6.10
	Octamer	-7.41	-1.67	5.74	-7.51	-1.42	6.09
PCNTH	Dimer	-8.20	-2.36	5.84	-8.46	-2.63	5.83
	Tetramer	-8.24	-2.54	5.70	-8.50	-2.77	5.73
	Hexamer						
	Octamer	-8.26	-2.54	5.72	-8.52	-2.80	5.72
PCNCY	Dimer	-7.84	-2.56	5.28	-8.04	-2.43	5.61
	Tetramer	-7.79	-2.68	5.11	-8.07	-2.55	5.53
	Octamer	-7.79	-2.68	5.11			
PCNFv	Dimer	-7.78	-2.82	4.96	-7.88	-2.51	5.37
	Tetramer	-7.72	-2.94	4.79	-7.91	-2.62	5.28
	Hexamer						
	Octamer	-7.73	-2.91	4.81			

Table 5.15: Valence band width (BW) for the polymers studied.

POLYMER	HOMO	HOMO-1	BW
PT(A2)	-7.778	-9.419	1.641
PT(Q2)	-7.534	-10.246	2.712
PCY(A2)	-7.353	-10.675	3.320
PCY(Q2)	-7.529	-11.000	3.470
PFv(A2)	-7.405	-9.983	2.578
PFv(Q2)	-7.518	-10.349	2.831
PCNTH(A2)	-8.262	-9.532	1.270
PCNTH(Q2)	-7.203	-9.453	2.250
PCNCY(A2)	-7.793	-9.540	1.750
PCNCY(Q2)	-8.399	-9.674	1.275
PCNFv(A2)	-7.727	-9.441	1.714
PCNFv(Q2)	-8.273	-9.567	1.294

The values of E_g corresponding to the most stable forms of the polymers are summarized in Table 5.13. We note that the trend for the parent polymers is as follows: PFv(Q2) has the lowest band gap in this group, followed by PT(A2) and PCY(Q2). Since the experimental value for E_g for PT(A2) is 2.1 eV, the above trend would indicate that PFv(Q2) and PCY(Q2) would have, respectively, band gaps slightly lower and slightly higher than 2.1 eV. Similarly, for the cyano compounds, the trend for the band gaps is as follows: PCNTH(A2) has the lowest energy gap, followed by PCNFv(Q2), PCNCY(Q2). This trend would indicate that, since PCNTH(A2) has an experimental value for the band gap of 0.8 eV, then PCNFv(Q2) and PCNCY(Q2) would have band gaps of the order of 1 eV with PCNFv(Q2) having slightly lower band gap than PCNCY(Q2). Once again we note that inclusion of the cyano group lowers the band gaps by approximately 1 eV and this is accomplished primarily by correspondingly increasing the values of EA more than the values of IP.

5.3.1 Ab Initio Oligomer Calculations

In order to test these trends with a higher level calculations, we have carried out molecular orbital calculations for short chain segments (dimers) for all of the stable compounds. The results of the *ab initio* calculations are included in the Table 5.13. Again we see a discontinuous jump in the values of E_g between the parent polymers and their cyano derivatives. Within each subgroup the order for E_g is as follows: PFv(Q2)

has the lowest band gap, followed by PT(A2) and PCY(Q2) for the parent polymers and PCNFv(Q2) has the lowest band gap, followed by PCNCY(Q2) and PCNTH(A2) for cyano compounds. Thus, overall the semiempirical and *ab initio* calculations predict similar trends for E_g for these compounds (with small rearrangement for the cyano compounds). Within the accuracy of these calculations we can not predict whether PCNFv(Q2) has a lower band gap than PCNTH(A2). We can only say that they will be comparable in value. Also, *ab initio* calculations clearly indicate that the LUMO eigenvalue is highly stabilized (i.e. lowered in energy) upon addition of a cyano group (thus increasing EA) whereas the HOMO eigenvalue remain virtually the same as in the unsubstituted compounds. Indicating once again, that the lowering of E_g for the cyano compounds is primarily due to the increase in their values for EA.

5.3.2 Cluster Size vs Band Gap Size

In Table 5.14, values for E_g are given for various cluster sizes. In the previous chapter, we showed that the heats of formation per monomer reaches a constant (bulk) values as the cluster size increases. The results in Table 5.14 show that band gap also levels off as the cluster size increases. That is, there is a very little difference between the band gaps obtained for octamer and tetramers. This confirms out previous conclusion that the cluster size consisting of four monomeric units is long enough to study the bulk electronic properties of the polymers.

5.3.3 Band Widths

Low IP and large EA together with large valence and conduction band widths suggests the possibility of obtaining, upon doping correspondingly with weak acceptors and strong donors or strong acceptors and weak donors, a transition from semiconductor to metallic state in the organic polymers [110, 111]. Thus, we briefly examined the valence band widths in the polymers studied. The approximate values for band widths, as determined from difference between the corresponding eigenvalues for the HOMO and the one less than HOMO (HOMO-1) eigenfunctions, are shown in the Table 5.15. PCY has the largest band width of all the polymers. The next largest band width is in PFv, followed by PT. In comparison, the cyano substituted polymers has band widths that are less than (approximately half the band widths) ones obtained for parent polymers. Of all polymers, PCNTH(A2) has the lowest band width (1.25 eV). The general trend obtained for the values of band width in the polymers agrees with the ones obtained in VEH calculations. However, it should be noted that there is a large disparity in the qualitative values for the band widths.

5.4 Presence of Donor and Acceptor Groups

From our calculations (refer to Fig. 5.39) it appears that PFv gives the lowest band gap for the unsubstituted polymers and its derivative, PCNFv, seems to give the lowest band gap of all the polymers studied. What makes this polymer a low band gap

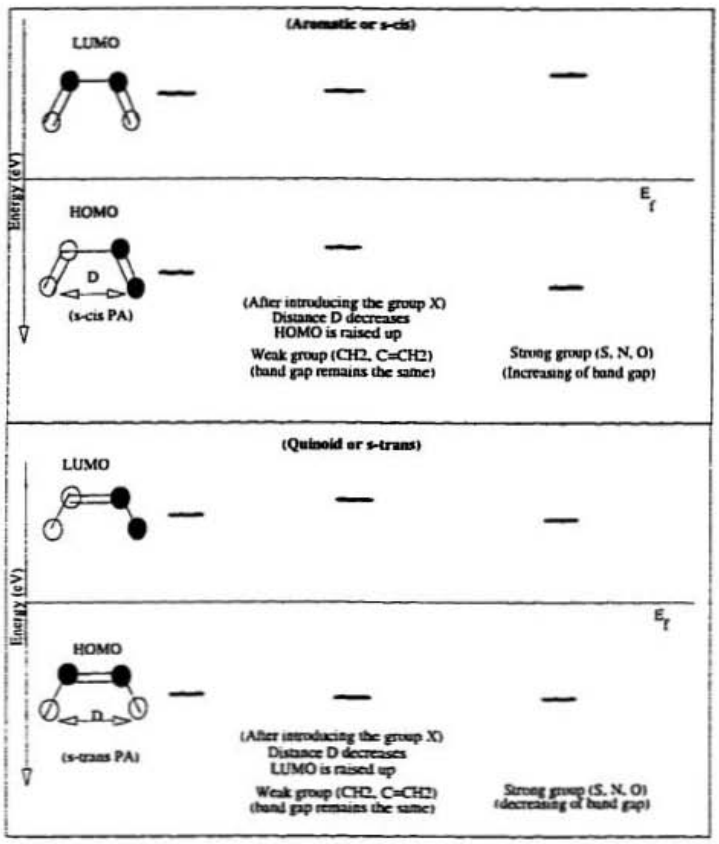

Figure 5.41: Effect of bridging groups X_d on the geometries and electronic properties of s-cis PA and s-trans PA.

polymer? It is not easy to answer this question. From the theoretical perspective the following details may possibly give some answers. Bridging groups X_d and Y_a play a very important role in defining the geometric and electronic properties of the polymers. Monomers in aromatic or s-cis (A1, A2) forms produce backbone skeletons of s-cis PA and quinoid or s-trans (Q1, Q2) forms produce backbone skeletons of s-trans PA if the bridging groups X_d were not present. First, we consider the effects of the bridging

groups, X_d, in PT, PCY and PFv parent polymers and then, the effects of cyano moiety on geometric and electronic properties are analyzed in PCNTH, PCNCY, PCNFv.

5.4.1 Effects of Electron-Donating (X_d) group

It is mentioned in our introduction trans or cis PA is a conducting polymer. So what will be the effect of attaching the proper donor substances X_d to bridge the carbons in s-cis PA? This would lead to the formation of five membered rings where X_d could be O, N-H, C, Si=H2, C=CH2 or CH2 or other similar group. In general, the inclusion of X_d modifies the geometry of the backbone, for example it can cause the C_α-$C_{\alpha'}$ distance in s-cis PA to decrease (see Fig. 5.41) [112, 38, 99, 101, 104] in order to accommodate the bridging groups X_d at the 1 position of the ring. The HOMO which is already antibonding between the orbitals of these atom in the A2 (s-cis) form of PA is raised due to further increased antibonding contribution from C_α and $C_{\alpha'}$ atoms. If the LUMO level remains unaffected this raising of HOMO eigenvalue would lower the band gap. We consider two case: (a)if the X_d is a strongly interacting group such as S, N-H or O the interaction pushes the LUMO eigenvalue up in energy as well, thus canceling the effect of the increased HOMO, the band gap may decrease but not by as much of the LUMO remained unaffected; (b) if the X_d group is weakly interacting group. the LUMO eigenvalue is not affected strongly, the net result is a decreased band gap. Similarly in s-trans PA, the introduction of the bridging group leads to raising of

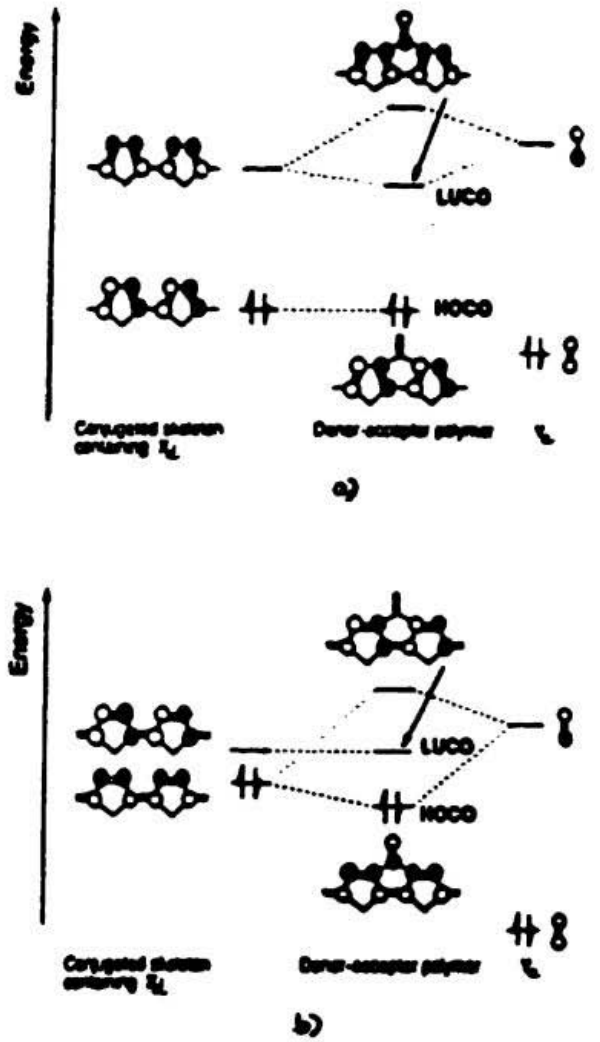

Figure 5.42: a) Schematic energy levels for the benzenoid form of donor-acceptor polymers. b) Schematic energy levels for the quinoid form of donor-acceptor polymers. The pseudo-π orbitals of X_d are omitted. Figure taken from A. K. Bakhshi et al., Synthetic Metals 79, (1996), 115.

the LUMO. If the HOMO level remained unaffected this would lead to an increase in the band gap. Again we consider two cases: (a) if the X_d is strongly interacting it also raise the HOMO causing the band gap to decrease; (b) if X_d is weakly interacting the raising of the HOMO is not very high hence overall the band gap will be increased.

Therefore, in either of the mesomeric forms, cases (b) are suitable for PCY and PFv like polymers where the electrons interact only weakly with the polymer backbones. Cases (a) are more suitable for PT, PPY, PAni like polymers where the electrons of the heteroatoms are highly diffused and strongly interacts with the polymer backbones.

5.4.2 Effects of Electron-Accepting (Y_a) group

As seen from the contour plots of eigenfunctions shown for substituted polymers from the top of the valence and bottom of the conduction bands, in aromatic or s-cis (A1, A2) forms of the polymer the contribution of the electron-withdrawing group, Y_a, to HOMO of the valence band is negligibly small. In the case of quinoid or s-trans (Q2, Q1) forms the contribution of Y_a group is negligibly small to the LUMO of conduction band. On the other hand, the electron-withdrawing group Y_a, makes a significant contribution to the LUMO of the conduction band in the case of aromatic or s-cis structures and to the HOMO of the valence band in the case of quinoid or s-trans structures (see Fig. 5.39). Therefore in the aromatic or s-cis cyano substituted polymers with a given electron-donating group, X_d, the band gap is primarily determined by the strength of

the bonding interaction between the LUMO of the conjugated skeleton containing X_d only and the LUMO of the electron-withdrawing group Y_a (see Fig. 5.42). Similarly, in the case of aromatic or s-cis structures, this band gap is largely determined by the interaction between the HOMO of the conjugated skeleton containing X_d only and the HOMO of the group Y_a only.

Since the LUMO of the Y_a group plays important role in defining the orbital symmetry, the LUMO of the cyano substituted systems found to be highly stabilized (i.e. EA is raised and the corresponding energy level is lowered) in PCNTH(A2), PCNCY(A2) and PCNFv(A2) mesomers. In these systems: PCNTH(A2), PCNCY(A2) and PCNFv(A2) HOMO eigenvalues remain almost the same as those for the parent polymers. For PCNTH(Q2), PCNCY(Q2), PCNFv(Q2), the HOMO eigenvalues are affected more by the presence of Y_a by increasing IP or lowering the corresponding eigenvalues relative to the A2 forms. In this case the LUMO is also affected by increasing EA and thus lowering the LUMO eigenvalues. The net effect is that in both cases, the band gaps of cyano substituted systems are lower than those for the parent polymers. In some cases, X_d or Y_a can be interchanged to obtain further reduction in the band gap values.

5.5 Electronic-Geometric Structure Correlations

From the above discussion, we note that there is a close relationships between the cyano substituted polymers and their parent polymers. In Table 4.7, 4.6 the geometric

structure parameters were given (see Chapter 4). In this section, we correlate the average bond length alternation, δr, along the backbone with the size of the band gap. We summarize the trend in Fig. 5.43. For the parent polymers we note that for PT(A2), PCY(A2) and PFv(A2) the absolute value for δr increases as E_g decreases whereas for the quinoid or s-trans form E_g decreases for PT with virtually no change in δr. Thus, for the quinoid or s-trans forms, a large decrease in E_g is strongly correlated with the presence of the sulfur atom in PT.

Next we consider the cyano substituted systems. The trends in the average bond length alternations as seen in Fig. 5.43 indicate that the decrease in E_g is accompanied by charge delocalization in PCNTH(A2) since δr in PCNTH(A2) (0.002 $\AA$ is smaller than δr in PT(A2) (-0.03 $\AA$). In contrast, the δr of PCNTH(Q2) (0.13 $\AA$) is larger than the δr for its parent PT(Q2) (0.11 $\AA$). Thus indicating that the lowering of E_g is now accompanied by the greater charge localization. The δr in PCNCY(A2) is -0.04 $\AA$ and in PCNCY(Q2) is 0.14 $\AA$ indicating that the decrease in E_g in PCNCY relative to PCY occurs when the electronic charge is less localized in PCNCY(A2) than in PCY(A2) and more localized in PCNCY(Q2) than in PCY(Q2). The same observations can be made for PCNFv which has δr equal to -0.04 $\AA$ for PCNFv(A2) and to 0.14 $\AA$ for PCNFv(Q2). The δr for PCNFv(Q2) (0.14 $\AA$) is larger than the corresponding values for the mesomers of PT, PCY, PFv and PCNTH with the exception of PCNCY(Q2). It appears from the corresponding values for δr that the attached vinylene group to

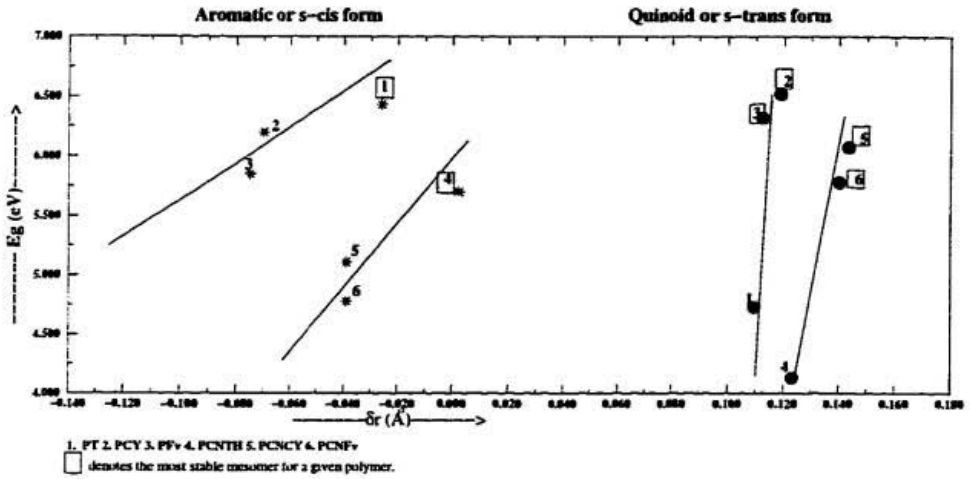

Figure 5.43: Bond length alternation (δr) plotted as a function of band gap (E_g) for the polymers (AM1 data) as indicated for the two mesomeric forms. The solid lines are drawn only for the purpose of guiding the eyes.

PCNCY does not significantly change the structure of PCNCY.

In summary, we note that while it was shown in section 5.3 that all cyano substituted polymers displayed a decrease in the band gaps relative to the corresponding values for their parent polymers, the respective trend in their geometric structures are not as straightforward. The structural analysis as summarized by the values of δr showed

that the cyano derivatives exhibited an increased aromaticity due to charge delocalization in their aromatic or s-cis forms but a decreased aromaticity in their quinoid or s-trans forms (see Fig. 5.43) when E_g is lowered. These trends are mainly attributed to electron-withdrawing property of the cyano group. In PFv and PCNFv the vinylene group has only a weak effect on the changing structures of PCY and PCNCY correspondingly. However, the presence of this group improves the planarity of these systems and thus increases the inter-cluster distances resulting in decreased interactions between the adjacent rings in the backbone [38, 99]. The more planar structure would favor the formation of the solid and films and may enhance the conductivity in the directions other than along the chain.

Chapter 6

Conclusions

We summarize our geometric structure findings as follows:

- The quasi one-dimensional polymers studied can exist in two mesomeric forms (aromatic or s-cis and quinoid or s-trans) that are produced as a result of lattice distortions. The two forms are nondegenerate (i.e. often correspond to energies that are widely different).

- Crystal packing and electronic energy associated with π-electron conjugation (that reduces strong steric repulsions) favor the appearance of coplanar conformations with monomers in *anti* orientation (A2, Q2 forms).

- With monomers in *syn* orientation (A1, Q1 forms), twisted conformations are generated due to large steric interactions between them.

- Comparing A1 and A2 structures reveal that both these structures are rather close in energy in some cases thus introducing the possibility of thermochromic behavior for these polymers.

- In general, the geometries are not significantly altered between A1 and A2 conformations and between Q1 and Q2 conformations, that is similar bond alternation patterns are present in the respective conformations.

- The consideration of the heats of formation, H_f, at the level of semiempirical calculations, shows that the trend in the stability is such that most favorable orientation preferred by the monomeric units in the polymer is *anti* (A2, Q2 forms) rather than the *syn* (A1,Q1 forms).

- The geometries and the heats of formation calculated using AM1 are considered to be more reliable than the corresponding MNDO values.

Next, we summarize our electronic structure findings as follows:

- The coplanar conformation maximizes the π orbital overlap.

- Our result for band gap indicate that PCNFv is a low band gap polymer similar to PCNTH of the order of 1 eV for the more stable form (see Table. 5.13. Semiempirical calculations overestimate the experimental values for E_g by approximately 3.0-4.0 eV.

- The average bond length alternation in PCNCY and PCNFv is increased (relative to PCY and PFv) upon addition of cyano groups resulting in the more quinoid-like structures than it is observed in their parent polymers. This can be correlated

with a strong influence of cyano groups on their LUMO eigenvalues (EA's) for these compounds.

- That is, in the cases of PCNCY and PCNFv, the band gaps decrease when PCNCY and PCNFv become more quinoid-like in comparison to their parent polymers. This is in contrast to the more "general" trend as shown in Fig. 5.39 which indicates that polymers with more aromatic-like structures tend to have smaller intrinsic band gaps.

- Interactions of different bridging groups with the backbone often results in the lowering of the band gaps. The strength of these interactions, in turn, determines by how much the band gap is lowered. For example, in the fulvene based polymers, PFv and PCNFv, the vinylene group does not contribute significantly to the lowering of the value of E_g. However it enhances the planarity to their backbones.

- In heteroatomic polymers, such as PT and PCNTH, the the lone pair electrons on sulfur atoms contribute extra π electrons (in contrast to the carbon atoms) to the backbone π system [38] - thus enhancing their conducting properties.

- Upon studying the relationships between the geometric and electronic nature of the planar polymers (A2, Q2 forms), it is observed that the less stable forms of the polymers have lower band gaps than the more stable ones.

- The IP, EA and band gaps of the polymers in (A1, A2, Q1, Q2 forms) calculated using AM1 are reliable than the values calculated using MNDO.

- Ab initio, molecular investigation of oligomer confirms our semiempirical findings. The 3-21G* basis set appears to be sufficient for this comparison. More ab initio calculations are planned for the future studies.

- Overall, in the monomers of the polymers studied, the cyano-group forms the electron-accepting group and the remaining structure of a given monomer forms the electron-donating group.

- Fig. 5.39 illustrates that the main role of the donor-acceptor groups in these polymers is to increase EA and decrease IP values and consequently to lower intrinsic band gaps.

Chapter 7

Appendix A

7.1 Nomenclature Followed in Semi-Empirical Methods

From Eq. 2.25 it is clear that the integrand of any molecular integral contains a certain one or two electron operators $\hat{A}$ and the appropriate atomic orbitals, which may depend on the local coordinate system. The natural origin of coordinates for an atomic orbitals is the nucleus of the corresponding atom. If $\hat{A}$ is one electron operator, a general one electron integral has the form

$$< \chi_\mu(r_A(1)|\hat{A}(r_B(1)|\chi_\nu(r_C(1) >$$

The subscripts A, B, C refer to atomic centers and ν, μ subscripts to individual orbitals. Depending on the coincidence of the origins of the various coordinate systems, the integral is referred to as a one- (A=B=C), two-(A=B, B $\neq$ C;B=C, A $\neq$ B), three-centre(A $\neq$ B; B $\neq$ C; C $\neq$ A) one-electron integral. Of particularly importance are

the following two-electron one- and two- centre integrals.

$(\mu_A\mu_A|\mu_A\mu_A)$ the one – centre Coulomb integral,

$(\mu_A\nu_A|\mu_A\nu_A)$ the one – centre exchange integral,

$(\mu_A\mu_A|\nu_A\nu_B)$ the two – centre Coulomb integral,

$(\mu_A\nu_B|\mu_A\nu_B)$ the two – centre exchange integral.

Bibliography

[1] J. S. Miller. *Advanced Materials*, 5(7/8,9):671, 1993.

[2] J. S. Miller. *Advanced Materials (Part-A).*, 4:587, 1993.

[3] G. Horowitz, F. Garnier, A. Yassar, R. Hajlaoui, and F. Kouki. *Advanced Materials*, 8(1):52, 1996.

[4] G. Horowitz, P. Delannoy, H. Bouchriba, F. Deloffre, J. L. Fave, F. Garnier, R. Hajlaoui, M. Heyman, F. Kouki, P. Valat, V. Wintgens, and A. Yassar. *Advanced Materials*, 6:752, 1994.

[5] J. M. Ziman. Principles of the theory of solids. *Edition 2, Cambridge University Press. New York*, 2:1, 1972.

[6] J. Farges. Organic conductors. *Marcel Dekker Inc., New York*, 1:1, 1994.

[7] L. Salem. Molecular orbital theory for organic chemists. *John Wiley and Sons. New York*, 1961.

[8] J. K. Burdett T. A. Albright and M-H. Whangbo. Orbital interactions in chemistry. *John Wiley and Sons, New York*, 1:1. 1986.

[9] J. A. Pople and S. H. Walmsley. *Mol. Phys.*, 71:1506, 1979.

[10] D. J. Berets and D. S. Smith. *Trans. Faraday soc.*, 64:823, 1968.

[11] T. Ito, H. Shirkawa, and S. Ikeda. *J. Polym. Sci. Polym. Chem. Ed.*, 12:11, 1974.

[12] H. Shirkawa, E. J. Louis, A. G. MacDiarmid, C. K. Chiang, and A. J. Heeger. *Chem. Commun*, 578, 1977.

[13] P. J. Nigrey, A. G. MacDiarmid, and A. J. Heeger. *Chem. Commun*, 594, 1979.

[14] D. M. Ivory, G. G. Miller, J. M. Sowa, L. W. Shackletter, R. R. Chance, and R. H. Baughman. *J. Chemical Physics*, 71:1506, 1979.

[15] A. F. Diaz, K. K. Kanazawa, and G. P. Gardini. *Chem. Commun*, 635, 1979.

[16] K. K. Kanazawa, A. F. Diaz, R. H. Geiss, W. D. Gill, J. F. Kwak, J. A. Logan, J. F. Rabolt, and G. B. Street. *Chem. Commun*, 854, 1979.

[17] G. Tourillon and F. Garnier. *J. Electroanal. Chem*, 135:173, 1982.

[18] T. A. Skotheim. Handbook of conducting polymers. *Marcel Dekker Inc., New York*, 1:1, 1986.

[19] A. Andreatta, Y. Cao, J. C. Chiang, A. J. Heeger, and P. Smith. *Synthetic Metals*, 26:383, 1988.

[20] R. L. Elsenbaumer, K. Y. Jen, and R. Oboodi. *Synthetic Metals*, 15:164, 1986.

[21] S. Bruckener and W. Porzio. *Makromol. Chem.*, 189:961, 1988.

[22] A. Bolognesi, M. Catellani, S. Destri, and W. Porzio. *Makromol. Chem., Rapid Commun.*, 12:9, 1991.

[23] J. Kurti and H. Kuzmany. *Phys. Rev. B*, 44:597, 1991.

[24] Terbeek, C. Zimmerman, and D. S. Burnell. *Mol. Phys*, 74:1027, 1991.

[25] M. Kobayashi, N. Colaneri, M. Boysel, F. Wudl, and A. J. Heeger. *J. Chemical Physics*, 82:5717, 1985.

[26] M. Satoh, M. Tabata, F. Uesugi, K. Kaneto, and K. Yoshino. *Synthetic Metals*, 17:595, 1987.

[27] G. leising. *Phys. Rev. B*, 38:10313, 1988.

[28] C. Taliani and L. M. Blinov. *Advanced Materials*, 8(4):353, 1996.

[29] Z. Vardeny, E. Ehrenfreud, O. Brafman, and B. Horowitz. *Phys. Rev. Lett*, 56:671, 1986.

[30] L. W. Shacklette, R. R. Chance, D. M. Ivory, G. G. Miller, and R. H. Baugman. *Synthetic Metals*, 1:307, 1979.

[31] R. E. Peierls. Quantum theory of solids. *(London, Oxford Press)*, 1955.

[32] S. A. Brazovskii and Kirova. *JETP Letters*, 33:1, 1981.

[33] M-H. Whangbo, R. Hoffmann, and R. B. Woodward. *Proc. R. Soc. Lond.*, 366(A):23, 1979.

[34] A. W. Overhauser. *Physical Review*, 167:691, 1968.

[35] J. M. Andre, L. A. Burke, J. Delhalle, G. Nicolas, and P. Durand. *Int. J. Quantum Chem. Symp.*, 13:283, 1979.

[36] J. L. Bredas, B. Themans, and J.M. Andre. *Synthetic Metals*, 11:343, 1985.

[37] Y. S. Lee and M. Kertesz. *J. of Chemical Physics*, 88(4):2609, 1988.

[38] S. Y. Hong, S. J. Kwon, and S. C. Kim. *J. of Chemical Physics*, 103(5):1871, 1995.

[39] A. J. W. Tol. *Synthetic Metals*, 74:95, 1995.

[40] Eiichi Tabei, Motoo Fukushima, and Shigeru Mori. *Synthetic Metals*, 73:113, 1995.

[41] M. Mizuno, A. F. Garito, and M. P. Cava. *J. Chem. Soc. Chem. Communication.*, 18, 1978.

[42] E. E. Havinga, W. ten Hoeve, and H. Wynberg. *Polym. Bull.*, 29:119, 1992.

[43] J. P. Ferraris, D. O. Cowan, and Jr. V. Walatka et al. *J. Am. Chem. Soc.*, 95:948, 1973.

[44] J. P. Ferraris and T. L. Lambert. *J. of Chemical Society., Chem Commun.*,, page 1268, 1991.

[45] J. M. Toussaint and J. L. Bredas. *Synthetic Metals*, 61:103, 1993.

[46] J. M. Toussaint and J. L. Bredas. *Synthetic Metals*, 69:637, 1995.

[47] J. L. Bredas, R. R. Chance, R. Silbey, G. Nicolas, and Ph. Durand. *J. Chem. Phys.* 75:1, 1981.

[48] M. J. S. Dewar, E. G. Zoebisch, E. F. Healy, and J. J. P. Stewart. *J. of Am. Chem. Soc*, 107:3902, 1985.

[49] P. G. Perkins and J. J. P. Stewart. *J.C.S. Faraday II*, 76:520, 1980.

[50] J. J. P. Stewart. Mopac 93.00 manual. *Fujitsu Limited, Tokyo, Japan*, 1993.

[51] H. Subramanian and J. B. Lagowski. *Submitted to Int. J. Quant. Chem.*

[52] S. Hotta, T. Hosaka, and W. Shimotsuma. *J. Chem. Phy.*, 80:954, 1984.

[53] S. Hotta, T. Hosaka, and W. Shimotsuma. *Synthetic Metals*, 9:87, 1984.

[54] C. X. Cui and M. Kertesz. *Phys. Rev. B*, 40(14):9661, 1989.

[55] W. L. McCubbin. Electronic structure of polymer and molecular crystals. *(J.M. Andre and J. Ladik, Eds.), NATO ASI Series*, B 9:171, 1975.

[56] J. L. Bredas, B. Themans, J. G. Fripiat, J. M. Andre, and R. R. Chance. *Phys. Rev B*, 29:6761, 1984.

[57] J. C. Scott, J. L. Bredas, P. Pfluger, K. Yakushi, and G. B. Street. *Synthetic Metals.*, 9:265, 1984.

[58] A. Szabo and N. S. Ostlund. Modern quantum chemistry. *Macmillan Publishing Company Inc.*,, 2:1, 1982.

[59] J. C. Slater. Quantum theory of atomic structure. *McGraw-Hill Book Company Inc., New York*, 1960.

[60] J. Sadlej. Semi-empirical methods of quantum chemistry. *John Wiley and Sons, New York*, 1:1, 1985.

[61] C. C. J. Roothan. *Reviews in Modern Physics*, 23:69, 1951.

[62] E. Huckel. *Z. Phys.*, 70:204, 1931.

[63] R. Pariser and R. G. Parr. *J. Chem. Phys.*, 21:466, 1953.

[64] J. A. Pople and G. A. Segal. *J. Chem. Phys.*, 43:S136, 1965.

[65] L. Oleari, L. Di Sipio, and G. De Michelis. *Mol. Phys.*, 10:97, 1966.

[66] M. J. S. Dewar, E. G. Zoebisch, E. F. Healy, and J. J. P. Stewart. *J. Am. Chem. Soc.*, 107:3902, 1985.

[67] J. J. P. Stewart. *J. Comp. Chem*, 10:210, 1989.

[68] J. J. P. Stewart. *QCPE Bulletin*, 3:43, 1983.

[69] K. B. Lipkowitz and D. B. Boyd. Reviews in computational chemistry. *VCH Publishers, New York*, 1:45, 1991.

[70] M. J. S. Dewar and D. M. Storch. *J. Am. Chem. Soc.*, 107:3898, 1985.

[71] F. Bloch. *Z. Physik*, 52:555, 1928.

[72] E. Huckel. *Z. Physik*, 76:628, 1932.

[73] K. Yates. Huckel molecular orbital theory. *Academic Press, Inc., New York*, 1:1, 1978.

[74] A. A. Levin. Solid state quantum chemistry. *McGraw-Hill International Book Company, New York*, 1:1, 1977.

[75] R. Hoffman, C. Janiak, and C. Kollmar. *Synthetic Metals*, 74:95, 1995.

[76] S. L. Altmann. Band theory of solids: An introduction from the point of view of symmetry. *Clarendon Press, Oxford*, 1:198–212, 1994.

[77] M-H. Whangbo. In extended linear chain compounds,. (Ed. J. S. Miller), *Band structures of one-dimensional inorganic, organic and polymeric conductors*, 2:127, 1982.

[78] T. Inui and Y. Umera. *Prog. Theoret. Phys. (Kyoto)*, 5:252, 1950.

[79] R. P. Messmer and G. D. Watkins. *Phys. Rev. Lett.*, 25:656, 1970.

[80] R. P. Messmer and G. D. Watkins. *Phys. Rev. B*, 7(6):2568, 1973.

[81] W. P. Su, J. R. Schrieffer, and A. J. Heeger. *Physical Review Letters*, 42:1698, 1980.

[82] Z. Iqbal, R. R. Chance, and R. H. Baugman. *J. Chem. Phys*, 66:5520, 1977.

[83] A. Almenningen, O. Bastiansen, and P. Svendsas. *Acta. Chem. Scan.*, 12:1671, 1958.

[84] G. J. Visser, G. J. Heeres, J. Wolters, and A. Vos. *Acta Crystallogr. Sect. B*, 24:467, 1968.

[85] G. Barbarella, D. Casarini, M. Zambianchi, L. Favaretto, and S. Rossini. *Advanced Materials*, 8(1):69, 1996.

[86] G. Horowitz, B. Bachet, A. Yassar, P. Lang, F. Demanze, J. L. Fave, and F. Garnier. *Chem. Mater.*, 7:1337, 1995.

[87] G. Barbarella, M. Zambianchi, A. Bongini, and L. Antolini. *Advanced Materials*, 4(4):282, 1992.

[88] A. Yassar and F. Garnier. *Advanced Materials*, 6(9):660, 1994.

[89] S. V. Meille and A. Farina. *Advanced Materials*, 6(11):848, 1994.

[90] K. Faid, M. Frechette, M. Ranger, L. Mazerolle, I. Levesque, and M. Leclerc. *Chem. Mater.* 7:1390, 1995.

[91] G. D. Stucky and J. E. MacDougall. *Science*, 247:669, 1990.

[92] P. P. Edwards, L. J. Woodall, P. A. Anderson, A. R. Armstrong, and M. Slaski. *Chem. Soc. Rev*, page 305, 1993.

[93] G. A. Ozin and C. Gil. *Chem. Rev*, 89:1749, 1989.

[94] C. Aleman and L. Julia. *J. Phys. Chem*, 100:1524, 1996.

[95] T. L. Porter, D. Minore, and D. Zhang. *J. Physical Chemistry*, 99:13213–13216, 1995.

[96] J. J. P. Stewart. *New Polymeric Materials*, 1:53, 1987.

[97] M. J. S. Dewar and M. L. McKee. *J. Comput. Chem*, 4:84, 1983.

[98] J. Pranata, R. H. Gribbs, and D. A. Dougherty. *J. Am. Chem. Soc*, 110:3430, 1988.

[99] S. Y. Hong and D. S. Marynick. *Macromolecules*, 28:4991, 1995.

[100] J. L. Bredas, G. B. Street, B. Themans, and J. M. Andre. *J. Chem. Phys*, 83(3), 1985.

[101] G. Brocks. *J. Phys. Chem.*, 100:17327, 1996.

[102] J. L. Bredas, R. L. Elsenbaumer, R. R. Chance, and R. Silbey. *J. Chem. Phys.*, 78:5566, 1983.

[103] J. L. Bredas, J. M. Andre, and J. Delhalle. Quantum chemistry aided design of organic polymers-an introduction to the quantum chemistry of polymers and its applications. *(World Scientific Co. Singapore)*, 2, 1991.

[104] A. K. Bakhshi, Y. Yamaguchi, H. Ago, and T. Yamabe. *Synthetic Metals*, 79:115, 1996.

[105] T. C. Chung, J. H. Kaufman, A. J. Heeger, and F. Wudl. *Physical Review B*, 30(2):702, 1984.

[106] J. J. Ladik. *Indian Journal of Chemistry*, 33(A):449.

[107] M. Kertesz. *Adv. Quantum Chem.*, 15:161, 1982.

[108] A. J. W. Tol. *J. Chem. Phys*, 11:1, 1994.

[109] T. Koopmans. *Physica*, 1:104, 1933.

[110] J. Tanaka, C. Tanaka, T. Miyamae, K. Kamiya, M. Shimizu, M. Oku, K. Seki, J. Tsukamoto, S. Hasegawa, and H. Inokuchi. *Synthetic Metals*, 55:121, 1993.

[111] N. Kirova and S. Brasovskii. *Synthetic Metals*, 76:229, 1996.

[112] Uli Salzner. Private communication. 1996.